# Structural style and evolution of the Caledonian foreland, northeast Tyrifjorden, Oslo Region

A MSc. thesis by Martijn Vlieg

June 29, 2015
Department of Geosciences University of Utrecht

Supervised by:
Prof. Roy Gabrielsen, Department of Geosciences University of Oslo
Prof. Dimitrios Sokoutis, Department of Geosciences University of Utrecht
Dr. Bjørn Larsen, Det Norske Oljeselskap ASA, Norway

**Abstract**

The Palaeozoic sediments present in the Oslo area reflect the outward growth of the Caledonian Orogen, making it a classical area for the study of frontal thrust systems. Bruton et al. (2010) proposed a revised structural model for the tectonic development of this basin, but detailed structural field data to support the model is still lacking. Analogue mechanical laboratory models were performed to better understand the structural inhomogeneities affiliated with the proposed structural model.

The present study covers two profiles; an 8 km N-S profile along the eastern shore of Tyrifjorden just south of Sundvollen and a 1.5 km profile along the western shore of Tyrifjorden just south of the first profile. The section along the shore south of Sundvollen shows open folding on the scale of hundred of meters and severe strain localized in the Utstranda pop-up generating an anticlinorium. Deformation in this section is strongly affected by back thrusting, which is localized below the mechanically strong Ringerike sandstone. Similar strain localization and strain transfer are observed in the analogue models.

The analogue models and field observations agree in terms of variation in deformation styles and presence of high and low strain regimes. The field observations also match the model from Bruton et al. (2010) and indicate a local tectonic transport direction towards the NW and a homogeneous fold axis of 060/10 throughout the area.

# Contents

# 1. Introduction

## 1.1. Research history

The Oslo region has for several centuries been an area of interest as a classical structural research area. The earliest studies done in the Oslo Region have recognized the major folding and faulting present and have associated it with the Caledonian orogeny *(Brøgger, 1882)*, especially after the Caledonian orogen itself was comprehended better *(Törnebohm, 1888; 1896 and Bjørlykke, 1901)*. Also the location of frontal-most thrust of the orogen has been a point of discussion. Classically it was recognized well northwest of Oslo, just southeast of Jotunheimen, though research has pointed out that the real thrust front is located south of Oslo *(Hossack and Cooper, 1986; Gee et al., 1985; Roberts et al., 1985; Nystuen, 1981)*. This thrust sheet is called the Baltic Cover sheet and comprises multiple thin-skinned nappes in Riphean to Silurian sediments *(Hossack and Cooper, 1986)*. The nappe of which the sediments in the Oslo area are compiled of is called the Osen-Røa thrust *(Nystuen, 1981)*. Later in the 20th century more detailed and modern studies were performed in order to place the Oslo region in the picture of an evolving Caledonian Orogen *(Nystuen, 1981; Ramberg et al., 1981 and Morley 1986a, b, 1987a, b, 1994)*. For example more detailed stress reconstruction was done, showing oblique emplacement in the Oslo area, compared to the Caledonian thrust front *(Hossack and Cooper, 1986; Sippel et al., 2010)* In the most recent structural study a new view was presented on the fold-and-thrust belt in the Lower Palaeozoic sediments in the Oslo area *(Bruton et al. 2010)*. In this study it is suggested that the Cambrian to Silurian strata is subdivided into four structural levels. Each structural level has its own deformation style, strain intensity and is associated (or bounded) by major thrusts. The four levels, from bottom to top, are: the basal thrust system, the middle thrust system, the upward ramping fault system which flattens under the Ringerike sandstone and the fault system that cuts through the Ringerike sandstone.
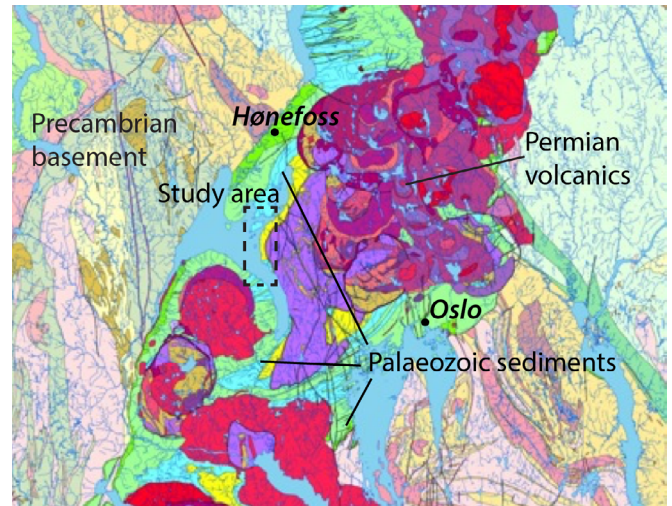


Fig. 1. Overview geological map of the Oslo area with the major lithological domains and the study area indicated. More details about locations that are mentioned in the text are presented in figure 2.

This structural model was used as a guide and as a correlation model for this study and it will be explained in more detail later in this introduction.

More detailed studies done at the coastline of Sønsterud and in the bay of Sælabonn, which are located respectively just north and south of this study's area (***Fig. 1 and Fig. 2***) *(Kleven, 2010; Hjelseth, 2010)*, go deeper concerning structural analysis of the theory presented in Bruton et al. 2010. At Sælabonn four distinct deformation styles are recognized, which all related to the Scandian deformation phase. The D1 phase represents early phase bedding-parallel shortening *(Morley, 1987)* and was followed by a phase (D2) of tight to isoclinal, disharmonic folding with upright axial planes and NE-SW trending fold axes. A phase of foreland-directed thrusting is followed (D3) and an out of sequence back-thrusting phase (D4) pursues this. All thrusting and folding is consistent with the main tectonic transport direction *(Hjelseth, 2010)*. Along the Sønsterud coastline also four stages (all in the Scandian phase) of deformation are recognized *(Kleven, 2010)*, however in this study back thrusting was particularly focused upon, as it had not been studied thoroughly and seems to be significant. Low and high angle back thrusting are found and categorized in their own thrusting stage. Furthermore the influence of back thrusting appeared to be bigger than

Fig. 2. Aerial photographs compiled to an overview map of the research area, with the study area indicated. Contemporary research by Van den Broek (2015) was executed in the northern part of the Ringerike area, by Verdonk (2015) at Fornebu and Bygdøy and by Weekenstroo (2015) at Slemmestad and along the coast northward.

expected in the Sønsterud area, it was a secondary process to the main foreland-directed thrusting and the mechanism behind the hinterland-directed thrusting was unclear *(Kleven, 2010)*.

The aim of this research is to enhance the understanding of the detailed structural development in the northeast Tyrifjorden area (***Fig. 1 and Fig. 2***) in light of existing regional tectonic models. This will be done using structural data from the field and mechanical observations from analogue models. In this study the focus will lie on the apparent dominant back thrusting *(Morley, 1994; Hjelseth, 2010; Kleven, 2010)* and its mechanism. Emphasis will be put on the strong heterogeneity of structural styles and strong homogeneity of deformation in the area.

## 1.2.  Methods

This study consists of two principle data set, namely a field set and an analogue modeling set. The latter has been performed in the Tectonics Laboratory at the University of Utrecht and will be discussed in its own part further on in this thesis. The field project was based on gathering data to be able to gain insights on the proposed questions. To achieve this, a number of sections were constructed along a NW-SE line and structural and lithological data was acquired. Due to the size of the Oslo area the project was combined with three other students (A. Verdonk, M. Weekenstroo and J. van den Broek), all working in a different part of the area with their own characteristic research question. The study by Verdonk et al., 2015 focused on the role of veining in the Caledonian deformation and the structural style of the Fornebu and Bigdøy outcrops, Weekenstroo et al., 2015 laid emphasis on the deformation tip of the foreland based on structural style and strain variations (Slemmestad area) and van den Broek et al., 2015 concentrated on the structural style of the basal decollement and strain transfer up section (Viul and Klekken area). Especially with van den Broek et al., 2015 a close combination can be made with this study, as our areas flow over into each other. In the end the data of the four projects is combined and correlations are made with the analogue models.

In the field master faults and relative

structures are documented, strike-dip relations and fold axes are measured and the structural style and lithologies are determined. The structural style is described by faults and folds classification, the frequency of deformation structures and the sequence of faulting. With this data maps and profiles are constructed in order to visualize the structures that are recognized from the field. For relative correlation the profiles (or sections), which are presented in an overview map of the study area (***Fig. 3***), have a partly (lateral) overlap.

Section A-A' is constructed from the Rytteråker peninsula in the north to, along the islands in the fjord; Haraøya, Storøya, Purkøya, Geitøya and it runs from Utøya to the main land, along the Utstranda coastline, ending at the Sønsterud coastline; section B-B' runs from the east of Storøya to the mainland; section C-C' runs along the Utstranda road parallel to the coast and terminates just south of the intersection of Utstranda with the connection road to the E16; section D-D' runs along the connection road between the E16 and Utstranda and finally section E-E' is constructed along the coastline on the other side of the fjord, where it is called Modum. Combined these profiles cover around 15 km of section in high detail. The sections were constructed in this way due to the average strike of the strata in the area. Most strata strike roughly SW-NE, so in order to gain the best view on the structures the sections are constructed perpendicular to the strike. Also data density is taken into account in the construction of the profiles. Structural data from the sections and the area will be analyzed using stereo plotting software; OSXStereonet and Stereonet *(Allmendinger and Cardozo, 2011)*.

## 1.3.  Position of the Oslo region in geological history.

### 1.3.1.  *Lower Palaeozoic*

In the early Palaeozoic the Caledonian orogen arose, of which the Scandinavian Caledonides embodies its northern branch. It represented the collision of three major continental terranes; Laurentia and Baltica in the north, and
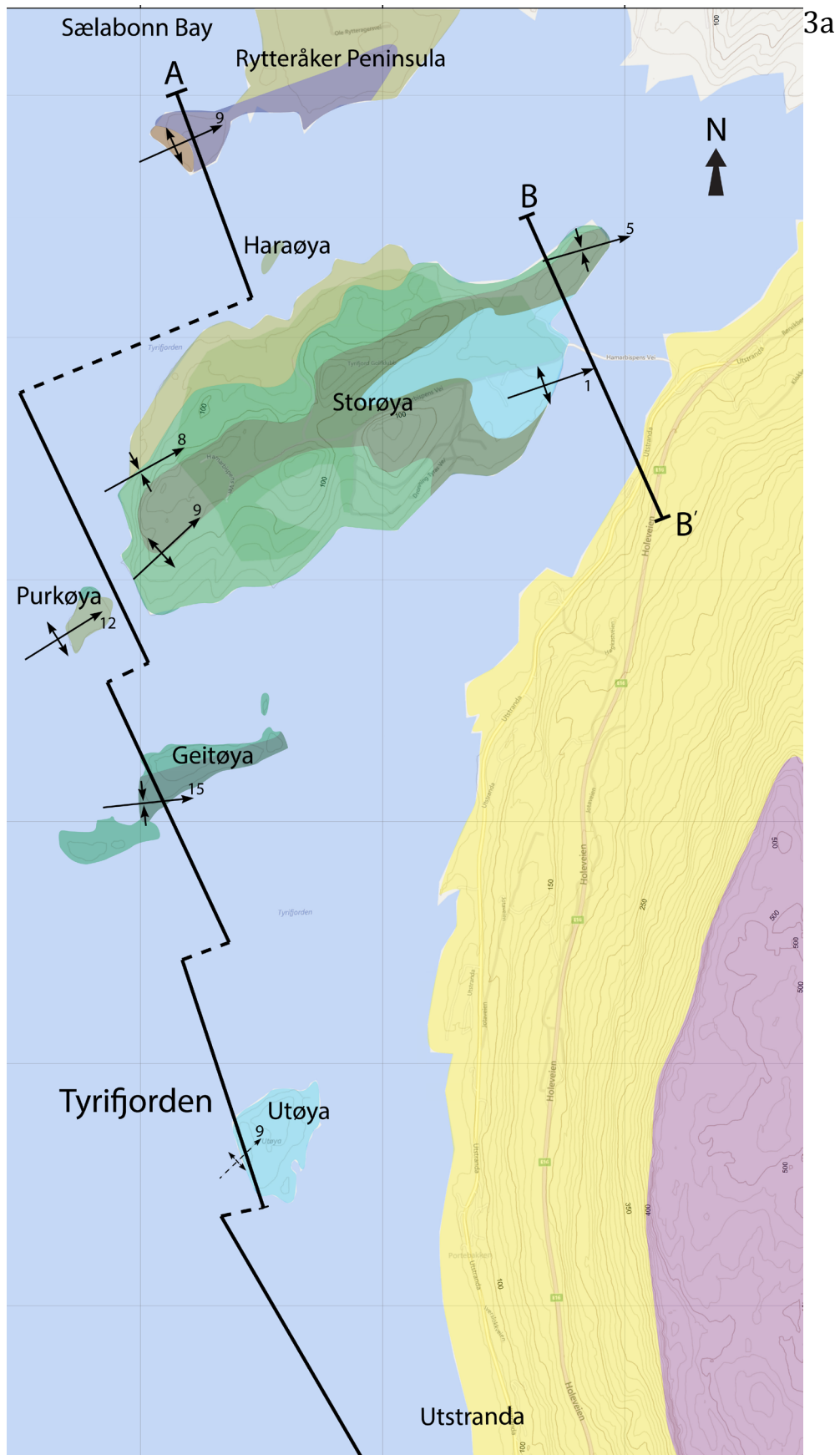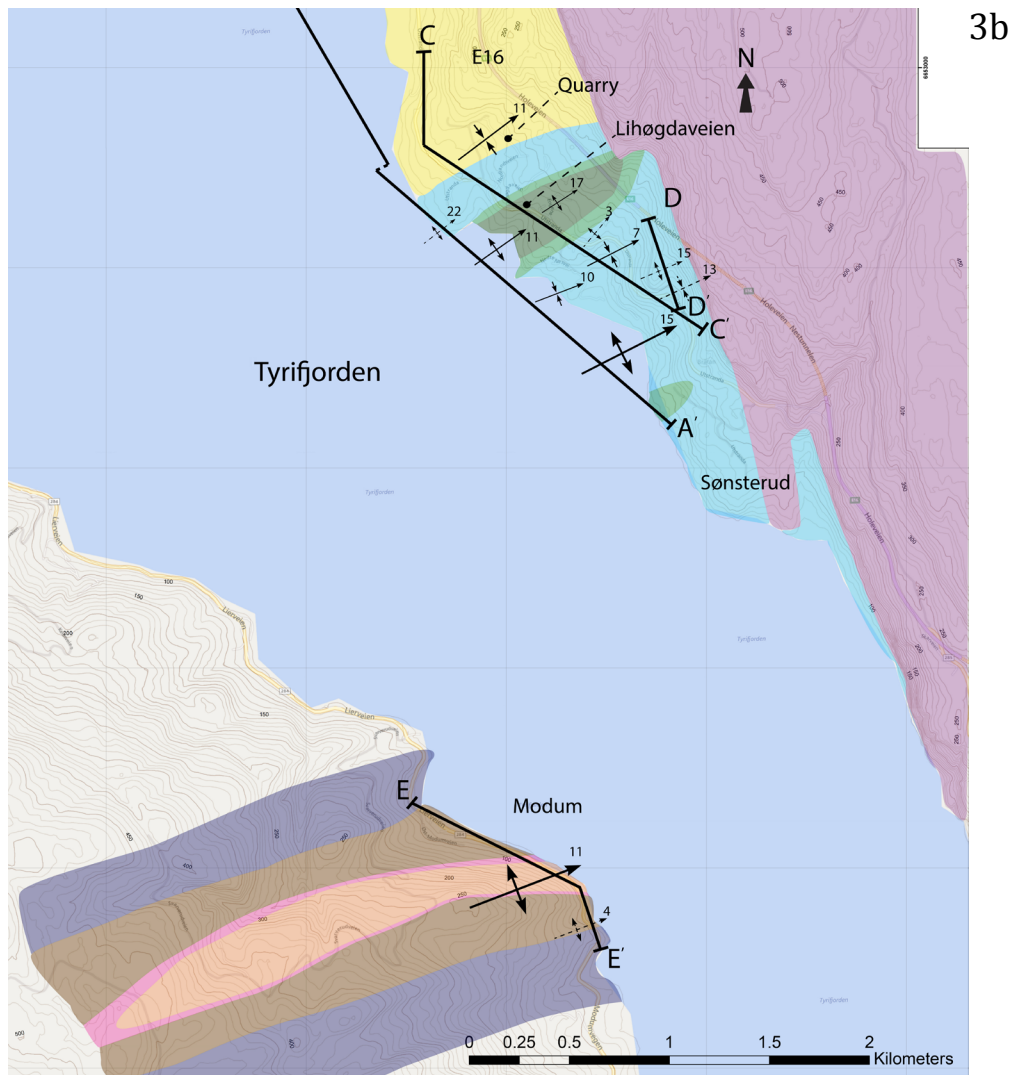
Fig. 3. Overview geological map of the study area. (A) The north part of the area showing the north coast of the Tyrifjorden and towards the NE the connection with the Steinsfjorden. The road between Hønefoss (N) and Oslo (S) (E16) runs through the area along the coast. (B) The south part of the area, directly connectible to the lower boundary of the north part map. Also the E16 can be recognized along the coast. (C) The legend for all lower Palaeozoic formations (Fm.) (mainly Silurian) that are found in the study area. Both 3a and 3b show the distribution of the formations throughout the area, schematically derived from the geological maps of Lier 1814 IV 1:50.000 (Gunby et al., 2003) and Hønefoss 1815 III 1:50.000 (Zwaan and Larsen, 2003). Also the locations of the five cross sections made through the area are presented in these two maps. Finally some of the most important fold axis are plotted that were measured or observed in the field; axis of big folds are solid arrows, axis of smaller or drag folds are dashed.

Ringerike Sst. (Sundvoll & Stubdal fm.)

Steinsfjorden Fm.

Braksøy Fm.

Bruflat Fm.

Vik Fm.

Rytteråker Fm.

Saelabonn Fm.

Langøyene Fm.

Bønsens/Sørbakken Fm.

3c

Laurentia and Avalonia more towards the south (*Fig. 4*). The orogeny is one of the events that formed the supercontinent Pangaea later in the Paleozoic era. The location of the Oslo region was on the southwest part of Baltica.

In general the Scandinavian Caledonides have been subdivided into in four tectonostratigraphic regions: the pre-Cambrian basement of Baltica, the lower to middle allochthons, the upper allochthon and the uppermost allochthon (*Fig. 5*).

The Baltic crystalline basement encloses structural and metamorphic relics from the old super continent Rodinia. The lower to middle allochthons represent the shelf and continental rise successions that are associated with the margin of Baltica. The upper allochthon embodies ophiolitic, magmatic arc and marginal basin associations all from the Iapetus Ocean (*Gale and Roberts, 1974; Stephens and Gee, 1985; Roberts, 2003*). On the very top, the uppermost allochthon has affinities with Laurentia (e.g. *Stephens and Gee, 1985*),

which has been confirmed in stable isotopic and radiometric dating (*Roberts et al. 2001; Melezhik et al., 2002, Yoshinobu et al., 2002*). In between there may be occurrences of micro continents that are rifted apart from either Baltica or Laurentia (*Gayer et al., 1987; Brueckner and van Roermund, 2004*). Within this classification the Oslo area is not incorporated, as it lies just southeast (maybe 100km) of the lower to middle allochthonous boundary. Still the area is included in the orogen as lithospheric processes like flexure and isostacy have a major impact on orogen proximal areas.

The Scandinavian Caledonides comprise four major compressive and transpressive tectonic events (*Roberts, 2003*); the Finnmarkian (*Sturt et al., 1978*), Trondheim (*Holtedahl, 1920*), Taconian (*Roberts, 1980*) and Scandian (*Gee, 1975*).

The Finnmarkian was determined as the earliest tectonothermal event; starting in the Late Cambrian, with a peak (eclogite) P-T condition around 505 Ma (*Mørk et al., 1988; Dallmeyer et al.,*
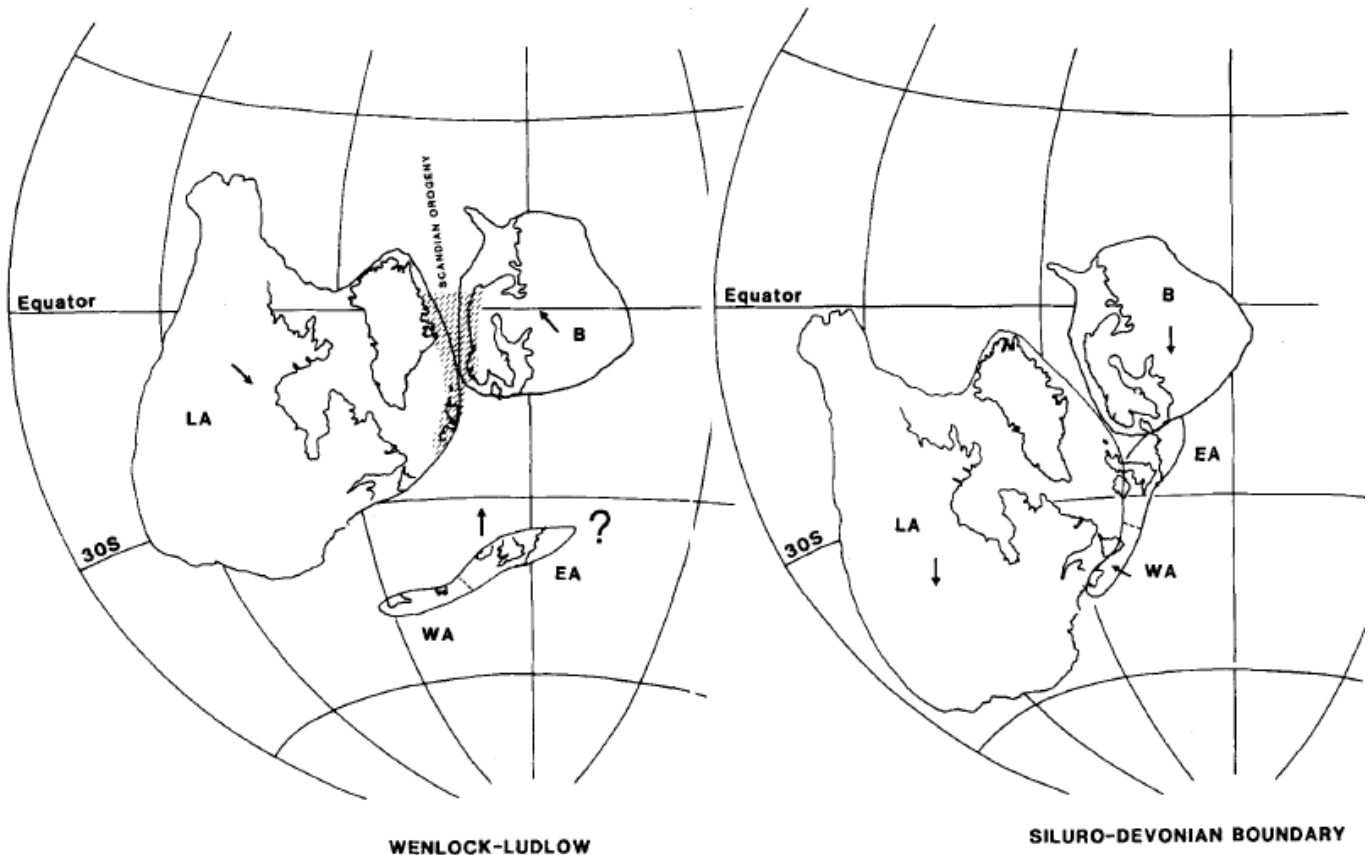


Fig. 4. Palaeomagnetic reconstruction of the Wenlock-Ludlow period and the Siluro-Devonian boundary, with emphasis on the positions of Laurentia, Siberia and Baltica. Based on data from Torsvik (1998), Torsvik et al. (1996), Cocks and Torsvik (2002) and small modifications by Roberts et al. (2003). (From: Roberts et al., 2003)
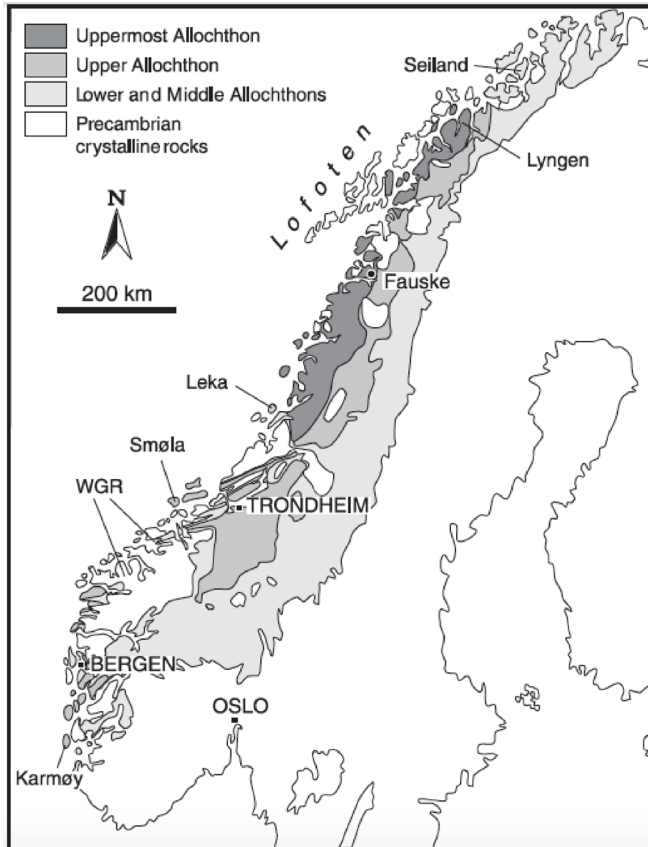
Fig. 5. Simplified tectonostratigraphic map of the Scandinavian Caledonides, with regions metioned in the text. (From: Roberts et al., 2003)

*1991; Essex et al., 1997).* This event is believed to be a result of accretion of a magmatic arc on the margin of Baltica by a seaward-facing subduction zone. This arc may be purely oceanic *(Torsvik and Rehnström, 2001; Hartz and Torsvik, 2002)* or it may originate from a micro continent *(Gayer et al., 1987).* In recent research contradictions have come to light that may reject the Finnmarkian event, it is suggested that the recognized thermal event may be involve an accretion event *(Kirkland et al., 2008).*

Although subsequently correlated to the Finnmarkian, the Trondheim event differs from the Finnmarkian in timing and palaeogeographic location *(Gee, 1986).* It characterizes a principal phase of deformation and metamorphism, in terms of ophiolite obduction and blueschists metamorphism *(Roberts, 2003).* Occurring around 25 million years after the Finnmarkian, in the early Arenig, anticlockwise rotation of Baltica had started gradually closing the Iapetus seaway *(Torsvik et al., 1996; Torsvik and Rehnström, 2001)* (**Fig. 4**).

During Mid to Late Ordovician a new, more significant tectonothermal event takes place: the Taconian event. This event is mostly recognized in the Uppermost Allochthon and covers metamorphism and magmatism and arc accretion complexes. Also a Late Ordovician to Early Silurian sedimentary sequence related to subduction polarity switch is associated to the Taconian orogeny *(Thon, 1985).* This event is the last stage before the evorogenic event.

In the oblique continental collision event between Baltica and Laurentia, the Scandian, the principal deformation and metamorphism takes place. Timing of the Scandian varies throughout the orogen, making a long-range correlation of orogenic events hard *(Roberts, 2003).* The actual event only lasted for around 10 million years. In the event all allochthons were involved, thus earlier formed structures and mineralogy were (partly) overprinted.

During later stages of continental collision, which persisted until Early Devonian, processes like gravitational collapse come into play, causing formation of major extensional structures found in the entire orogen. In sediment record the period from Early Devonian to Late Carboniferous is scarce as the land lies above sea level at that time, minimizing accommodation space for sedimentation. Sedimentary sequences that are from this period show clear signs of weathering and erosion, for example brecciation and deep red coloring. It is assumed that the area was again leveled into a peneplain in middle Permian *(Henningsmoen, 1978).*

The foreland sequence typically starts with a transgressive succession, which was southward in the Oslo region and occurred from Early to Middle Cambrian. It was followed by a epicontinental sea with low sedimentation rate from Late Cambrian to Middle Ordovician in which the lowest recognizable formation of the area is deposited: the Alum Shale *(Bergström & Gee, 1985; Nielsen & Skovsbo, 2007).* The Alum shale is found throughout Baltoscandia, indicating a major flat platform with high sea level. The Alum Shale is part of the Røyken group and is a succession of dark shales alternated with dark, organic rich limestone beds. The limestone fraction normally occurs in shell-like concretions

Fig. 6. Limestone concretion in the dark Alum shale (lithology on the left), which is strongly foliated and sheared at this locality. The lithology on the right is a basaltic or syenitic dyke.

(*Fig. 6*). Other distinct formations of the epicontinental stage are the Huk- and Bjørkåsholmen formations, which are recognizable throughout the area due to fossil content and appearance.

Eventually the orogen becomes more proximal, creating silt- and sandstones and shallow marine warm water carbonates from Late Ordovician to lower Silurian. Typical formations of this group are fine sandstones like the Sealabonn and Bruflat formations and nodular limestones like the Sørbakken and Steinsfjorden formations. Finally the environment becomes continental with the deposition of sediments from meandering rivers and coastal alluvial planes in Late Silurian. These sediments are the molasses sediments from the Caledonides and are called the Ringerike Group.

### 1.3.2. Upper Palaeozoic

Related to the Variscan Orogeny (Late Carboniferous/Early Permian), the Oslo rift originated north of the Tornquist (strike-slip) fault system. The asymmetry of the rift, with in the south part an east dipping half graben (Vestvold Graben) and in the north part a west dipping half graben (Akershus Graben) which, together with the volcanics takes a dominant position in the present landscape. The two grabens are separated by a strike-slip fault that runs just north of the Tyrifjorden area. All volcanic rocks found in the area are associated with this Permian rifting stage, for example syenitic sills that are found in the base of the lower Palaeozoic rocks and dykes throughout the whole Palaeozoic sequence *(Larsen et al., 2008)*.

### 1.4. Structural outline

Based on the older structural studies in the Oslo area (e.g. *Brøgger, 1882; Bjørlykke, 1902; Nystuen, 1981, 1983*) modern structural perspective is used to further understand the Palaeozoic deformation in the Oslo region. The leveled fold-and-thrust belt model suggested by Bruton et al., 2010 is a good base for this, and thus it is used as a guide and correlation model for this study. Again, the model is build up out of, from bottom to top: the basal thrust system, the middle thrust system, the upward ramping fault system which flattens under the Ringerike sandstone and the fault system that cuts through the Ringerike sandstone (*Fig. 7*).

The first level is characterized by a detachment zone, which is situated in the lower part of the succession, but most likely not at the basin-basement contact. This basal thrust runs through the weak Alum Shale; a black shale with limestone concretions, and is the most prominent tectonic discontinuity in the area. In the Oslo area the basal thrust is an equivalent of the Osen-Røa thrust, which is recognized more properly towards the northwest. Towards the south, near the Skien-Langesund area the basal thrust dies out, most likely in a blind thrust *(Oftedahl, 1943; Nystuen, 1983; Morley, 1986a)*. This level is recognizable by very high strain intensity, at some places all primary structures are obliterated over a distance of a few centimeters *(Bruton et al. 2010)*. Multiple generations of cleavages are distinct and asymmetric folding is the most common geometry. Also nice piggybacks can be recognized in some parts of the formation. The Alum shale is around 75m thick throughout the Oslo area but intense deformation is focused in only 10 to 50 meters of the formation *(Bruton et al. 2010)*.

The second structural level, known as the middle thrust system, still comprises major amounts of strain, though now more localized in fault zones in a ramp and flat system. This
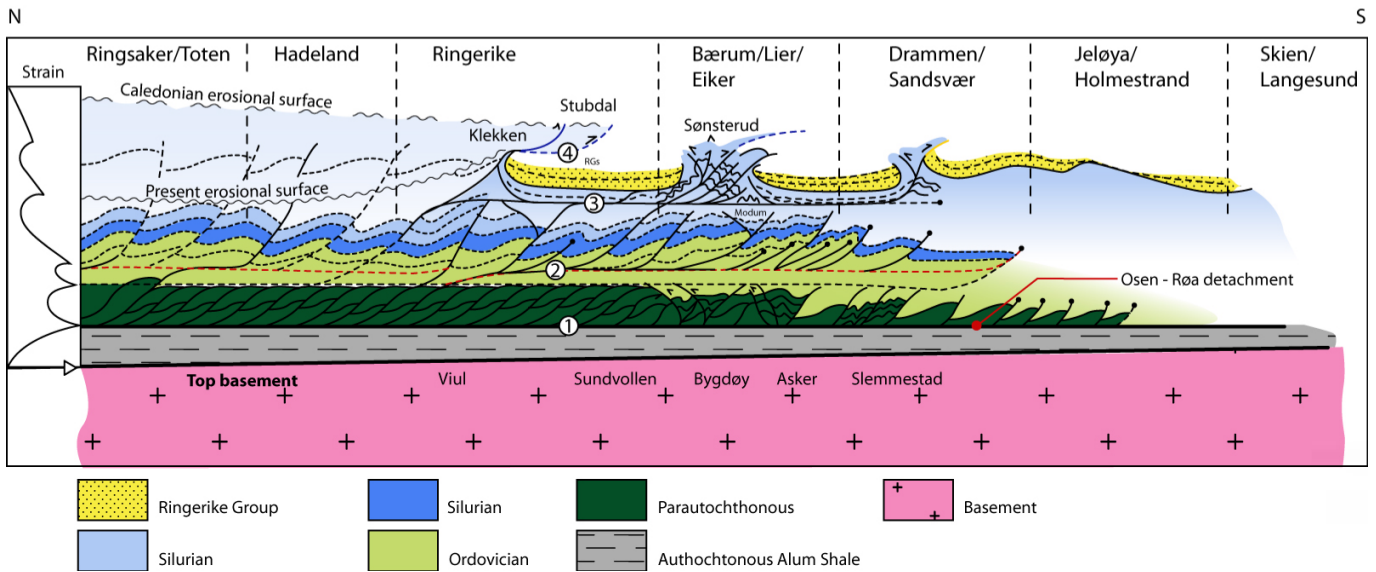
Fig. 7. NNW-SSE schematic section through the Oslo area showing the four structural levels that are presented in the text. Strain intensity is indicated schematically in the left part of the figure, showing the highest strain intensity in the sole thrust through the Alum shale. Key areas for this research lay around the major Sønsterud popup. (From: Bruton et al., 2010)

level runs through almost the entire sequence from lower Ordovician rocks to Silurian rocks. The lithologies mainly consist of shales alternating with carbonates and small sandstone. This structural level varies in thickness between 100 and 400 meters. Deformation is characterized by: reverse faults, imbricate thrust sheets and asymmetrical, overturned folds above listric-shaped contractional faults *(Bruton et al., 2010)*. No regional detachment zone is present, though layer parallel (back-) thrusting can be recognized in this structural level.

The third level is characterized by faults that are linked to the second level, but the key feature is that they become flatter below the Ringerike group. At localities where the thrust system is able to go through the Ringerike group the deformation is very localized and intense, sometimes having the characteristics of a tectonic mélange *(Halvorsen, 2003)*. This level shows major (back) thrusting and horses and very open folding in the parts where no thrusting is present.

The upper structural level is closely related to the thrusting in structural levels two and three.

It can be found at the localities where the thrusts have ramped through the Ringerike Group, for example at Sønsterud and Stubdal. Structures found in this level become flatter if they are through the Ringerike group. Also significant differences in deformation style can be recognized between level four and for example level three.

Throughout the area these tectonic levels can be recognized between for example level four and level three. Deformation styles can vary on the basis of fold geometry (amplitude, wavelength and classification), type of deformation (brittle or ductile), fault presence (for example fault zone with fault gouge or small faults creating duplexes and lenses) and fault direction (fore- and hinter-land directed). Structural style tends to vary both laterally and vertically (*Fig. 7*)

## 1.5.   Lithostratigraphy

The Oslo area has carefully been study in terms of lithostratigraphy. Several stratigraphic (e.g. *Worsley et al., 1983; Bockelie, 1978; Owen et al., 1990*) and paleontological (e.g. *Bruton et al., 2010*)

studies contribute to a highly detailed stratigraphic column. In area studied for this research (Ringerike area) only the Silurian sequence is found, thus formations of this sequence will be specified further. All formation can be found in the lithostratigraphic column (*Fig. 8*). The majority of the formations found in the study area (northeastern part of the Tyrifjorden) are deposited in a marine environment (shales and limstones). Towards the top of the sequence (Ringerike Group) continental deposits are introduced, creating a terrestrial deposition environment. This occurred during late Silurian.

### 1.5.1. Bønsnes Formation

The lithology of the Bønsnes Formation is limestone and calcareous shale. In the base the limestone is dark and the overlying limestone beds are lighter and contain corals. In the upper part of the formation nodular limestones are found. Fossil content ranges from algae to trilobites and brachiopods. According to the fauna content, a Rawtheyan age (before-last stage of the Ordovician) is suggested *(Owen et al., 1990)*. This formation represents a depositional environment of a shallow carbonatic sea. The thickness of this unit in the study area is around 200m and is found along the Modum section on the west side of the fjord (*Fig. 3b*).

### 1.5.2. Langøyene Formation

This formation mainly compiles sandstone with minor abundance of limestone and shale. Its thickness is around 50m in this study area and within the sandstone channels and storm surge beds can be recognized. Also evidence for seismic activity is found, suggesting basement fracturing during this period *(Brenchley & Newall, 1977)*. Fauna (mainly trilobites and brachiopods) in this formation suggest a Hirnantian age (final stage Ordovician) *(Owen et al., 1990)*. Concerning a depositional environment this formation would be a shallow sea with continental input.

### 1.5.3. Sælabonn Formation

The Sælabonn Formation is characterized by sandstone, siltstone and shale and is demonstrated the best in the small Sælabonn bay (*Fig. 3a*), in the north part of the Tyrifjorden in the Ringerike district, where it is approximately 110m thick. The base can be recognized at a sequence of silty shales and minor thin limestones lies on top of a karstic surface. This develops into thickly bedded and coarser
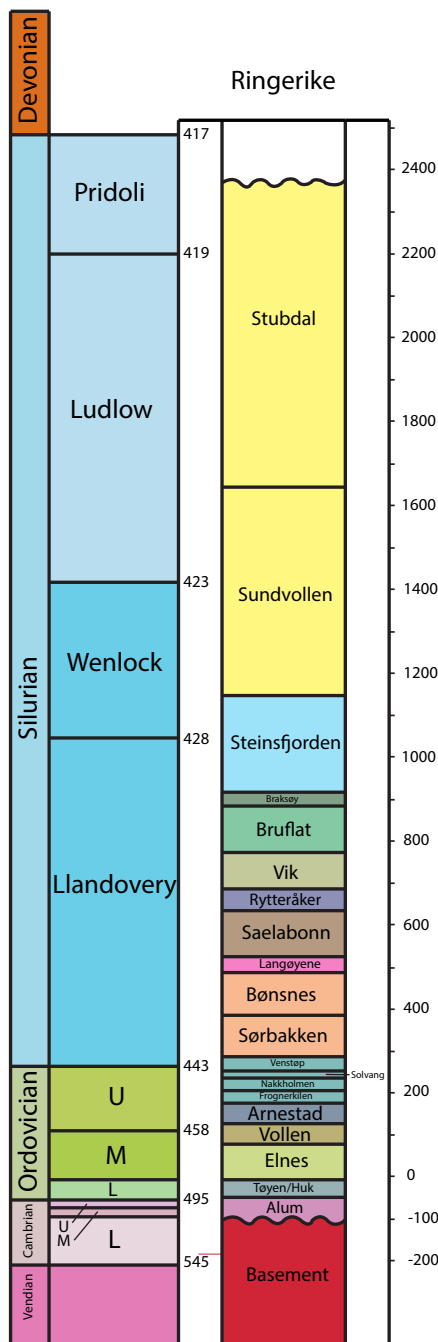


Fig. 8. Stratigraphic column of the Ringerike area. Formations from Bønsnes to the Ringerike Group (Stubdal fm. and Sundvollen fm.) are described in the text.

sandstones, which then fine up into siltstones and shale with increasing limestone content, going towards the boundary with the Rytteråker formation. In terms of depositional environment an early Silurian transgression can be recognized in the base of the Sælabonn formation, followed by a short progradational episode in a coastal environment and in the top of the formation the transgression is renewed. This formation is Rhuddanian (first stage of the Llandovery) of age *(Worsley et al., 1983).*

### 1.5.4. Rytteråker Formation

This formation is nicely exposed at the peninsula just south of the Rytteråker farm. In the type area the formation is around 50m thick and is dominated by limestones filled with pentamerids, corals and stromatoporoids. Towards the base a transition to siltstones and shales occurs, which agrees with the Sælabonn formation below. Bioherms are present above a thick limestone interbed. Towards the top of the formation shale and silt is introduced again, creating an alternation between limestone and shale/silt beds. The Rytteråker formation indicates the development of a shallow carbonate depositional environment when meanwhile early sources for clastic material were submerged. The presence of the above mentioned fossils indicate shallow water depth *(Worsley et al, 1983).*

### 1.5.5. Vik Formation

This formation is of Llandovery age and is found in the area of Skien and Ringerike, where its thickness is respectively 40 to 80m. It can be subdivided into three members: the Storøysundet, Garntangen and Abborvika members. In the base the Storøysundet Member (12-20m thick) is comprised of red shales (*Fig. 9*), minor bioclastic limestone concretions, some calcareous nodules and some interbeds of green/grey shale. The red shales can only be found in the Ringerike and Asker area. Fossil content may be crinoids, brachiopods, tabulate corals and stromatoporoids. The Storøysundet Member is followed by the Garntangen Member, which is 25m thick and is comprised of more thinly bedded limestone layers. Also calcareous



Fig. 9. Typical red shale bed in the Vik formation.

nodules and green/grey shale interbeds are present. Corals and stromatoporoids are abundant in this part of the Vik Formation. In the top part of the Vik formation the Abborvika Member lies with a thickness of 35m. It has higher shale content than the other two members but for the rest it is comparable. The boundary between the Vik formation and the above lying Bruflat formation is sharp. In terms of depositional environment the Vik formation represents a coastal/marginal environment with during deposition of the Garntangen Member a more secluded environment, shielded from clastic input due to the abundance of corals and stromatoporoids *(Worsley et al, 1983).*

### 1.5.6. Bruflat Formation

The Bruflat Formation is thought to be 400-450m *(Worsley et al., 1983)* and consists of fine sandstones (*Fig. 10*), siltstones and shale. The formation is deposited from Llandovery to Wenlock and can be recognized by the first introduction of sand into the system and throughout the formation an alternation occurs between sandstones siltstones. In the upper part the beds become thicker and shale interbeds are present. In the Ringerike area the Bruflat formation is only 115m thick, and the contact with the overlying unit is erosive. In this formation a coarsening upward trend can be recognized indicating progradation and depositional environment around the wave-base *(Worsley et al., 1983).*

Fig. 10. Well-bedded fine sandstone in the Bruflat formation, beds are approximately 10 cm thick.



Fig. 11. Black bituminous limestone with corals and small fractions of shale, typical for the Braksøya formation.

### 1.5.7. Braksøy Formation

This formations name is derived from the island of Braksøya in the Steinsfjorden (fjord that links in the northwest of the Tyrifjorden), on which the entire 27m thick succession of carbonates and minor amount of marls and shales can be found. It can be subdivided into two members; the lower and upper member. The lower member consists of biohermals surrounded by marl. The upper part of the lower member is compiled of black bituminous shale (*Fig. 11*) with a high amount of in situ corals and stromatoporoids. The upper member consists of well and thickly bedded limestones with occasionally marl and desiccation cracks. Below an interval of thinly bedded shales and limestones the boundary between the Braksøy Formation and the Steinsfjorden Formation is placed. Regarding depositional environment this formation embodies a marginal carbonate ocean with shallow water depth, as there are plenty of coral colonies present. The existence of desiccation cracks and marls suggest possible periods hyper saline conditions. The age of the Braksøy Formation is Wenlock *(Worsley et al., 1983)*

### 1.5.8. Steinsfjorden Formation

The Steinsfjorden Formation is also of Wenlock age and is subdivided into three members; the Sjørvoll, Brattstad and Ranberget members. The formation is approximately 260m thick and consists mainly of shales and limestones. The Sjørvoll member covers the lower 200m of the formation and is compiled of thin interbeds of grey shale and limestone. In this part of the Steinsfjorden Formation also mudflake conglomerates and desiccation cracks are abundant. The Brattstad member is around 30m thick and is composed of thick limestone beds with interbeds of marl and dolomitic limestone. The first occurrence of nodular limestones (*Fig. 12*) is the boundary with the overlying member, the Ranberget member. This member also contains, apart from lumpy nodular limestones, mudflake conglomerates, desiccation cracks and bentonites. This member is around 30m thick and the boundary with the overlying formation is defined by the transition from a typical greyish color to a red color of the red mud and sandstones of the Ringerike group. A typical environment that fits the Steinsfjorden



Fig. 12. Typical lumpy, nodular limestone from the Steinsfjorden formation.

formation would be a very shallow sea where tides have influence (recognizable in the desiccation cracks and mudflake conglomerates). The alternation between limestone and mud could represent a transgression and regression system, on a small scale, as the beds are thin. *(Worsley et al., 1983)*

### 1.5.9. *Ringerike Group*

The contact between the Steinsfjorden formation and the overlying Ringerike Group is conformable and gradational. The Ringerike group mainly is of Devonian age. Above this group either the Asker group is situated (which is of Carboniferous age *(Olaussen, 1981a)*) or the Permian lavas. The group consists of approximately 1250m of red sand- and siltstone beds and has been subdivided into two formations: the Sundvollen (lower 500m) and Stubdal (upper 750m) Formations. Overall a typical continental depositional environment is represented in the Ringerike Group, like estuaries, river systems and fluvial fining upward sequences *(Worsley et al., 1983)*. The transition from Sundvollen Formation to Stubdal Formation essentially shows a difference in paleo-current, most likely triggered by the activation of the Caledonian thrust front in the Skien area, creating a topographical high *(Davies et al., 2005)*.

To synthesize; the Oslo region has undergone a transition from a shallow carbonatic sea, with transgression – regression cycles causing a variation in sediment influx resulting in alternation of sand or carbonate dominated formations, to a continental based environment, caused by a major regression. This major regression occurred in the late Silurian and was caused by the finalization of the Caledonides *(Worsley et al., 1983)*.

## 2. Observations from the field

Description of the profiles constructed in the study area. The orientation of each profile is presented in the overview map *(Fig. 3)*, along with the structural measurements. Stereoplot data is presented in Appendix A and further on in this chapter.

### 2.1. Section A-A'

This section *(Fig. 13)* starts at the Rytteråker peninsula and runs along the islands to the south *(Fig. 3a)*. The north part shows very open folds on a large scale and when going south the folding geometry becomes tighter and thrusting becomes more dominant. The lithologies also change comparably, going from the Vik and Rytteråker formations at the peninsula, to Bruflat and Braksøya formations on the islands. Halfway the section, on the island of Utøya, hinterland-directed thrusts are recorded and folding only occurs in association with the thrusts. This locality comprises only the Steinsfjorden Formation. When approaching the mainland the section runs trough the Ringerike Group, which makes a big syncline until a major back thrust separates the Ringerike Group with the Steinsfjorden. Just south of to the back thrust strong folding is recorded, decreasing in frequency but increasing in size, when moving away from the fault.

The open large scale folding in the north is visible on the peninsula *(Fig. 13)*. An anticline is visible in the Vik (easily recognizable as red muds), Rytteråker and Sælabonn formations with a wavelength of almost a kilometer, a very low (1-3m) amplitude and a fold axis of 66/9. A similar style of folding, though lower amount of shortening, occurs more to the north at a section next to the gas station of Vik and in the bay north of the Rytteråker peninsula *(Hjelseth, 2010)*. A difference in shortening would require strain accommodation and intensity differences.

Going towards Storøya the south (SE dipping) limb of the open anticline lies underneath the fjord (also visible on Haraøya) and at on the north of Storøya a syncline can be recognized with similar geometry, in terms of amplitude and wavelength, as the anticline on the peninsula and a fold axis of 61/8. On the south of the island though a tighter fold appears with a more significant amplitude (10-15m), a lower wavelength (several 100 meters) *(Fig. 14a)* and a fold axis of 47/9. The north flank of this fold also shows some meter scale parasitic folding and smaller scale deformation structures, like meter scale back thrusts and smaller (cm-m) en echelon (back thrust) structures *(Fig. 14a)*. On Purkøya the continuation of this tight anticline is
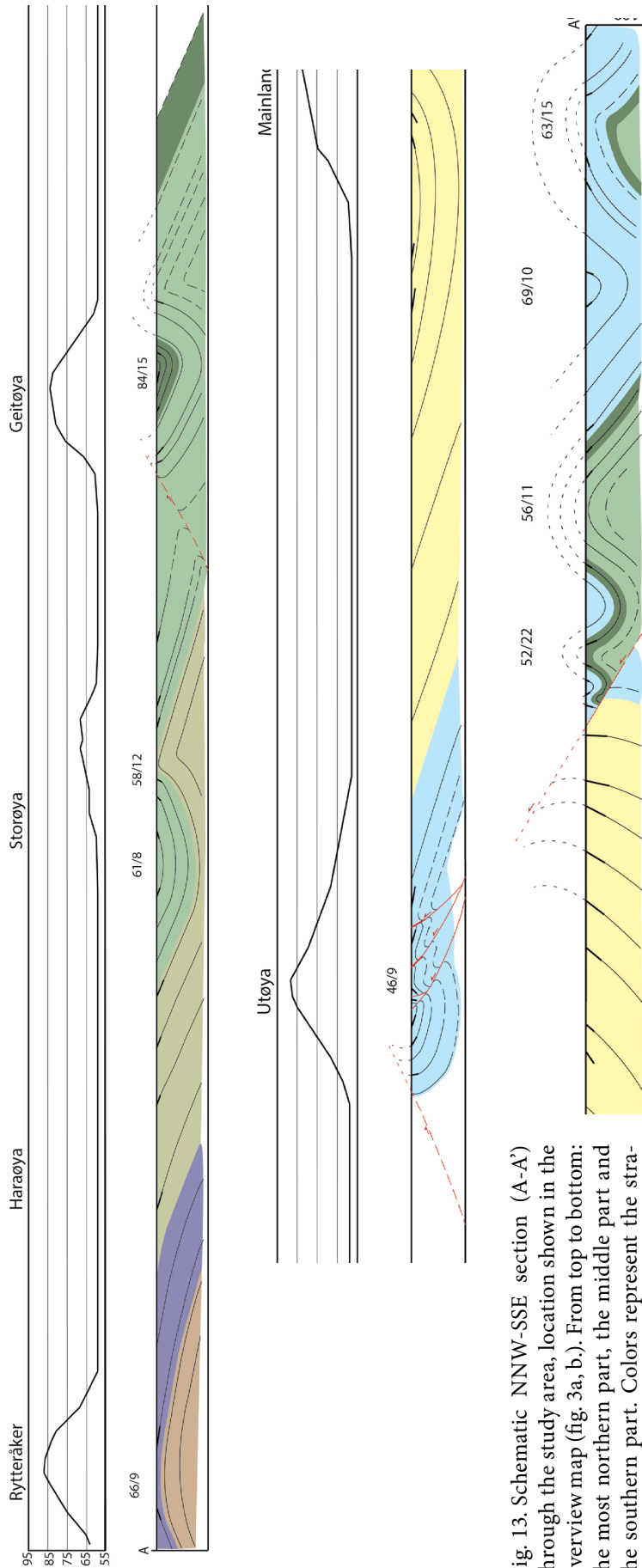
Fig. 13. Schematic NNW-SSE section (A-A')
through the study area, location shown in the
overview map (fig. 3a, b.). From top to bottom:
the most northern part, the middle part and
the southern part. Colors represent the stra-
tigraphy as in fig. 3c. Length of the profile is
8500m.

even more faulted (both in backward and forward direction), especially in the hinge and also comprises parasitic folds. The fold axis derived from the measurement of both limbs results in 58/12. Strata on Storøya and the Rytteråker peninsula dips either SE or NW with varying dip (*Appendix A*).

Going south along the profile, the south limb of the anticline on Storøya continues underneath the fjord and at the next island, Geitøya, this limb becomes very steep (dip of ±75° south). Along the north side of the island this dip is fairly constant and at the south side of the island the dip changes to the north, thus the hinge of a syncline runs across the island with a fold axis of 84/15. At west side of the island this change in dip is very significant (in the order of 50° change), here the strata turns to almost vertical. Though on the east side of the island it appears to be a normal syncline, possibly the flattening strata defines the transition to the anticline that is located just south of this location.

The stratigraphical units exposed at the island are the Bruflat and Braksøy formations, and at several localities along the coastline conjugate sets of N-S orientated, steeply dipping white veins of cm scale are present. The veins are most likely associated with Caledonian compression Along the southeastern coast of the island a nice section runs parallel to the strike of the limb, in which smaller structures within the limb can be recognized. For example several parasitic (asymmetric) folds on meter and decimeter scale can be recognized (*Fig. 15*). At some localities the parasitic folds in the north limb of the Geitøya syncline are very big, in the order of 10-30 meter. These structures are also located relatively close to the hinge of the syncline. Fold axes measurements of parasitic folds on the south coast of Geitøya range from 51/10 to 91/8 (*Appendix A*). Dips on the southwestern beach also show some major deviations from the general dip of the limb, this may also be due to the parasitic folding present in the limb, or due to the back thrusting that is present at the west part of the island (*Fig. 16*).

A



B



Fig. 14. (A) A cliff on the southwest side of the island of Storøya, with a much steeper north limb than similar scale folds on the north side of the island. Also interlimb deformation (parasitic folding Cand en echelon folding) has not been observed on other parts of the island. (B) A cliff on the northeast side of the island, showing a very different style of deformation compared to 14a, much lower amplitude and more open folding.

On Geitøya dominant dip direction is NW-SE.

The first visible outcrop south of Geitøya, along profile A-A' (*Fig. 13*), is situated on the west side of the island of Utøya. Outcrops on the west side of Utøya show both faults and folds with axial planes parallel to the fault planes. Thus folding always coincides with the major faults that are present. Fold axis of these drag folds range from 90/1 to 23/7, still cluster mainly around 50/10. In the 500m of cliff that represents the west side of Utøya three major back thrusts are visible all accompanied by a hanging wall anticline and footwall syncline (*Fig. 17*). At the north side of the cliff the strata dip close to vertical, which is not consistent with the rest of the cliff section, suggesting a different mechanism. Almost all of the strata dips towards the southeast or more dominantly east and almost no strata dips NW, only in the relatively small (compared to the major open folds in the north part of the section) drag folds. The entire cliff is build up out of a single formation, the Steinsfjorden Formation. This can be recognized in the massive coral reef boundstone, which is the top deposition of the Steinsfjorden Formation, located in the footwall of the most northern back thrust.

At a smaller scale (cm-m) both harmonic and parasitic foldz can be recognized and at some localities fault propagation folds are present (*Fig. 18*). The fault propagation folds exist on regular basis, normally in a hinge of a larger drag fold,
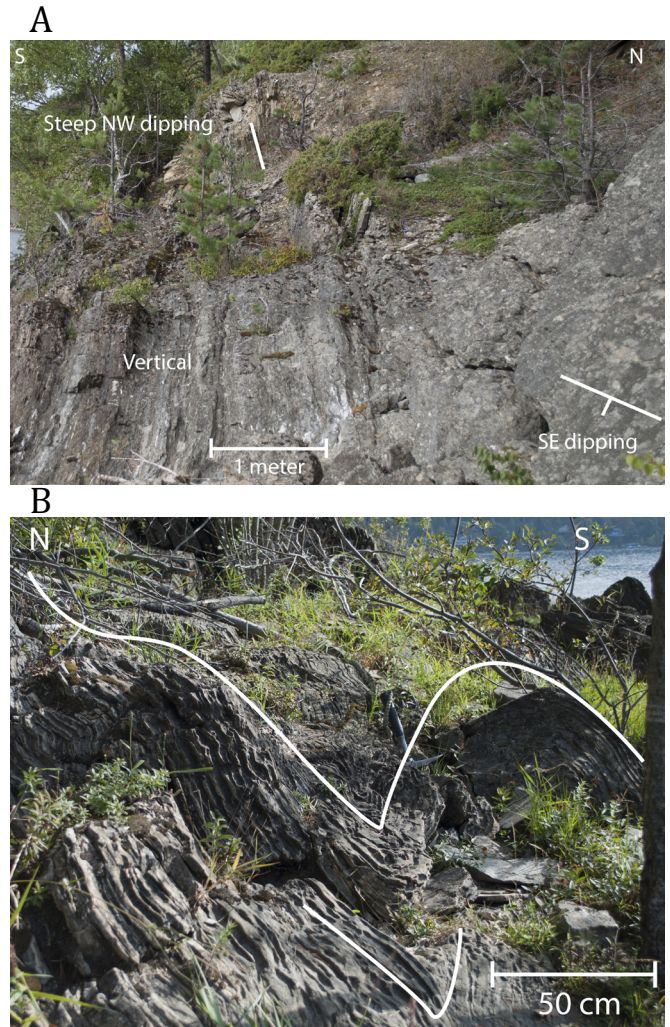
Fig. 15. Two localities on Geitøya with parasitic folding in the south limb of the Geitøya syncline on tens of meters scale (15a) and centimeter to meter scale (15b)
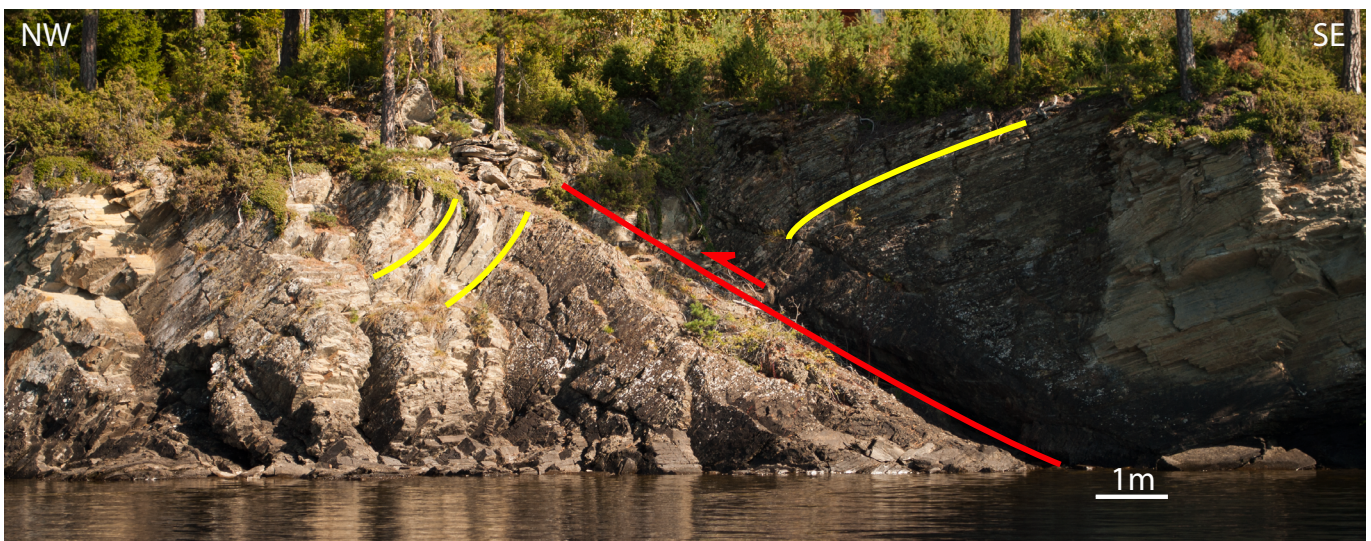
Fig. 16. Back thrust on the southwest tip of Geitøya, in the south limb of the Geitøya syncline (profile A-A', figure 8).

Fig. 17. North side of the cliff on the west part of Utøya, the back thrust is the first of three. A nice hanging wall anticline can be recognized. The structure on the northern most tip is interpreted as a footwall syncline of a fore thrust. The massive coral reef boundstone can be observed in the centre part.

suggesting consistent accommodation problems in the major drag folds. Drag also occurs on much smaller scale near the fault plane (cm scale). On these fault planes slick and slides can be recognized and measured giving an idea on the direction of movement. Also stylolites can be identified in the north part of this section (*Fig. 19*), which can provide an indication of the stress direction, as they form normal to the highest stress. The stylolites have an orientation of 86/85 and 83/84 prior to formation of the small fold it was measured in (larger scale folding may have rotated it also).

Towards the south the profile runs to the mainland gradually into the Ringerike Group (boundary is under the fjord). On Utøya the strata dips SE, but on the mainland the strata dips NW, so a major anticline lies under the water between Utøya and the mainland. Going south the strata becomes steeper to almost vertical near

the transition to the Steinsfjorden Formation, which must be bounded by a fault as a large part of the Steinsfjorden is missed. At the boundary between the two formations a small valley runs towards the northeast, suggesting a similar orientation of fault (dip between 20 and 50 towards SSW), thus a back thrust. The gradual steepening of the strata north of the fault provides prove for a back thrust and also the strong deformation in the hanging wall suggests a backward movement. Considering the size of the drag faults (50-100m)





Fig. 18. Fault propagation and refolded folds on the west side of Utøya. Picture is taken in a N-S orienation, width of the image is approximately 2m.

Fig. 19. Stylolites in a fault propagation fold on the west side of Utøya, also layer parellel slip can be recognized in the more shaly layers. Image was taken roughly N-S and the width of the image is around 15cm.

Fig. 20. The last anticline on profile A-A' with the north and south flank visible. The style of the fold seems assymetric with its axial plane dipping towards the north.

implies that a significant movement has taken place along this fault plane. In the hanging wall a series of folds are present with relatively small amplitudes and wavelengths (tens of meters) signifying the localization of deformation in this part of the section. Further away from the major back thrust between the Ringerike Group and the Steinsfjorden Formation the folding becomes larger scale, visible in anticlines and synclines succeeding one another within 300-500 meters. Folding remains symmetrical and relatively open, only the last anticline on the section may be broken in the hinge, making it asymmetrical with the hinge pointing towards the south (*Fig. 20*).

## 2.2.  Profile B-B'

This NNW-SSE profile (*Fig. 21*) is a correlation profile for the first part of A-A'. It starts on the east side of Storøya and runs through the fjord to the mainland (*Fig. 3a*). At the east side of Storøya the Bruflat, Braksøya and Steinsfjorden Formations

are outcropped (*Fig. 13a*). Deformation in this part is recognizable in very gentle folding. Going SSE the Ringerike Group is encountered in the mainland, which almost shows no deformation at this locality. The east coast of Storøya displays similar structures like the west coast; an open syncline on the north side and an anticline in the south (*Fig. 14b*), a contrast though is that the anticline in the east has a much more open character, larger wavelength than on the west side of the island (in order of a kilometer in stead of hundreds of meters). Also the orientation of the fold axes of both the syncline and anticline on the east side varies slightly from those on the west side of the island, relatively 74/5 and 71/1 (*Fig. 13a, Appendix A*). Apart from this also the lithological formations differ from east to the west. Due to a moderate dip of the entire sequence towards the east an upward motion in stratigraphy is established when going east, thus it is higher in stratigraphy. In the east the Steinsfjorden and Braksøy Formations are present, while in the west the outcrop is comprised
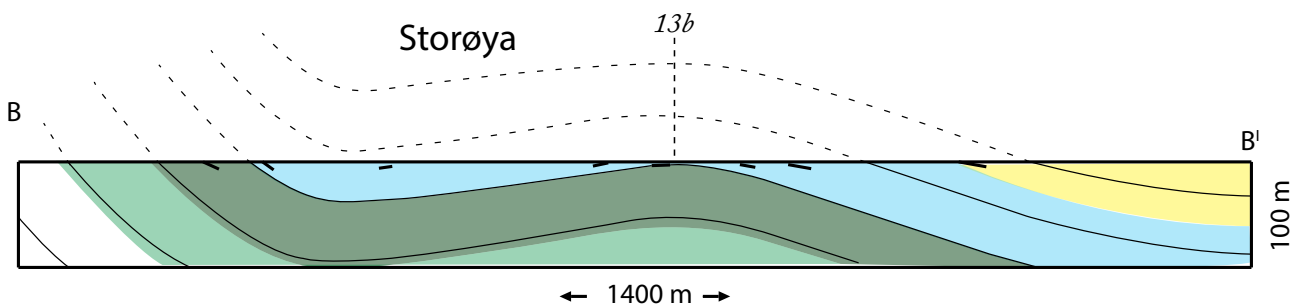


Fig. 21. NNW-SSE profile (B-B') from the east of Storøya to the mainland, colors represent the stratigraphy and are presented in figure 3c.

of the Vik and Bruflat formations (*Fig. 3a*).

## 2.3. Profile C-C'

As a partial correlation the section along the Utstranda road (C-C') can be used for the last 2200m of the A-A' section (*Fig. 22*). Lateral distance between both sections is a few hundred meters (*Fig. 3b*), thus similar structures are observed along this transect: a major syncline in the Ringerike Group, followed by the major back thrust and subsequent large scale folding in the Steinsfjorden Formation. In the south of the section structures are identified that indicate (back) thrusting.

The gradual increase in dip in the north part of this section is not constant. If going from north to south one would encounter a rapid increasing dip, then a sudden drop to almost horizontal and then a rapid increase again. This occurs around four subsequent times (possible more as exposure is not optimal) and these dip changes are thought to be duplexes or tectonic lenses. Faults between these duplexes are not clearly observed though likely to be present. The fifth time the strata becomes steeper it ends at the boundary between the Ringerike Group and the Steinsfjorden Formation. Here a major back thrust thus lies, which has also been observed at the coast section. The footwall of the major back thrust has undergone brittle deformation in the form of duplexes/tectonic lenses. Near the major back thrust, measurements at the road section show almost vertical layering and an outcrop more landward in a quarry, which is located between the E16 and Utstranda, shows steep southeast dipping Ringerike Group layers, suggesting and overturned sequence at that locality. Combining these localities results in a major footwall syncline that is at least 200m wide and with a fold axis of 53/11.

The first outcrop (Steinsfjorden Formation)

on the south side of the back thrust comprises a small fault of which the movement sense is unknown. The orientation of the fault though is close to layer parallel (thus around 60/55 NW) and some small drag folds show fold axis of around 40/10 (*Appendix A*). These observations may indicate a small antithetic fold, originating at the major back thrust. Along the next curves in the road a regular (steep) dip is documented until the ramp of the Lihøgdaveien (*Fig. 3b*), where a big change in deformation style occurs. Going further inland the same regular steep dip is recognized and thus this can be correlated laterally with the Utstranda section. The ramp of the Lihøgdaveien consists of characteristic very tight and even isoclinal folds, combined with a brittle signature (*Fig. 23*) and some minor parasitic- and fault propagation folding. All these intense deformed structures are present in only a few tens of meters of outcrop, making it a very local deformation style. The lithology at this locality is also different, namely the Braksøy Formation, which is only around 50 meters thick and orientated close to vertically here. In the next major outcrop the style of deformation already is very different again. Distinctive here is the local faulting (back thrusts) without major deformation in footwall and hanging wall (at this locality also a dyke is intruded into an older fault), some tectonic lenses with layer parallel faults and a 100 meter wide anticline (*Fig. 24*) with slight accommodation problems in the hinge and a fold axis of 57/17.

Going south along the profile into the Braksøya Formation in the south flank of the big anticline in the hanging wall of the back thrust. When going through the bend of the road the Steinsfjorden Formation outcrops and a relatively small (several tens of meters) parasitic fold with a fold axis of 41/3 is identified. The outcrop here runs nearly parallel to the fold axis thus the structures
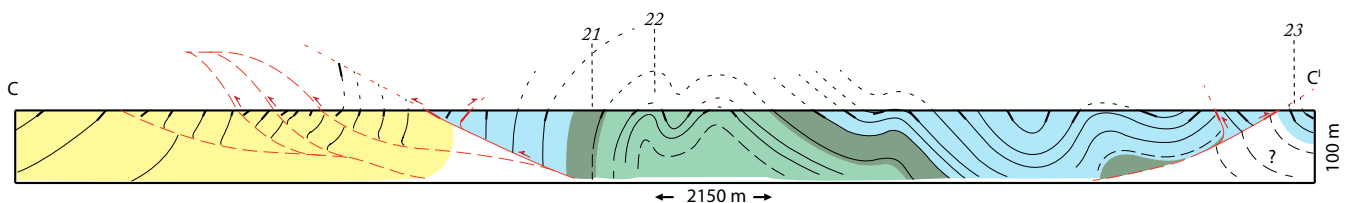


Fig. 22. NNW-SSE profile (C-C') along the Utstranda road on the main land. Colors indicate stratigraphical formations and can be found in the legend of figure 3c.

23

Fig. 23. Outcrop at the Lihøgdaveien ramp, mostly compiled of shaly Braksøy formation. Few stronger layers show a brittle signature, like this popup. Image is taken roughly NE-SW.



Fig. 24. Outcrop just south of the Lihøgdaveien ramp, in Bruflat formation, showing a rather open fold and some tectonic lenses in the north part of the image.

are rather unclear. Also the deformation style in the Braksøya Formation is again very different and intense. Refolded folds, fold propagation faults and layer parallel slip can be recognized around this parasitic fold. Following the bend, and walking perpendicular to the strike again, some 50° SE dipping layers are recognized, still in the limb of a fold. Several hundred meters south the limb dips steady NW, creating a syncline with a fold axis of 53/7. In the south limb of this syncline another small parasitic fold is present, though it is very poorly outcropped at this locality. Deformation in this part of the section is very much concentrated in small faults that all dip to the SE. This results in a large amount of tectonic lenses and splay faults at this locality. Finally a syncline is recognized with an axis of 55/13 at the place where profile D-D' starts in the south (the same north limb of this syncline can be recognized on profile D-D'. All folds in the part south of the back thrust have an open to sometime tight geometr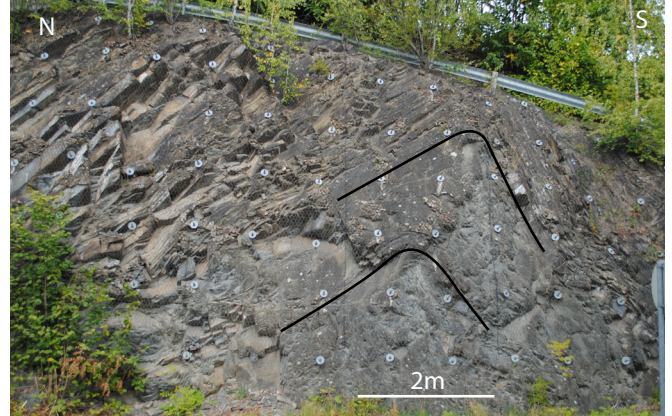y and are between 50 to 150 m in size. Just south of there a major fore thrust is recognized with an antithetic component cutting of the south flank of the 55/13 syncline. The hanging wall of this fore thrust is full of splay faults and lenses and zones of weak material, and poor exposure, are present at the place where the faults run. The footwall of this fore thrust contains a drag fold of around 10-20m wide.

## 2.4.   Profile D-D'

This profile runs along a road that connects the E16 and the coastal road Utstranda (*Fig. 3b*). This causes the orientation of the profile (*Fig. 25*) to deviate slightly from perpendicular to the strike, though the structures are still relatively well recognizable. In the south it starts with the north flank of the syncline that is discussed above in profile C-C'. Subsequently it forms a similar anticline (in terms of wavelength and amplitude) with a slightly tighter geometry than the anticline on C-C' and a fold axis of 67/15. The overall structure for around 200m to the north looks like a big syncline, though the syncline is faulted in the hinge by back thrusts. These back thrusts can be recognized by zones of weak material (fault gouge) (*Fig. 26*) and cause all kinds of strong deformation features, like drag folds (*Fig. 27*), fold propagation folds (*Fig. 28*), layer parallel slip (*Fig. 26 and Fig. 28*), tectonic lenses, splay faults and ductile deformation, all on varying scales. The smaller scale folding can be tight to very tight. This all occurs in a single lithology, that of the Steinsfjorden Formation. All the fold axis of the smaller folding ranges between

Fig. 26. Deformation in the footwall of the northern most back thrust on profile D-D'. The back thrust is present in a zone with high amount of fault gouge.
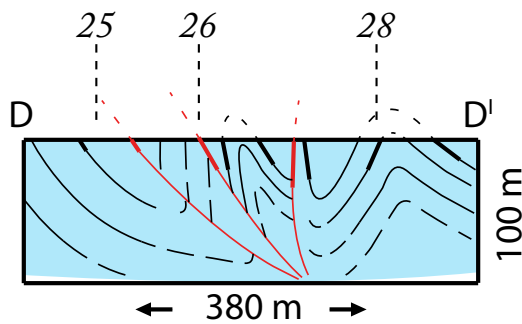


Fig. 25. Profile D-D', orientated N-S along the crossroad from Utstranda to the E16. This section entirely consists of Steinsfjorden formation (legend figure 3c).

73/19 and 40/10 (*Appendix A*). An interesting feature also is a dyke that runs through an older fault when the dyke meets the fault (*Fig. 29*). This locality contains also a lot of information on the very small scale. Apart from fossils and bentonites that are typical for the Steinsfjorden Formation also small scale (cm-m) en echelon folding and back thrusting (*Fig. 30*), tension gashes and all kinds of sedimentary structures are present.

## 2.5.   Profile E-E'

This profile (*Fig. 31*) lies at the other side of the fjord, along the Modumveien (Modum in *Fig. 3b*). It is situated a slight bit south of the rest of the
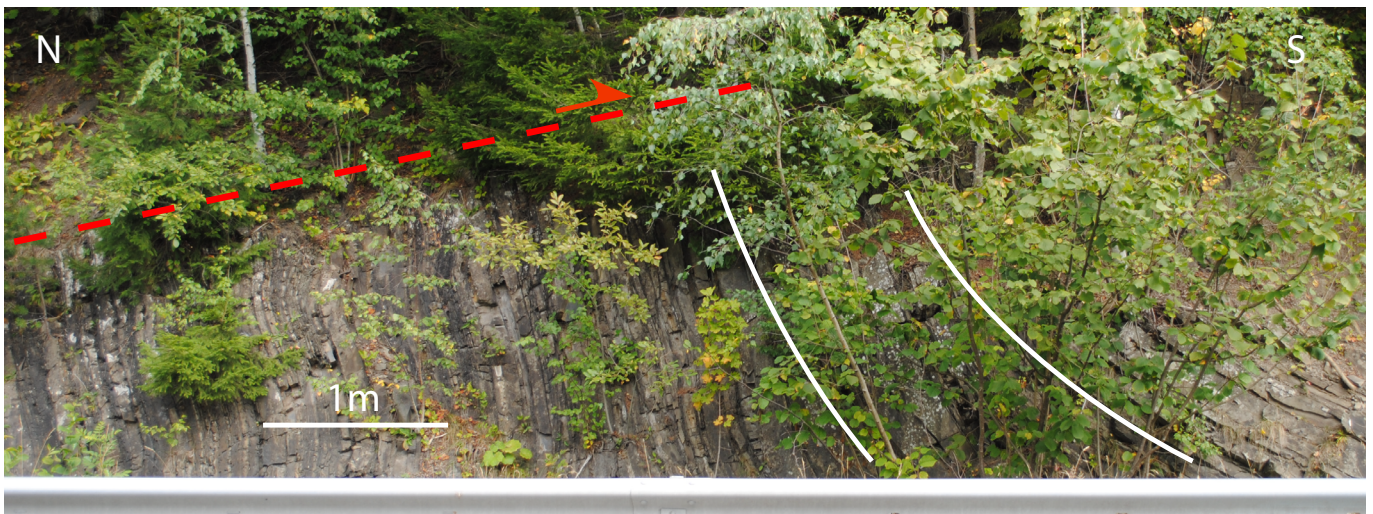


Fig. 27. Syncline with an abrupt change to poor exposure interpreted as a fore thrust with a footwall syncline. Outcrop is just south of the cross road from Utstranda to the E16, south on the C-C' profile (figure 20).
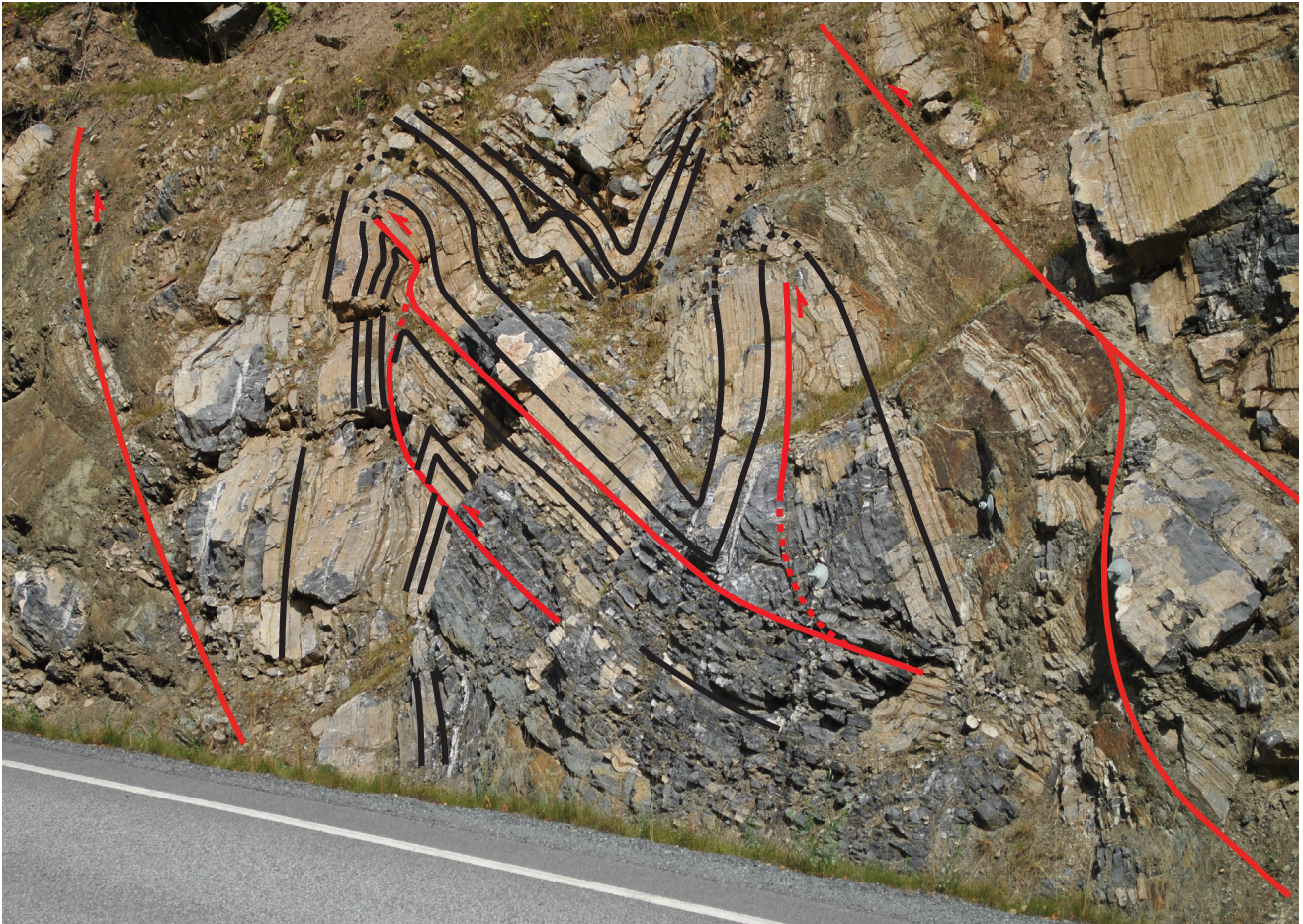
Fig. 28. Fault propagation fold zone in between two major fault zones with fault gouge. Orientation of the image is roughly N-S on on profile D-D'.



Fig. 29. South part of the D-D' profile, with a Permian dyke intruding layer parallel and into a pre-existing back thrust. Back thrusting occurs regularly in this outcrop, though displacement is not very significant as no drag has been recorded in the foot or hanging wall.

Fig. 30. Small scale en echelon back thrusts in the Steins-fjorden formation in profile D-D'. Orientation is roughly N-S.

# 3. Interpretation of structures

The significant hinterland-directed thrusting in the area is interspersed by foreland-directed thrusting at some locations. Two similar localities in profile A-A', both north sides of Utøya and Geitøya show possible evidence of this statement. At both localities a very steep dip in the layering is observed (*Fig. 13*). This is a feature that is not consistent with the rest of the outcrops on both islands. A solution to this problem may be a major fore thrusts that lay on top of these steep dipping outcrops, resulting in a footwall syncline of similar scale as the large scale folding in the area. Fore thrusting is more default in other parts of the Oslo region (e.g. *van den Broek, 2015; Weekenstroo, 2015; Verdonk, 2015*).

Analyzing fold axes measured on the islands, it turns out the directions of the axes vary laterally (*Fig. 3a and b*). For example on Purkøya in the west the direction is 60°; while on the east side of Storøya it is around 75° (*Appendix A*). The plunge usually stays the same; between 15 and 0. This small deviation may be caused by local variables, or younger deformation. Rifting in the Oslo graben may have had influence on this area, the very slight dip of the whole area towards the east, causing younger lithologies to crop out in the east and older in the west may be associated with tilting by rifting. The big strike-slip fault, which forms the boundary between two major tilted grabens, runs NW-SE just north of the study area. This strike slip zone may leave a subtle mark on structures

profiles, so it does not have any overlap, though still it gives an idea of the deformation style in this stratigraphic level. The stratigraphy at this locality ranges from Rytteråker to Bønsens/Sørbakken formations. The locality comprises one major anticline of profile scale (±500 meters wide), with a rather tight to isoclinal geometry and a fold axis of 68/11 (*Appendix A*). Starting in the north the layer measurements along the Modumveien increase to vertical rapidly and stay near to vertical for a few hundred meters. In the south part a smaller fold appears, with a width of around 20-50m and a fold axis of 68/4. At this part of the profile this is the biggest structure but, unlike in the north part of E-E', this locality consists of many smaller folds (repetition every 10 or 20m) that follow up on each other, like a fold train. The geometry of these individual folds is open to tight and fold axes range from 82/8 to 56/14, and there is also a population with a SW dipping fold axis (e.g. 242/8) (*Appendix A*).
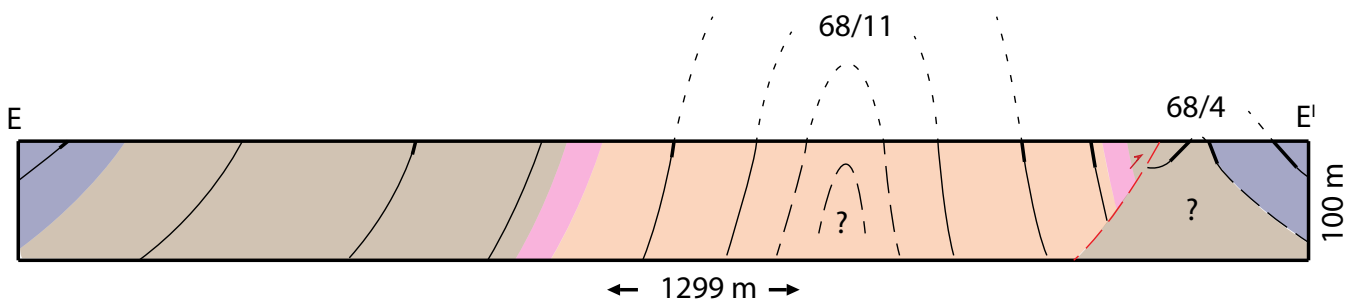


Fig. 31. Profile along the east coast of the Tyrifjorden, constructed at an outcrop along the Modumveien. Orientation is NNW-SSE, colors represent the different formations and can be found in the legend of figure 3c.

in this area. The variance that is documented on Storøya, is something that is seen throughout the area, on Storøya it is a gradual transition from west to east, though on other locations the variation is less sorted. This poor sortation implies a general deviation and defining a structural subarea thus is not possible, especially when considering the range of variability (not more than 10-15°). This range is minor for a normal fold-and-thrust belt, and taking into account measurement error margins a subarea is not eventual.

A different locality with structures of ambiguous origin is the Ringerike Group outcrops along the Utstranda road (C-C') in the footwall of the major back thrust. Along this section (going from N to S) a gradual increase in dip is recorded, which suddenly drops and starts again. The layers that have a gradual increase in dip are most likely part of one block (lens/duplex) and the sudden drop in dip can be explained with a fault. Faults are not observed at this locality, though the exposure is poor. Orientation of these faults may be either back- or fore thrusts (assumed that these faults have similar orientations as the rest of the faults in the region and thus the section runs perpendicular to the strike of these faults). It is proposed that these faults can be associated with the major back thrust and that they are back thrust, cutting through the footwall syncline of the back thrust. In this scenario this would be footwall collapse and this locality would comprise of tectonic lenses. This would also explain the local character of these lenses/duplexes, as at the coast section (A-A') these lenses are not observed.

On the other side of the fjord, at profile E-E', another interesting sequence of structures is observed. In the north part of this profile a tight hanging wall anticline seems to be present, requiring a fore thrust south of the steep dipping strata. South of this interpreted thrust a zone of stronger deformation is present, interpreted as a fold train. In this case the local high strain intensity in the fold train outcrop can be explained by localized deformation in the footwall of a thrust. Also the similarity in fold axis of both the tight hanging wall anticline and the folds in the fold train and the agreement with fold axis of the other profiles support this

scenario. This locality lies lower in stratigraphy than the Utstranda coastline with the islands.

The majority of the folds in the east Tyrifjorden area can be classified as parallel folds or class 1b *(Ramsay, 1987)*. Folds that are not influenced by drag generally show an upright, open to tight character. Large scale folding in the north part of the study area, for example at the Rytteråker peninsula, is gentle to open and upright, though sometimes asymmetric (figure profile A-A). At a smaller scale layers may be folded tight to isoclinal and sometimes disharmonic and refolded (figure Utoya). This ductile character of the layers may be due to high fluid content during deformation. At multiple locations this disharmonic folding occurs, suggesting differential fluid distribution. Age constrains of the structures are not evident, though the large scale upright open folding seems to precede the faulting as most faults end in an anticline or initiate in a hinge. Most likely this is a progressive sequence of events, with at first small scale folding and faulting of originally flat layers, then larger scale upright folding with fore thrusts following the (and initiating in) hinges and finally back thrusting.

Comparing the lateral overlapping parts of the sections some striking differences can be observed. As mentioned before, the geometry dissimilarity in the east and west anticlines on Storøya is one of those differences, but also the lack of smaller scale (10-50m) deformation features in the Ringerike group lithologies. In sections A-A' on the islands small-scale deformation structures are present in terms of folding and faulting, but in the Ringerike group (which lies on top of the lithologies present on the islands) no deformation on this scale is observed. Only in association with the major back thrust in profile C-C' similar scale deformation features are recognized, but not further away from the back thrust.

Based on the structural data several deformation styles can be recognized. In the north part of the fjord (*Fig. 3a and b*) large scale, low amplitude folding can be recognized as a style and is defined as a subarea (subarea 1). More to the south, closer to the popup deformation becomes intensified and more brittle (dominantly hinterland-directed) thrusts are present. This can

be determined as a second structural style, thus a second subarea (subarea 2). The boundary between both subareas is positioned between Geitøya and Utøya (*Fig. 3a and b and Fig. 13*) as on Utøya a dominance in back thrusting is recorded and on Geitøya only one small back thrust is present in the limb of a major fold. In terms of structural style the Ringerike Group also stands out as deformation is minimal in this formation, compared to the lithologies below. Defining this as a subarea (subarea 3) also urges the need to define the boundary of it. The rheology of the Ringerike Group seems to influence its surroundings *(Morley, 1987; Bruton et al, 2010)*, thus lithologies located close to the Ringerike Group show similar structural style. Though the other way around also applies; the faulting structural style also influences the Ringerike Group, for example in the major footwall syncline in profile C-C' (*Fig. 22*). In this way subarea one (folding) consists of the islands north of Geitøya plus the Rytteråker peninsula, subarea two (faulting) compiles Utøya and everything south of it along the coast, with exception of the Ringerike Group that forms subarea three.

A final subarea then is defined on the other side of the fjord, at the Modum locality. Here the fold geometry and fault size varies significantly from the eastside of the fjord and it is therefore treated as a subarea (subarea 4).

# 4.  Analysis

Data from the field is plotted in a stereogram using OSXStereonet *(Allmendinger and Cardozo, 2011)* creating diagrams with the poles of the measured planes and the determined fold axes of each subarea (*Fig. 32*). The data is give in different colors, representing the exact outcrop or location the measurement was taken, following the legend (*Fig. 34e*).

Planar and fold axis data from subarea one (*Fig. 32*), compiled of the islands of Geitøya, Storøya and the Rytteråker peninsula, shows an average fold axis of around 67/15 and a spread of planar measurements. The poles of the planes do show populations, for example at Storøya more low angle planes have been measured than on Geitøya, where the spread is larger. In general

the data is cohesive and representative. The low amount of data from the Rytteråker peninsula fits nicely in the data from the islands and the geographical spread of the data is significant (the area is ±6km2). Plotting the axial planes of the folds measured in this subarea gives a possible clustering in a NNW-SSE orientation (on 162/70) (*Fig. 33*).

Subarea two (*Fig. 32*) also shows a coherent data spread. The poles to planes tend to avoid the middle part of the data cloud suggesting more steep dipping layers than flat dipping layers. There are no outcrop/localities that stand out in terms of plane pole distribution. The fold axes show an average of 60/17 with the folds on Utøya deviating the most from this average. From all localities more than 50 measurements are incorporated, except from Sønsterud, though this area fits in this subarea in terms of structures and measurements *(Kleven, 2010)*. The area the measurements were taken in is around 4km2, so the geographical spread is decent. Plotting the axial planes of the folds measured in this subarea (*Fig. 33*) shows a strong population in the NNW and a possible spread along the great circle that runs NNW-SSE (162/70). There are also some smaller populations deviating from this great circle, some aligning like for example a population around the NW. This population coincides with a population which groups more around the SE on a NW-SE line (325/88).

Subarea three (*Fig. 32*) shows no folding and also a low amount of deformation. This results in the population seen around the center of the plot; all close to horizontal planes. The population in the lower part of the plot is taken in the part where the back thrusts go through the Ringerike Group (*Fig. 22*), creating duplexes and thus higher angle planes. This data is taken along the coast from the bridge to Storøya to the major hinterland-directed thrust, so along a line of around 5km. Subarea three does not have any folding, thus no axial plane plot can be made.
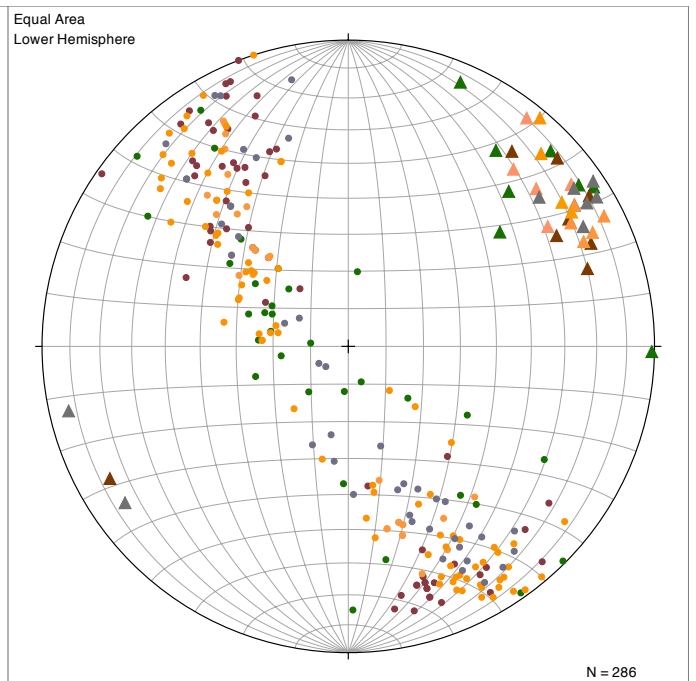
Subarea four, along the Modumveien (*Fig. 32*) is strongly folded with an average fold axis of 60/10. Striking in this subarea is the high amount of fold axis dipping SW instead of NE. The planar data shows a spread and dominant dip is steep as most of the poles are situated
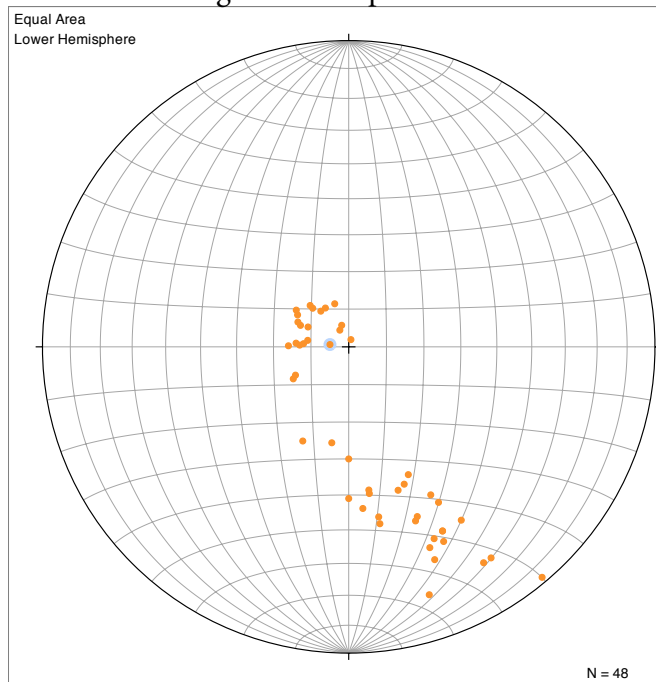
## Subarea 1: Folding
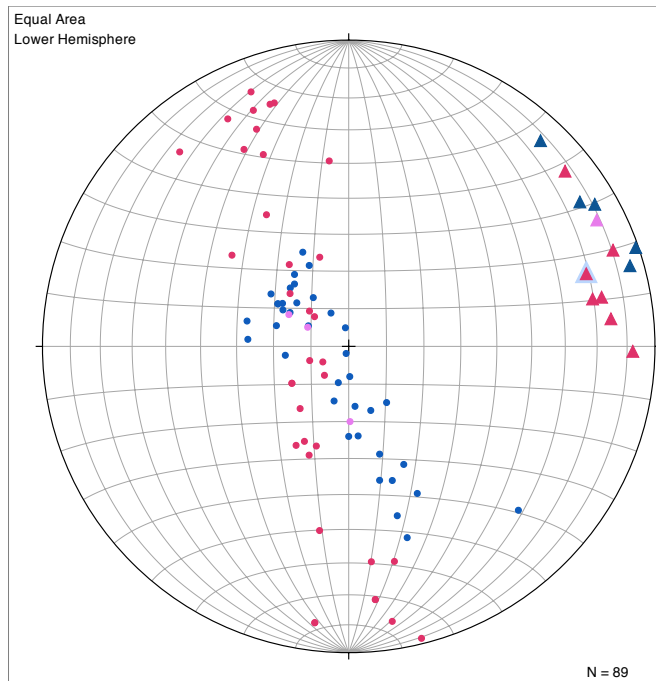


## Subarea 2: Faulting



## Subarea 3: Ringerike Group
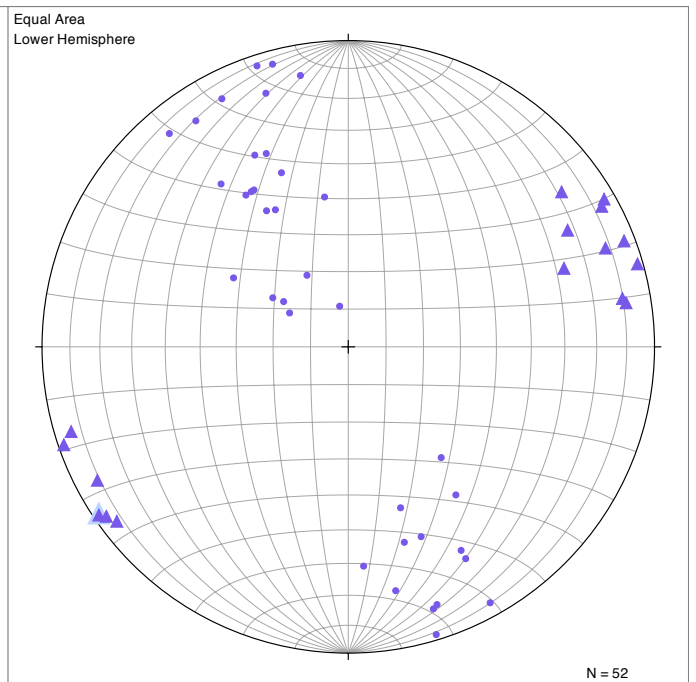


## Subarea 4: Modum



Fig. 32. Measured data from the field; dots are poles to planes and triagles are fold axes either measured in the field or derived from limb measrurements. The different colors of the data represent different outcrop localities, following the legend in figure 34e, Grouping of these measurements (the four subareas) is based on structural style recognized in the field and is discussed in more detail in the text.

## Subarea 1 axial planes
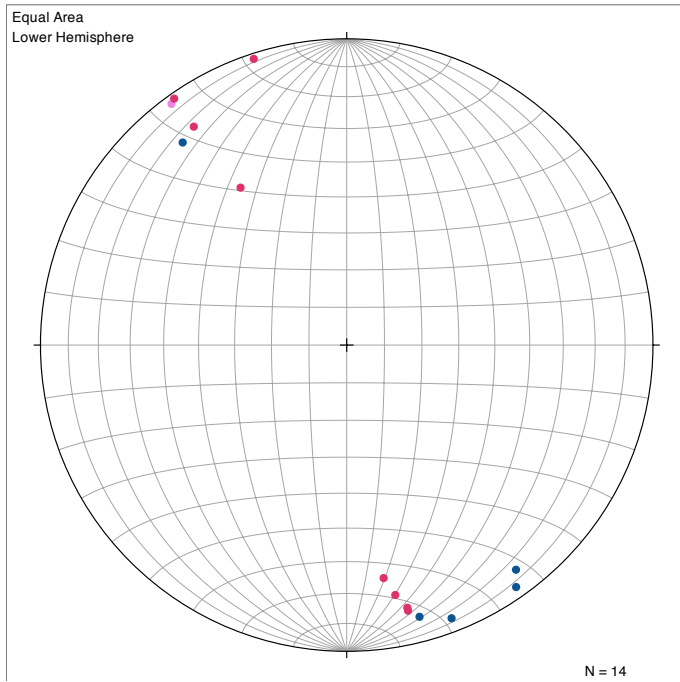


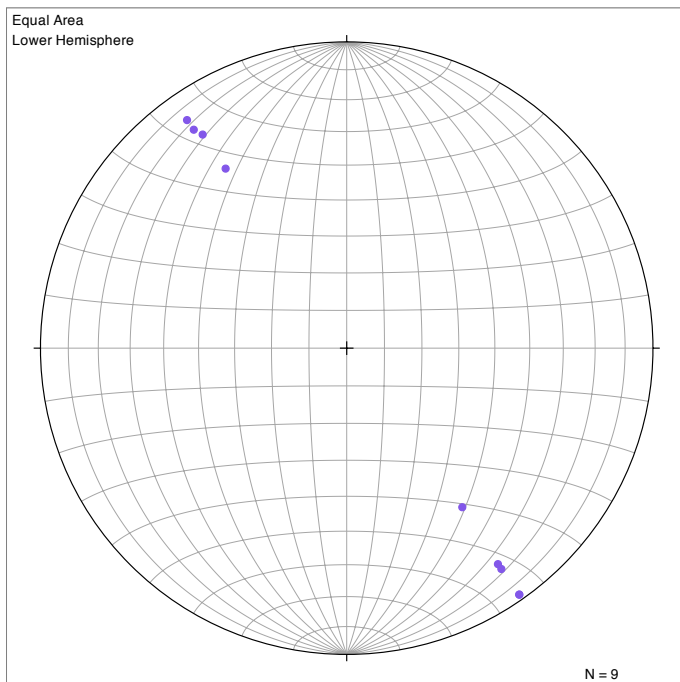## Subarea 2 axial planes
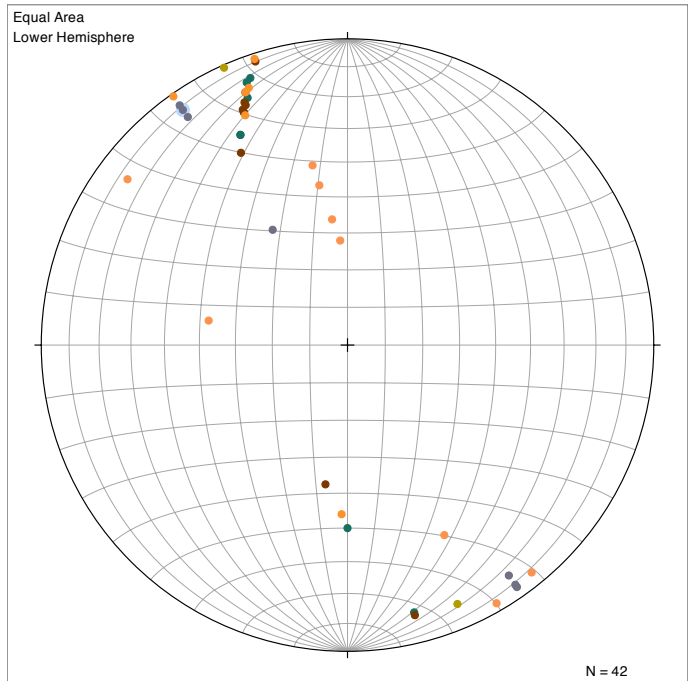


## Subarea 4 axial planes



Fig. 33. Axial planes determined from the measured and derived fold axes in each sub area. Subarea 3 did not have any folding, so no axial planes could be determined. Colors indicate the outcrop locality, present in the legend (figure 34e).
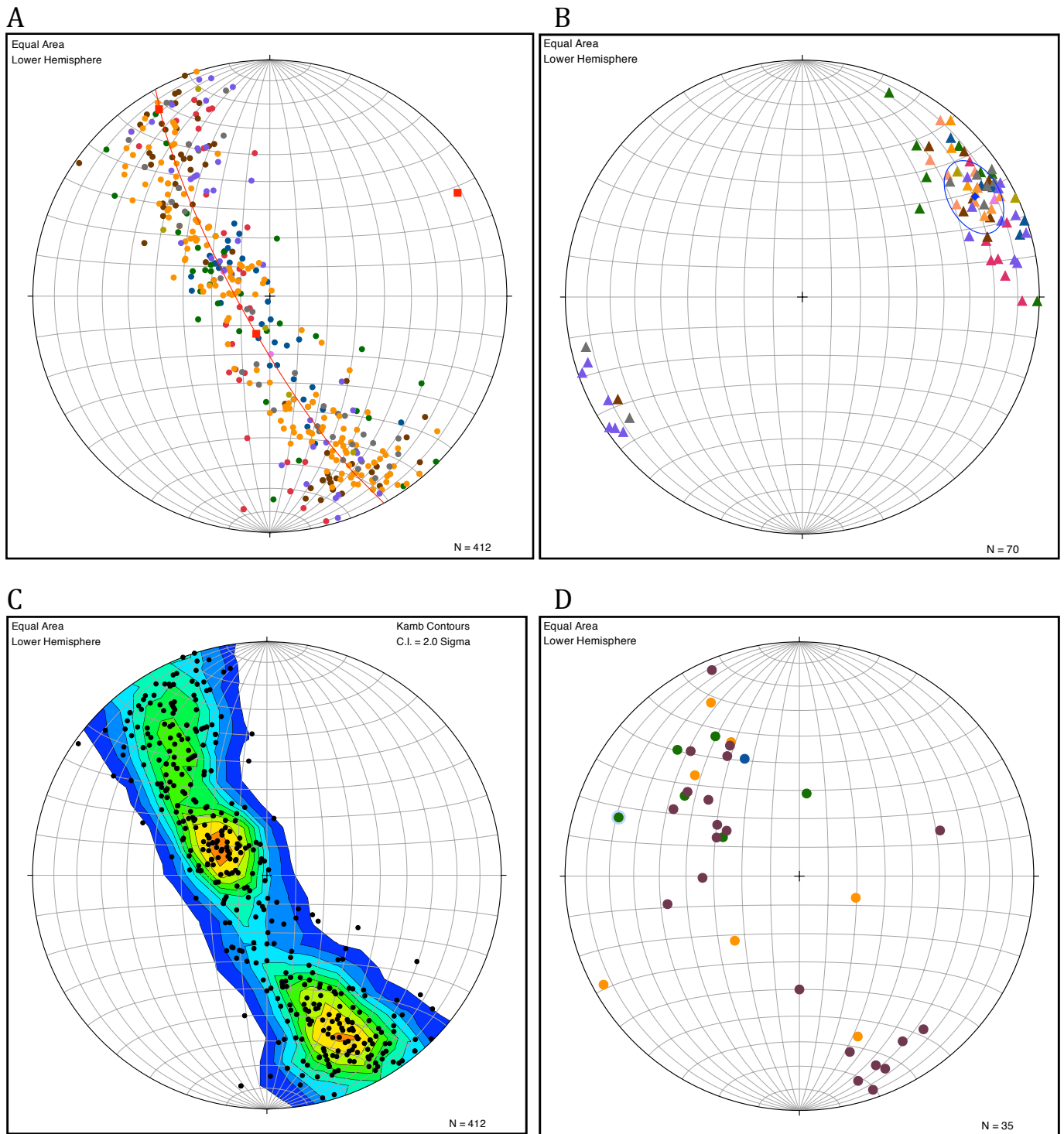
Fig. 34. Stereoplots with data from the study area, plotted in OSXStereonet (Allmedinger and Cardozo, 2011). (A) Plot with poles of all measured planes, the colors represent the areas or profiles the measurement was made in (legend in 34e). A best fit was done presenting an axis all planes are folded over (average fold axis) of 62/11. (B) All fold axis, serperately measured or derived from two flanks, plotted in one stereonet, colors again represent the locality. A mean vector was constructed, representing a mean fold axis, of 62/9. (C) A stereoplot with again poles of all measured planes from the study area, no locality color was added, but a kamb contour was constructed with the data, showing density contours in the data. (D) Stereoplot with poles of the fault planes measured in the area, colors indicate the localities. (E) Legend linking the localities to the colors used in the stereoplots, profiles are indicated, profile B-B' and A-A' are combined and devided into separate localities.
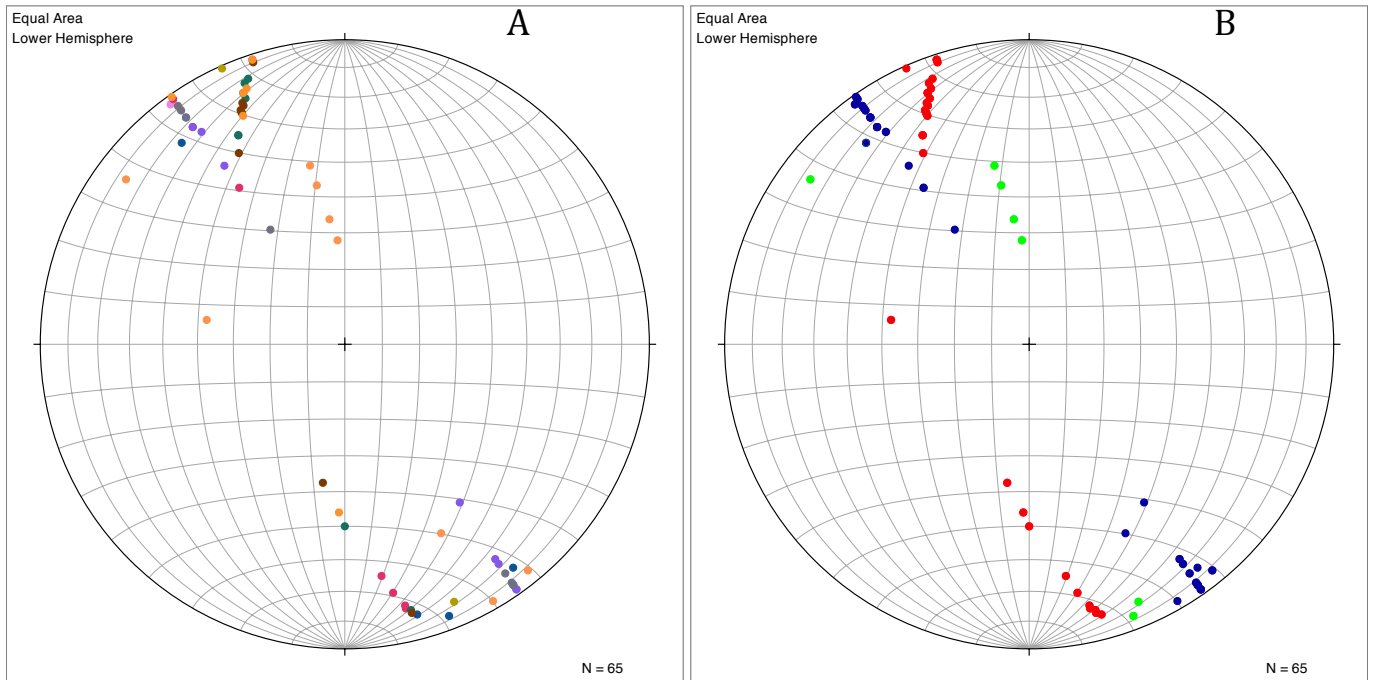
Fig. 35. Plots with axial planes with location label (A) and cluster label (B). Colors in plot 35a represent different localities (same legend as 34e). Colors in plot 35b show the two clusters lining up on two great circles. Blue is the folding cluster and red is the faulting cluster (see text for more details). The green data have uncertain origin, they may either belong to the folding or faulting cluster, or to a new population.

away from the middle part of the plot. The axial plane plot of subarea four (*Fig. 33*) shows a nice clustering along a NW-SE great circle (325/88).

In terms of planes and fold axes the subareas do not seem to show any variability (*Fig. 34a*). The combination plot of the poles to the measured planes makes a band along a NNW-SSE orientation. Scatter along this orientation is minimal and all 412 measurements are taken in an area of around 10km2 making it a quality dataset influenced by a single stress regime. The average fold axis of the entire dataset is 62/11.

Plotting separately the fold axis of all the measured folds (combining the subareas) gives a similar mean fold axis of 62/9 (*Fig. 34a and b*). What stands out is that especially fold axis measured at Modum on the other side of the fjord show a wide spread, also dipping towards 230-250 in stead of 60. Analyzing purely the poles of all the measured planes (*Fig. 34c*) a better estimation of average fold geometry can be made. Two populations can be recognized using a density contour tool; one representing low angle SE dipping planes (poles cluster around 280/70) and

the other representing steep NW dipping planes (poles cluster around 145/30). Thus most south dipping planes are shallow and most north dipping planes are steep, which is in agreement with the field observations (*Fig. 13,* profile A-A'). An asymmetrical system that would agree with tectonic transport towards the SE *(Bruton et al. 2010)* would be the exact opposite of this situation (with steep south dipping planes and shallow dipping north planes). More than half of all the bigger faults measured in the area have a backward sense of direction (*Fig. 34d*). Especially on the island of Utøya and the south part of the coast section (profiles C-C' and D-D') show significant back thrusting. The asymmetrical character of fold, suggesting a local reversed transport direction, agrees with the dominance in back thrusts in the area.

The axial plane plots do show a variance (*Fig. 33 and Fig. 35a and b*). Especially subarea one and two show presence of multiple populations. Combining the plots of subarea one, two and four shows two main populations can be recognized (*Fig. 35*). One population is spread over the great circle of 325/88 and the other over 162/70. A few (maybe 10 out of 65) data points

do not fall in one of these populations, though usually they are close. Clearly these populations are not associated with the previously suggested subareas, as the faulting (2) and folding (1) sub-area both show both populations. When looking into detail on which data points falls into which cluster it shows that in one population the data mostly is measured in pure folds (325/88) and in the other the data is measured in fault-associated folds (162/70) (*Fig. 35a and b*). Thus one population is mainly associated with thrusting (measurements in red) in terms of drag faults in the foot- and hanging- wall. The other population (in blue) is measured in pure folds that were formed during a more viscous stage of the system.

Data shows that the structural style in the study area is heterogeneous, though deformation was homogeneous with an average fold axis of 62/9 and transport along a NNW-SSE line. The appearance of two populations in the axial plane plot suggests a difference in timing and implies a difference in deformation mechanism. It is proposed that an early, more viscous stage, created folds in the research area associated with the folds axial plane population (325/88) while after slight rotation a more brittle stage created faults with related folds associated with the faults axial plane population (162/70). This early viscous stage can also be the explanation for certain fold geometries that do not appear in purely brittle systems with a single deformation event, like fold propagation folds and refolded folds.

# 5.  Lab report

## 5.1.  Introduction

Combining the data from this study with previous studies (e.g. ***Bruton et al., 2010; Van den Broek 2015***) provides a reasonable conceptual model for the Ringerike area. The basal plane study by Van den Broek (2015) shows a strongly deformed basal plane running from the north of the Ringerike area (Viul) all the way to Slemmenstead, with its subsequent deformation of overlying units. This deformation is recognized in major frontal and back thrusts and large scale folding in the area but also in smaller scale structures like splay faults and fault propagation folds. The occurrence of these structures still raises questions, which may be answered by varying rheological and mechanical parameters in an analogue study. Due to the limitations of analogue modeling in terms of scaling and rheology the Oslo region cannot be modeled precisely, though influences of certain mechanical and rheological variations may be analyzed.

Previous studies have shown that deformation in foreland basins has its own characteristics, which are essential to include in a mechanical analysis *(Chapple, 1978)*. Deformation in foreland basins occurs in belts that are thin-skinned, so folding and thrusting is limited to a certain stratigraphic horizon. This horizon is usually near the crystalline basement, but may also be higher in stratigraphy. This basal layer is commonly composed of weak material, often over pressurized shale or evaporites *(Chapple, 1978)*. The key is that it is not about the mechanical strength contrast between the sequence and crystalline basement, but about the presence of a layer of weak material to create a thin-skinned fold-and-thrust belt.

Type of lithology of the weak basal layer also has influence on the deformation characteristics in the fold-and-thrust belt. For example a salt detachment results in a very narrow cross-sectional taper and an abrupt change in deformation style at the margins of the salt basin. The sedimentary infill of the basins is wedge shaped, so thicker closer to the

orogen and thinner further away from the orogen. In general the basal layer slopes backward (towards the orogen) and the surface slopes towards the foreland, which was the basis for the 'critical taper theory' *(Chapple, 1978; Davis et al., 1983; Davis and Engelder, 1985; Smit et al., 2003)*. The final characteristic of a thin-skinned fold-and-thrust belt is strong thickening and shortening of the wedge. The structural style, or mode of compression, varies between belts but also between different localities in the belt. For example the back end of the wedge (closest to the orogen) can be transported 200km, whereas the most frontal thrust only accommodates a few kilometers. In this case the difference is accommodate in the shortening within the fold-and-thrust belt *(Chapple, 1978)*.

Brittle-ductile systems in foreland basin settings have been studied by Smit et al. 2003, arguing whether coupling is a function of the magnitude and ratio of differential stresses. This ratio drops towards the front of the wedge, increasing the brittle-ductile coupling *(Smit et al., 2003)*. It is also shown that the mode of coupling (strong/weak) influences structures sequence and geometry.

The Oslo area as a foreland basin comprising all the above mentioned characteristics; it has a shale décollement, it is a thin-skinned fold-and-thrust belt, the sediments are present in a wedge-shape (near Oslo the sequence is much thinner than in the Ringerike area) and there is a variation in deformation styles in depth as well as laterally in the basin. The careful field study carried out by Bruton et al. (2010) provided a good understanding of the Oslo area as a foreland basin, though further questions have risen on the role of certain structural and mechanical parameters in the evolution of the Oslo foreland basin. The parameters that raise questions are: 1) the origin of deformation intensity variations, 2) the high dominance of back thrusts and 3) the role of rheological stratification. In order to understand the above-mentioned constraints the analogue modeling approach is used. The analogue models performed give better insights on the evolution of the fold-and-thrust belt system, but also on impacts of rheological contrast within the sedimentary infill of the foreland basin.
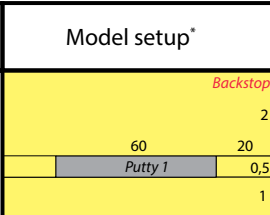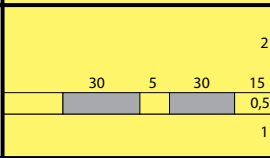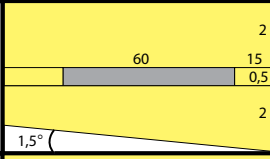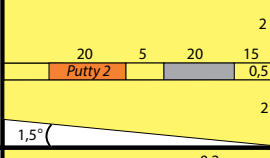
The analogue models will be compared
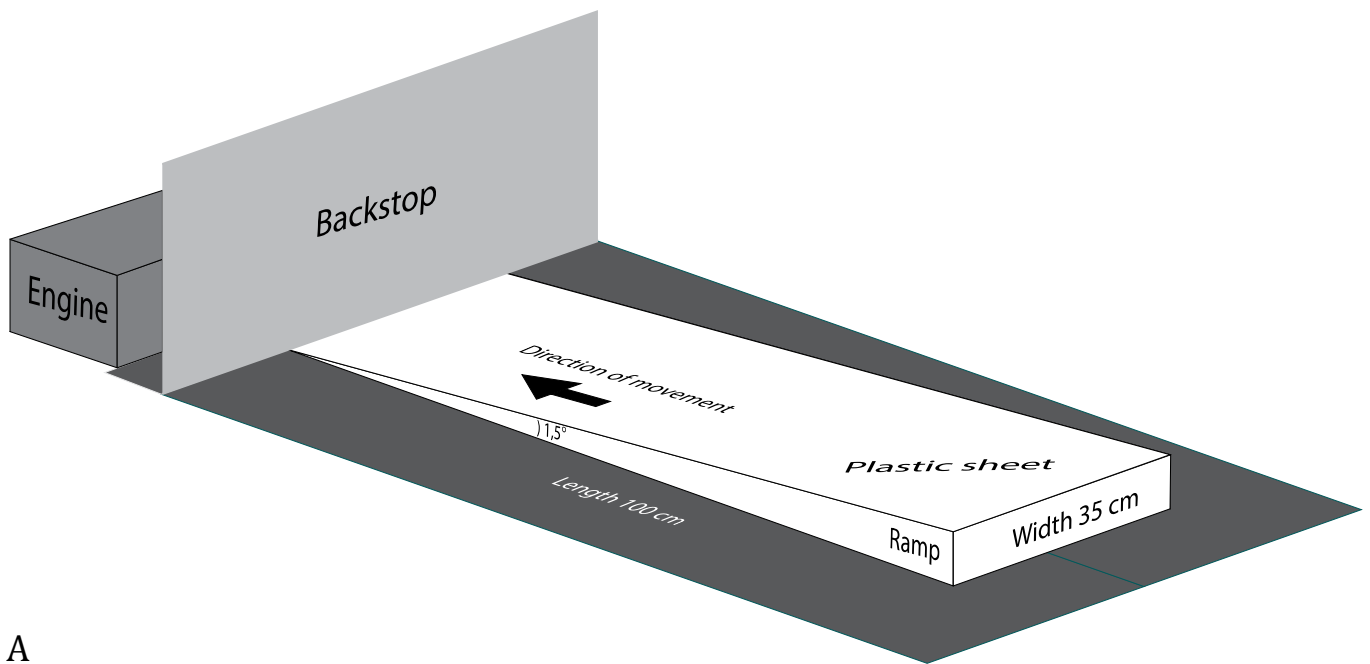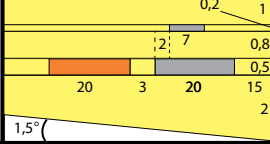
A
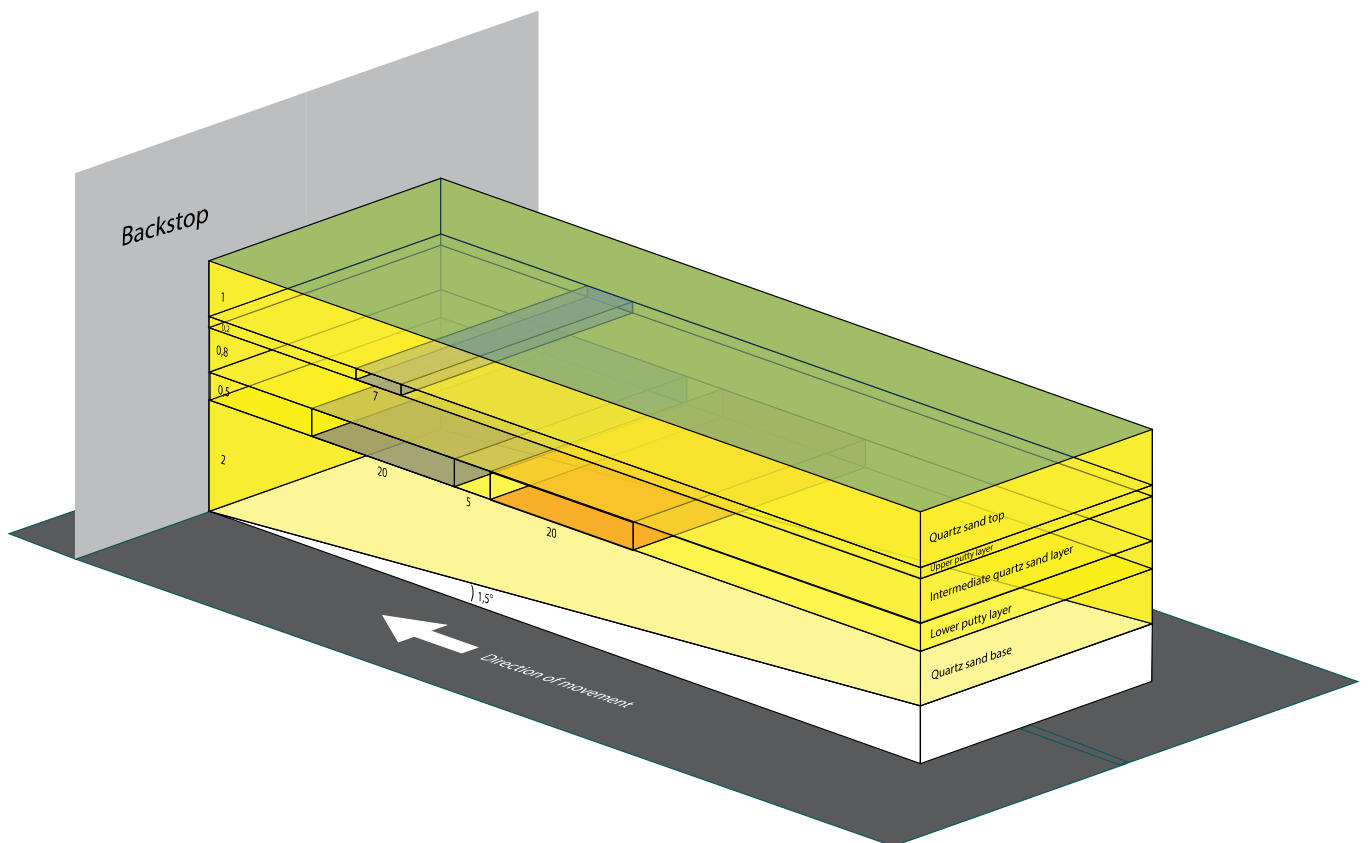


B

Fig. 36. Experimental setup used in this study. (A) Technical setup with variable basal angle and constant dimensions of the bounding box. Driving mechanism of the models is displayed by the plastic sheet on top of the basal (wooden) layer, which is pulled under the backstop by the electrical engine. (B) Example of the stratigraphical setup of the experiments indicating different layers, materials and their dimensions. This perticular example is model 5 (table 1) with weak layers (grey) and a strong object in the foreland (orange) in a quartz sand system. The other experimental setups can be found in table 1.

with the field studies of Bruton et al., 2010, Weekenstroo, 2015; Verdonk, 2015; van den Broek, 2015 and the present study.

| Model # | Model setup* | Mechanical setup |
|---|---|---|
| 1 |  | Basal (strong) quartz layer with a thin centered (weak) putty layer on top, followed by a thick section of quartz sand. *BS (bulk shortening): 13%, v (velocity of convergence): 5 cm/h.* |
| 2 |  | Basal (strong) quartz layer with a discontinuous (weak) putty layer on top (which lays closer to the backstop), followed by a thick section of quartz sand. *BS: 20%, v: 5 cm/h.* |
| 3 |  | Basal (strong) quartz layer with a thin, centered (weak) continuous putty layer on top, followed by a thick section of quartz sand. Basal inclination of 1,5°. *BS: 15,5%, v: 5 cm/h.* |
| 4 |  | Additional discontinuity in the putty layer, putty 2 is very strong compared to putty 1. Basal inclination of 1,5°. *BS: 10%, v: 5 cm/h.* |
| 5 |  | Additions: Shorter sand part inbetween two putties and the introduction of a second stage of weak layer in the upper part. Basal inclination of 1,5°. *BS: 13%, v: 5 cm/h.* |

*Thickness and lengths are given in cm.*

Table 1. Experimental setup table with mechanical variations explained. Material use and setup considerations are discussed in the text.

## 5.2. Modeling strategy

### 5.2.1. Materials

To achieve a model that is most representative for the Oslo area several setups scenarios were used. The overview table (*Table 1*) and schematic setup figure (*Fig. 36*) above illustrate the model setups and the mechanical variability within the five models. Two main types of analogue models have been studied, one without a basal inclination and one with a basal inclination. Furthermore variations are made on the location of weak and strong zones. The basal inclination The analogue models are performed in the Tectonics Laboratory (TecLab) of the department

of Geosciences at the University of Utrecht.

The analogue materials that were employed to construct a multilayer brittle/ductile system are derived from the structural model presented in Bruton et al. 2010. For the weak lower layer, which would represent the detachment zone of the fold-and-thrust belt (Alum shale or any other weak layer within the Palaeozoic sequence) silicon putty was used. This silicon polymer exhibits a non-Newtonian fluid behavior and has a density of 1,00 g/cm3, a viscosity of 1,98·104 g/cm3, an n-value of 1,2 and an A-value of 1·10-5. In all experiments this material was used as non-basal weak zone, in these cases it would still represent a weak, interlayered rock, like for example shale. The bulk strong part of the model consists of quartz sand, which is analogous to the stronger limestones and sandstones in the sequence in the Oslo region. To keep the models simple and more general no distinction was made between limestones and sandstones. The used quartz sand has a density of 1,5 g/cm3 and an angle of internal friction of 32°. Finally for a very strong component in the system, which may be analogous to the Ringerike Group, silicon polymer mixture was used that was constructed for a previous study which has a density of 1,823 g/cm3 and a, high viscosity, n-value of 1,6 and an A-value of 2·10-8. This component thus acts more or less as a rigid object in the system. In appendix B the strength profiles through various locations in the models are presented.

### 5.2.2. Brittle behaviour

Brittle material deforms according to the Mohr-Coulomb criterion *(Byerlee, 1978)*. Following the Mohr-Coulomb criterion the maximum differential stress of the brittle layer increases linearly with depth and is independent of strain rate. For the brittle part of the model, in compression mode, the following equation applies:

$$(\sigma_1 - \sigma_3) = 2\frac{\mu\rho gz}{(\mu^2 + 1)^{1/2} - \mu}$$

Where $\sigma_1$ and $\sigma_3$ are the maximum and minimum principle stresses, $\rho$ is the density of the brittle material, g is the gravitational constant, z is the depth of the brittle part of

the model and μ the density of the material.

### 5.2.3. Ductile behavior

The ductile material being used in this study is silicon putty. This material is a non-Newtonian viscous material that is linearly dependent on strain rate. The ductile strength of the putty in a compressional setting can be describe by:

$$(\sigma_1 - \sigma_3) = 2(\frac{\dot{\varepsilon}}{A})^{1/n}$$

In which $\sigma_1$ and $\sigma_2$ represent the maximum and minimum principle stresses and $\varepsilon$ represents the strain rate, A the material parameter function of temperature, compression and material properties and n the stress exponent.

### 5.2.4. Model scaling

In analogue modeling scaling is of the greatest importance to preserve results that are comparable to nature. The models were scaled following the principles of geometric and dynamic-rheological similarity *(Hubbert, 1937; Ramberg, 1981; Weijermars and Schmeling, 1986; Sokoutis et al. 2005)*.

Scaling relationships between nature and the model are maintained by the strength of the ductile layers scaled with respect to the strength of the brittle layers in the equation of dynamics *(Brun, 1999; 2002)*:

$$\frac{\delta \sigma_{ij}}{\delta x_{ij}} + \rho \left( g - \left( \frac{\delta^2 \epsilon_{ij}}{\delta t^2} \right) \right) = 0 \; with \; (i, j = 1, 2, 3)$$

Where $\sigma_{ij}$ stands for the components of stress, $\varepsilon_{ij}$ for the components of deformation $x_{ij}$ for space coordinates, $\rho$ for density of the material, $g$ for gravity acceleration and t for time. This makes that the ratio of stresses has a relation with the ratio of density, gravitational acceleration and length, giving:

$$\sigma^* = \rho^* g^* L^*$$

and

$$\epsilon^* = g^* (t^*)^2$$

Where L stands for length and ($^*$) refers to the ratio between the model and nature *(Brun, 1999)*. The latter equation can be left out as inertial forces can be neglected in geological processes *(Hubbert, 1937)*. Experiments that are done under normal gravity have a gravitational acceleration ratio of 1 and since materials with similar densities are used in the models as in nature also this ratio approaches to 1, which results in:

$$\sigma^* \approx L^*$$

So the ratio of stresses becomes almost equal to the ratio of lengths *(Brun 1999)*.

### 5.2.5. Time scaling

Taking time equally into account as the other scaling ratios results in a problem *(Ramberg, 1981)*. The problem is based on the requirements for velocity in modeling:

$$l_r t_r^{-2} = a_r = 1$$

With $l_r$ as length ratio and $t_r$ as time ratio and as $a_r$ acceleration ratio, following from the fact that both nature and model are both exposed to the same gravitational acceleration. For example in a model with a length ratio of $10^{-5}$, so 10 km in nature is 10 cm in the model, a time span of approximately $10^6$ years is reasonable for the formation of the natural structure. Following the equation the time required to do the experiment is 3160 years, which is not ideal for scientific research *(Ramberg 1981)*.

The fact that acceleration of a body in a tectonic process is negligible the equivalent is to say that inertial terms are negligible in fluid-dynamic equations when applied to tectonic processes. Therefore the length ratio and time ratio can be treated independently, which makes it possible to do experiments in a shorter time.

The validity of neglecting inertia has been discussed and the simplification seems acceptable with a low Reynolds number (Re) *(Wickham, 2007; Del Ventisette et al., 2007)*.

$$Re = \frac{\rho v l}{\eta}$$

With ρ as the density, v as the velocity of convergence, l as the length and η as the viscosity. In both the models and nature the Reynolds number turns out to be relatively low (Re = $10^{-8}$), making the simplification valid.

### 5.2.6. Model setup and deformation

The analogue models were constructed using a plastic sheet that is being pulled underneath a backstop by a motor (*Fig. 36*). The velocity on which the motor is pulling the sheet underneath the backstop is kept constant, at 5 cm/h, to be able to compare the results of experiments mutually. The backstop causes shortening to occur in the body of sand that is put in front of the backstop (on the plastic sheet) in a 100 cm long and 30 cm wide area bounded by metal bars. The body of sand was sieved in layers with different colors of 2/4/8mm thick, with thin black layers in between for optimizing the contrast in the cross sections. The framework is fixed using weights and clamps to ensure that during the running of the model no movement is possible in framework and no volume alteration in the body of sand is possible. In some experiments the basal inclination was varied which was achieved by building the model on an inclined (inclination of 1,5°) wooden plate with the plastic sheet on top (*Fig. 36*). Variable setups were constructed (*Table 1*) changing the position of weak silicon putty layers within the model, bulk shortening (BS), basal inclination (ß) and introduction of a strong object (stiff putty) in the system. Bulk shortening is defined as:

$$\frac{L_U - L_D}{L_U} \cdot 100 = bulk\ shortening$$

with $L_u$ the length of the model before deformation and $L_d$ the length after deformation.

### 5.2.7. Limitations

Nature is too complex to be exactly modeled; thus analogue models are only simplifications of natural situations. For example the strong and weak parts of the crust are not as homogeneous in nature as they are in the analogue models. Temperature dependency is limited in sand and putty models. Also flexural and isostatic variations, with corresponding processes like erosion syn-tectonic sedimentation and denudation, are not present. Finally the materials used in the analogue models are only a close approximation to the natural materials.

These limitations must always be taken into account when interpreting the models and make conclusions about the models. However from the models the first order interpretation can be derived.

### 5.2.8. Nomenclature

As a framework for discussing the performed brittle-ductile experiments, the common types of contractional faults observed are identified (*Fig. 37*). Fore thrusting is the most basic type of faulting that occurs in contractional settings and is usually accompanied by minor back thrusts that accommodate internal deformation in the hanging wall (*Fig. 37a*). In some cases the master fault is the back thrust and hanging wall deformation is accommodated in smaller fore thrusts (*Fig. 37b*). As deformation progresses and multiple fault system start interacting with each other a so-called 'flip' may occur where a minor fault becomes a master fault and thus a more symmetrical pop-up-like structure is formed (*Fig. 37c*). Finally the basic pop-up structure, with two equally important thrusts, is also recognized (*Fig. 37d*).
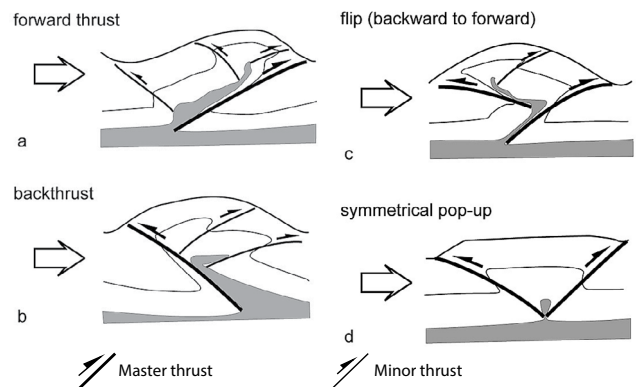


Fig. 37. Typical nomenclature for fold-and-thrust belts, see text for more details. Figure after Smit et al., 2003.

## 5.3. Observations

### 5.3.1. Model 1

Deformation in this model is concentrated relatively close to the backstop. The first major fault (#1, *Fig. 38*) is a foreland directed thrust fault (fore thrust) and is followed within a few cm by a second fore thrust of significant size (#2, *Fig. 38*). Subsequent with the first fore thrust a hinterland directed back thrust is formed (#1r), which is poorly visible on the top view, though nicely recognizable in the section (*Fig. 41*). This back thrust clearly is influenced by the presence of the backstop, as it steepens when it approaches the backstop. These structures form during the first 5% of bulk shortening (*Fig. 38*)
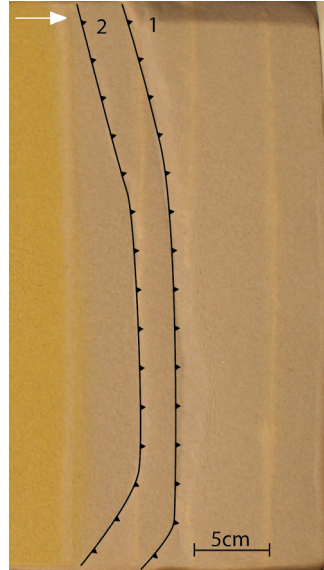


Fig. 38. Model 1 fault pattern after 5% BS. The white arrow indicates the transport direction.

The thin-skinned fold-and-thrust belt develops in sequence with foreland directed thrusts of varying scale; for example thrust 2 is significant enough to be recognized in the top views but also several smaller thrusts can be identified in the cross section (*Fig. 41*). These smaller thrusts do not cut through to the surface, though they do accommodate strain. After 10% of bulk shortening (*Fig. 39*) a major back thrust (#4r, *Fig. 39*) dominates the region where before the fore thrusts #1 and #2 were laying. This back thrust originates near the boundary of the weak interlayer with the quartz sand, as can be seen in the cross section (*Fig. 41*). Towards the foreland more fore thrusts are identified (#5 and 6, *Fig. 39*), creating a major popup combined with the previously mentioned back thrust. In the frontal part of the popup the strain is being accommodated by three thrusts (#6, 7 and 7b). Sequence of these thrusts relative to each other is hard to tell, as they are barely visible on the top views, though it very much looks like they are formed in sequence.

Deformation in the popup is significant, especially the weak layer is deformed intensely, but also the brittle layers in the root are strongly folded and faulted. After more strain the deformation becomes localized more, as strain is being transferred through the weak layer towards the foreland (*Fig. 41*). This results in a thrust far in the foreland
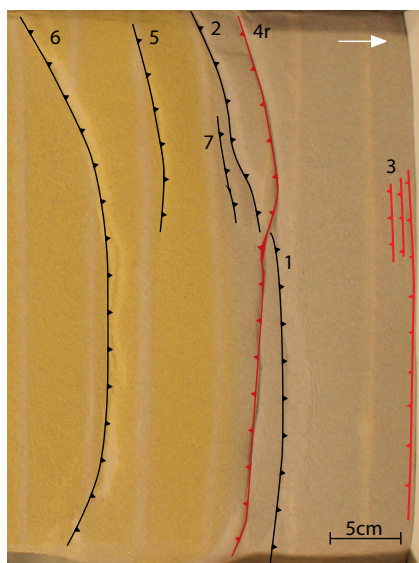


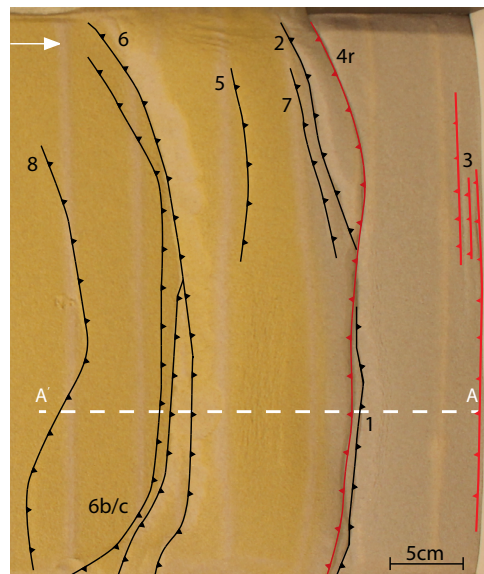Fig. 39. Model 1 fault distribution after 10% BS; Formation of a major popup is visible.



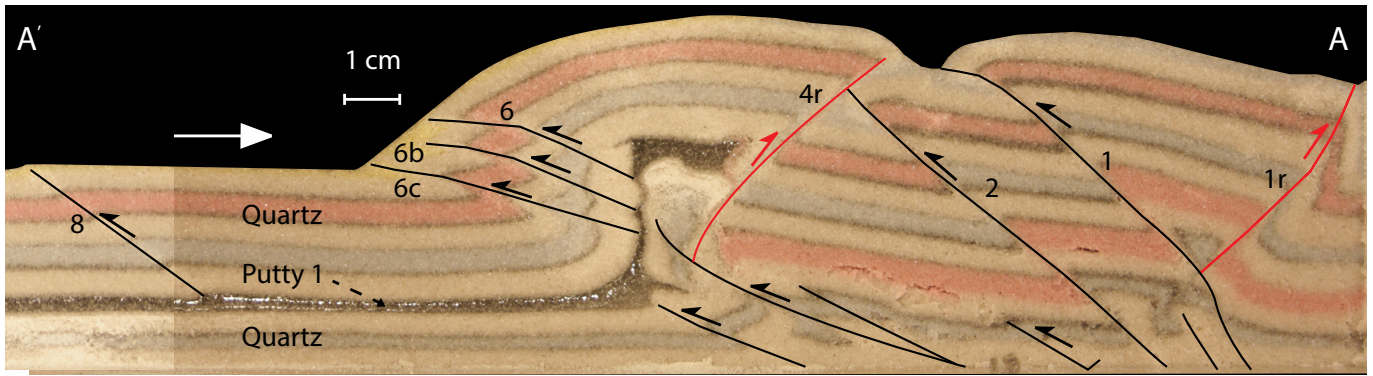Fig. 40. Model 1 final fault distribution (16% BS). Cross section A-A' is presented in fig. 37.

Fig. 41. Model 1 cross section along line A-A' (indicated in figure 36) after 16 % BS.

(#8, *Fig. 40 and Fig. 41*) and a zone in between (between thrust #7 and #8) of low deformation, maybe some large scale folding or back thrusting..

The final fault distribution (*Fig. 40*) can be described as two major popup systems of which the second (most foreland based) is the most complex with strain partitioning occurring in the foreland-directed thrusts and high mobility deformation of the weak layer at depth (*Fig. 41*).



Fig. 42. Model 2 fault pattern after 5% of BS.



Fig. 43. Model 2 fault distribution after 10% of BS.

### 5.3.2.    Model 2

In this model the weak interlayer was made discontinues and placed 5 cm closer to the backstop and a higher bulk shortening (BS) was generated, but further the model is similar to model 1. Results thus are comparable; with a major popup close to the backstop and due to the more proximal presence of the weak interlayer the second foreland directed thrust already runs through the weak interlayer (*Fig. 44*). The first two foreland directed thrusts already form within the first 15 cm of the model (*Fig. 42*). After more strain (10% BS: *Fig. 43*) new thrusts form and in the back nappes are stacked on top of each other (*Fig. 44*). The top view also shows significant lateral variation in this model, as in the top of the image a tectonic domain is present which has been joined in the lower part of the image. Further towards the foreland the strain is again transferred through the putty and creates a new popup at relatively great distance, though due to higher strain this system eventually becomes involved in the first popup system, creating a complex set of thrusts and back thrusts in the top part of this popup (*Fig. 44*). This part of the model most likely has become very complex
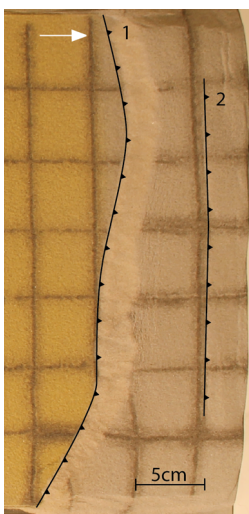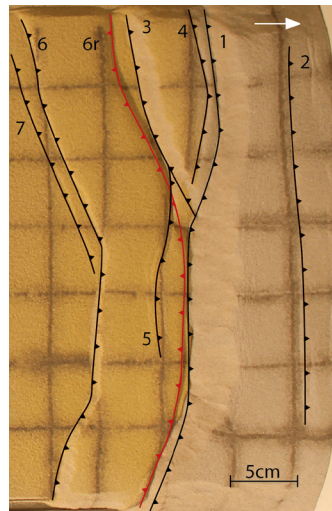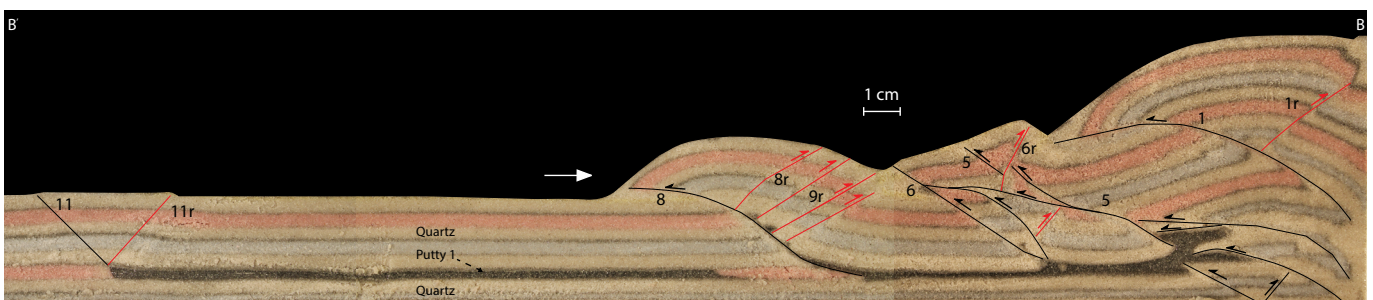


Fig. 44. Cross section through model 2 along line B-B'. Line B-B' is indicated in the last top view (after 20% BS) in figure 47.
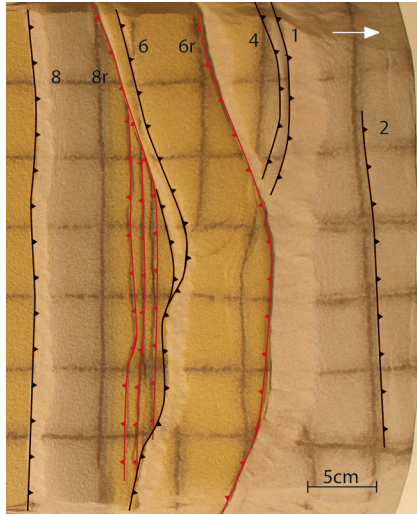
Fig. 45. Model 2 top view after 15% of BS.

due to interaction of the first popup system and this popup system. The third popup is much clearer visible in the section and develops at the final boundary of the first domain weak interlayer putty. A clear fold propagation fold is visible, with a foreland directed thrust (#8, *Fig. 44 and Fig. 45*) that almost runs flat near the surface. The back thrusting is dispersive and results in four separate back thrusts, which are nicely recognizable in after 15% BS (*Fig. 45*). Within the popup and especially in the root and weak zone major deformation has taken place (*Fig. 44*). In the front of the model also a small popup can be recognized (after 20%
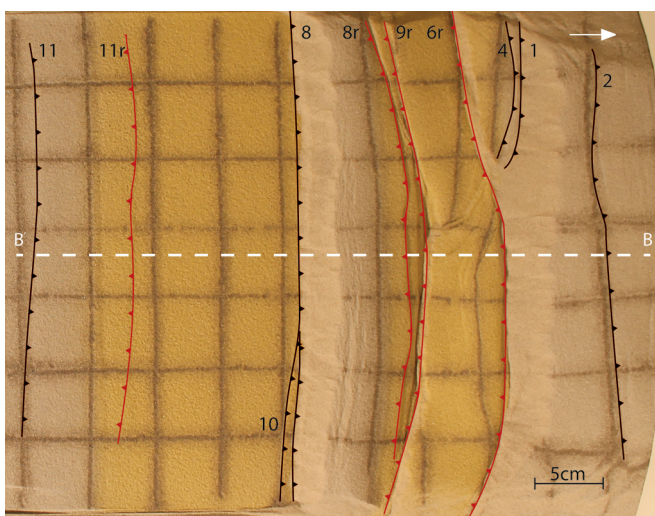


Fig. 46. Model 2 final top view (after 20% BS), with three popup systems visible at the surface. Line B-B' shows the section, presented in figure 40.

BS: *Fig. 46*), this means that through the weak interlayer strain is transferred. This also means that through the discontinuity, the brittle part between the two weak interlayers, some horizontal shear most have occurred, as no other deformation structure could have cause this strain transfer to the second weak interlayer domain (*Fig. 44*).
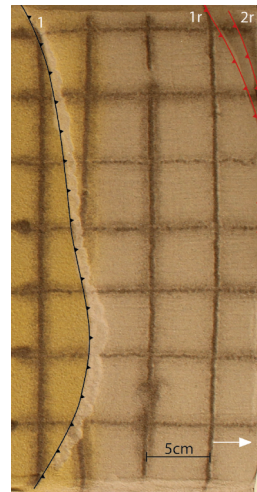


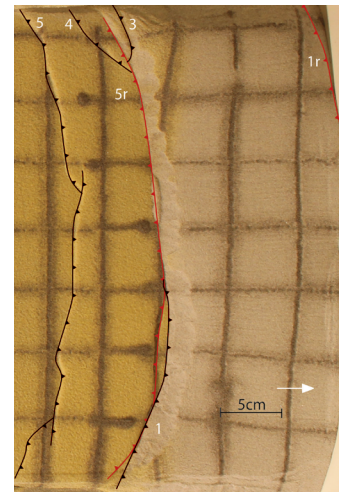Fig. 47. Model 3 (5% BS) top view fault distribution.



Fig. 48. Model 3 top view after 10% BS showing two popups.

### 5.3.3. Model 3

This experiment (and the following experiments) was constructed with a 1,5° basal angle and a continuous weak interlayer (*Table 1*). The basal inclination results in a thicker (thus stronger) succession near the backstop than more towards the foreland. This causes a big popup to form early in the experiment close to the backstop; the fore thrust #1 and the back thrusts #1r and #2r are components of this popup (*Fig. 47* and *Fig. 49*). The second foreland directed thrust originates at around the same place, causing a nappe- or antiformal stack, just like in model 2 (*Fig. 44*). The first foreland directed thrust (#1) has rotated to a very horizontal orientation by this antiformal stacking process. The weak interlayer again accommodates and transfers the strain, in the middle of the model this results in the formation of two clear-cut popups. The first one is formed after 10% BS; fault #5 and #5r are components of this popup (*Fig. 47*). The second popup compiles thrust #8 and back
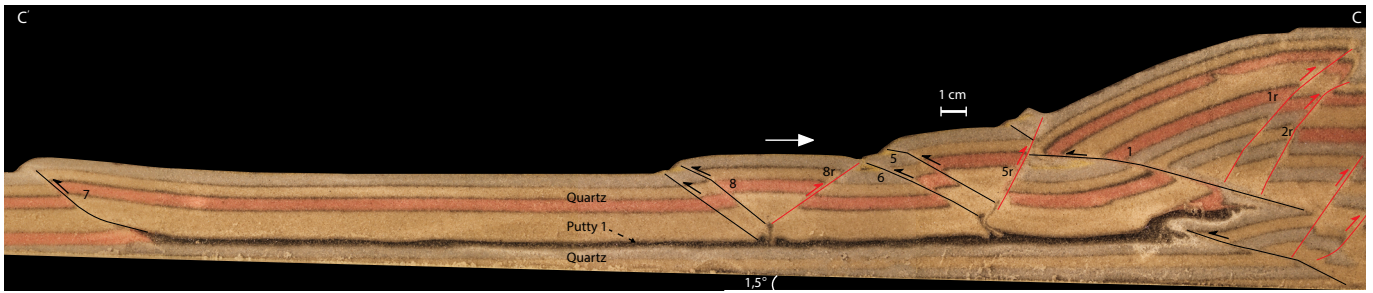
Fig. 49. Cross section made along line C-C' indicated in figure 51. The section shows a major popup near the backstop and some smaller popups in front with interesting structures at the root of the popup (discussed in the text).
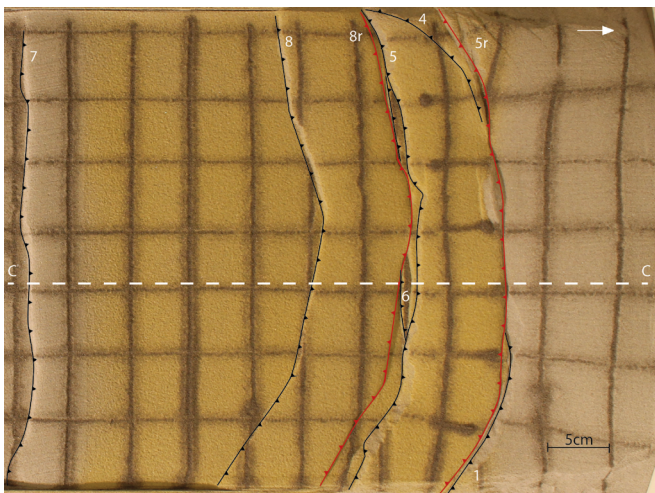


Fig. 50. Model 3 final fault distribution on the surface of the experiment. Along line C-C' a section was made given in figure 50.

### 5.3.4. Model 4

For experiment 4 a different viscous material was used; putty 2. The goal was to see the effect of a very stiff component in the frontal part of the model. As can be seen in the cross section (*Fig. 52*); the first thrust forms in the strong part and the second thrust runs into the weak viscous material. The effect of the weak viscous material is nicely recognizable in the top view after 5% of BS (*Fig. 51*). In the middle part of the experiment, where fault #1 is closest to the backstop, the fault has not been influenced by the weak interlayer, though in the top part of the image the thrust did interact with the putty, resulting in more foreland situated thrust. Besides that, thrust #3 is also introduced

thrust #8r and is formed in the final stage of deformation (*Fig. 50*). Deformation in the root of these popups is significant; the weak interlayer almost seems to be intruded into the strata above the weak layer (*Fig. 49*), deformation in the popups itself is minor. Striking in this experiment is the significant thrust in the end of the model and the domain of no deformation between this thrust and the last popup. The weak interlayer looks folded on a large scale, probably due to strain transfer and accommodation, but the stronger layer above is relatively undeformed. The final strain distribution in this experiment shows three domains: a popup domain near the backstop, with first a major pop-up which is part of an antiformal stack, followed by two minor popups with significant deformation in the root. The second domain comprises minor folding to almost no deformation and the third domain is the frontal fore thrust that originates at the end of the weak interlayer (*Fig. 49*).



Fig. 51. Fault distribution observed on the surface of model 4 after 5% of BS.
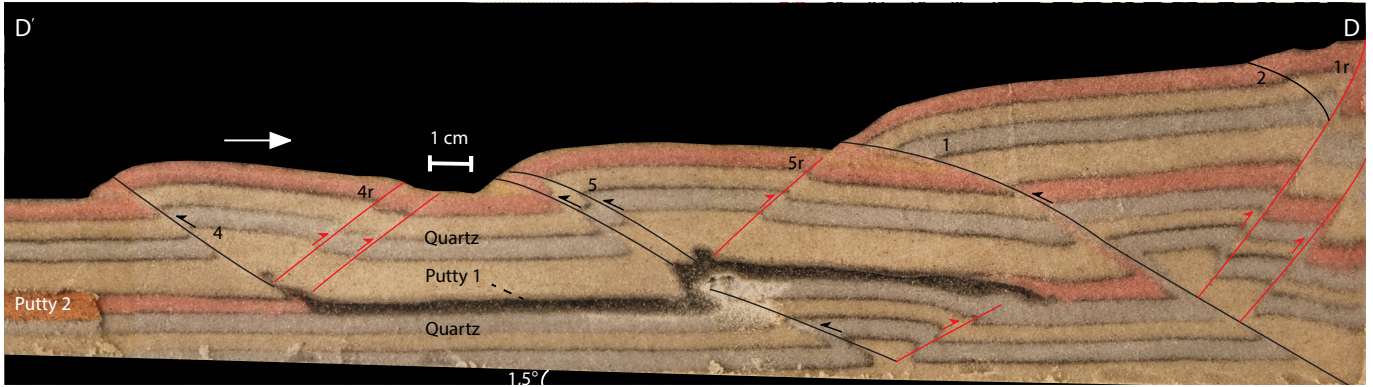
Fig. 52. Cross section in model 4 along line D-D'. Location of line D-D' is presented in figure 54. Influence of the frontal strong putty on the model is minimal, most likely due to low bulk shortening in this serie (only 10% BS).

in the top part of the image, but merges with #1 around the middle, showing dispersion by interaction with the putty. Close to the backstop a major popup forms, with #1 and #1r as components (*Fig. 51 and Fig. 52*). During the final stage of the experiment (after 10% of BS) the middle part also starts interacting with the putty, resulting in thrust #5 and creating a popup of which the back thrust is not visible on the top view as it forms close to fore thrust #1 (*Fig. 53*). The popup that forms in front is nicely recognizable in the cross sections, at the end of the weak interlayer it originates and

it branches up in two components: fore thrust #4 and two back thrusts, of which one can be identified on the top views as #4r (*Fig. 53*). Due to low strain (only 10% BS) there is no significant nappe stacking near the backstop. The deformation in the root of the popups does occur at low strains, the deformation pattern is already comparable to the root deformation in the previous experiment. Interaction with the very stiff viscous material (putty 2) has not really occurred yet.
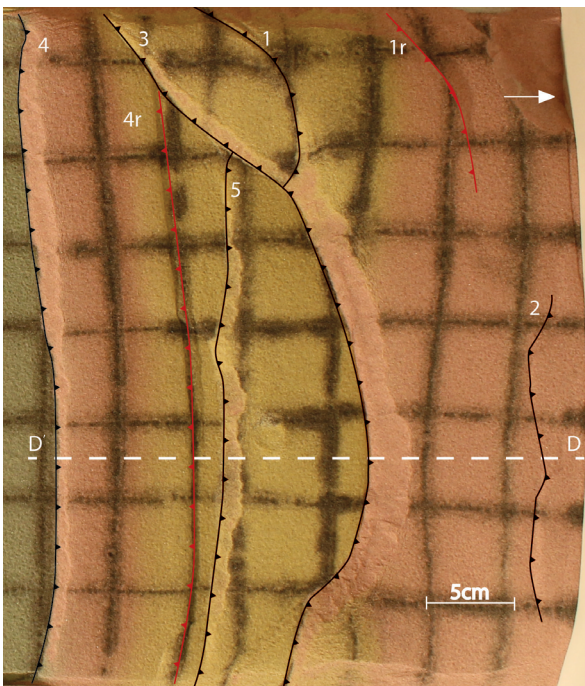


Fig. 53. Top view of model 4 after 10% of BS, with several recognizable popups. Line D-D' represents the line of the cross section given in figure 53.
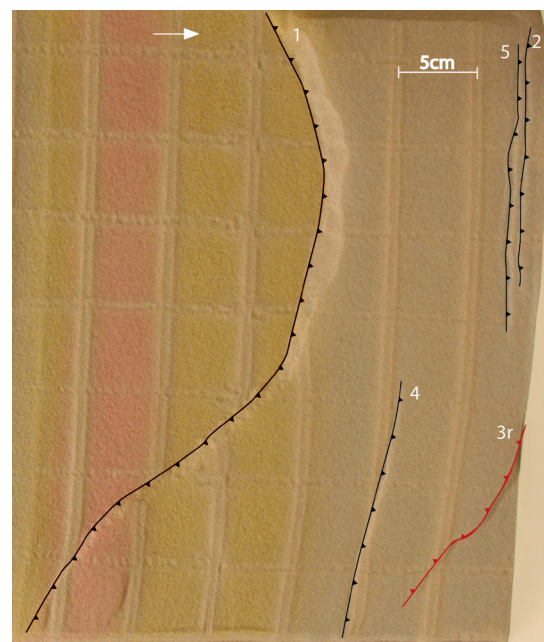


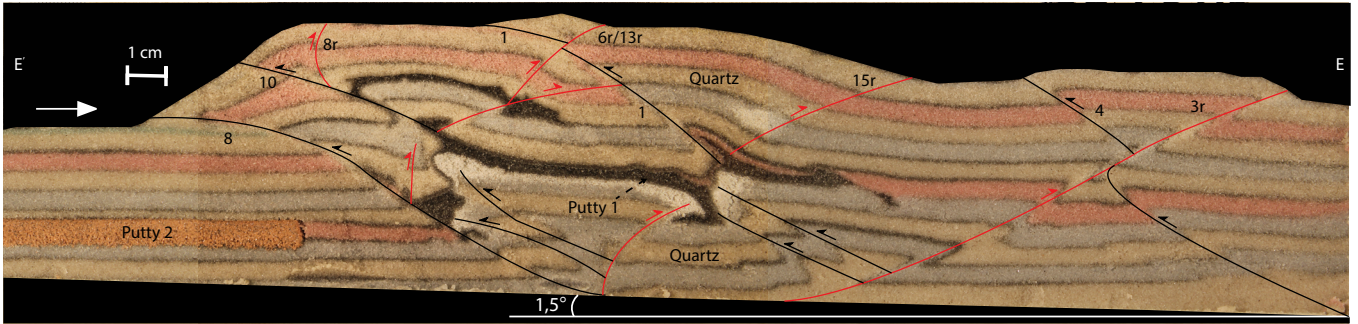Fig. 54. Top view of model 5 after 5% of BS.

44

Fig. 55. Cross section through model 5 along line E-E' (given in figure 58). Influence of the strong viscous material (putty 2) clearly visible, strong deformation with several sizes of popups visible in the middle part of the model (detail description in text).

### 5.3.5. Model 5

The final experiment comprises multiple weak interlayers in the first putty domain and a, similar to model 4, stiff domain in the frontal part of the model. Just like in the other experiments the lateral variation is significant; the first major thrust that is being formed (#1) runs through the strong (brittle) part in the top part of the image (*Fig. 54*) but runs through the first and ends even above the second putty layer in the lower part of the image. This results in almost 15 cm of horizontal distance between both thrust fronts. Out of sequence fore thrusts are present close to the backstop in terms of fault #5 and #2, but also #4 which forms a popup combined with #3r (*Fig. 54* and *Fig. 55*). After 10%

BS (*Fig. 56*) the big lateral variation has decreased, fore thrusts like #10 and #8 run relatively straight through the model. Also back thrusting becomes more dominant; the top view (*Fig. 56*) reveals that there are several smaller popups, for example in between fault #10 and #8r or between fault #1 and 6r/13r. The section (*Fig. 55*) though shows that these smaller popups have formed within one major popup, namely the domain between fault #8 and #15r. The interaction with the putty causes dispersion of the faults and formation of tectonic lenses. Deformation is localized in the roots of the popups, or in the weak interlayers within a pop-up (for example the popup with component fault
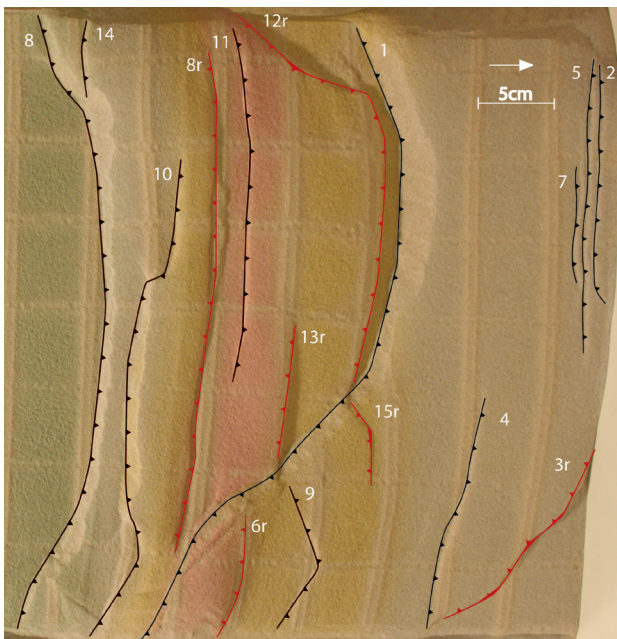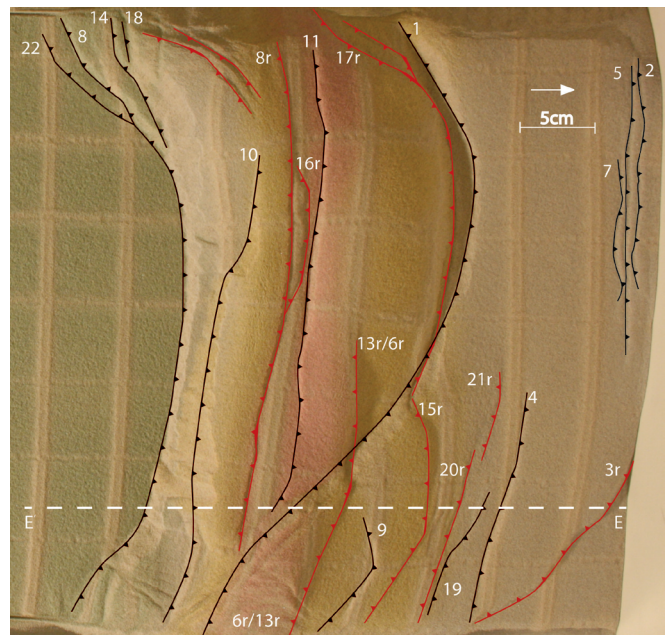


Fig. 56. Top view image after 10% BS of model 5.



Fig. 57. Surface image of model 5 after 13% of BS. Concentration of faults clearly visible in the middle part of the image.

45

#8a and #6r/13r). The weak layers are strongly folded and displaced and also the quartz layers are strongly deformed. The final stage of the experiment (13% BS) further extends the deformation features there were present after 10% BS (*Fig. 57*). Some faults that formed on either sides of the model have joined, for example fault #13r and #6r. During the final stage of the model no new faults are formed in the frontal part, only the very stiff putty is indented into the strongly deformed weaker part and a significant uplift is recorded. Overall the amount of back thrusts in this model is relatively high compared to the other models.

## 5.4.  Model analysis

### 5.4.1.  *Role of weak layers*

Considering the development of the fold-and-thrust belt towards the foreland, both the position of the weak layer(s) compared to the velocity discontinuity (backstop) and the amount of bulk shortening play a significant role. By comparing the results of experiment 1 and 2 (respectively *Fig. 41* and *Fig. 44*), the more proximal weak layer and higher BS causes strain to localize in bands and an antiformal stack to form near the backstop. Also the development of the thrust front towards the foreland is greater with a higher BS, caused by layer parallel shortening (horizontal strain transfer through the weak zone). Of special interest is the transfer of strain that can be recognized in experiment 2 (*Fig. 44*), which runs through the brittle part in between the two weaker layers. Another interesting feature is the ramp-flat-ramp system in the middle popup (between #8 and #8r), and the dominant back thrusting (*Fig. 44*). The effect of weak layers in the system, in any position in the basin (either in the base or somewhere in the middle) can be describe be coupling between the ductile layer and the brittle overburden. Brittle-ductile coupling is a function of the magnitude and ratio of differential stresses in the brittle and ductile layers *(Smit et al., 2003)*. The geometry of the brittle and ductile layers, but also fluid pressure (in nature), strain rate and viscosity, play an important role in the magnitude of the differential stresses. Weak BD-coupling (brittle-ductile-coupling)

has proven to give dominantly back thrusts and the spacing between thrusts increases with decreasing coupling *(Smit et al., 2003)*.

### 5.4.2.  *Role of a basal inclination*

The introduction of an inclination in de basal plane gives a better representation of the research area (experiments 3, 4 and 5), as usually strength also decreases towards the foreland in nature. In terms of structures there is not much change compared to the previous experiments (3 compared to 2) (respectively *Fig. 49* and *Fig. 44*), the deformation is less pronounced due to a lower BS. What is interesting the see is the large region with low deformation between the frontal thrust and the rest of the deformation (*Fig. 50*). The strong deformation at the base (or roots) of the popups is another point of interest (*Fig. 49*). The weak material seems to be 'intruded' upwards; the weak layer has been very active in the root of the popup. Comparing the coupling between the brittle and ductile components in different parts of the model shows an agreement with findings from Smit et al. (2003); an increase in coupling occurs going towards the tip of the deformation front.

### 5.4.3.  *Role of a rigid component*

Introducing a strong viscous material in the frontal part of the system that acts as an obstacle concentrates the strain more in the back. In experiment 4 (*Fig. 52*) a similar evolution has taken place as in experiment 2 (*Fig. 44*), where the frontal popup originates at the end of the weak zone and due to continuation of convergence multiple back thrusts are being formed. As can be seen by comparing model 4 and 5 (respectively *Fig. 52* and *Fig. 55*), by increasing the bulk shortening the strain intensifies rapidly in the part of the model where the weak zone is present. The difference in bulk shortening between the two experiments is only 3%, though as the system cannot progress towards the foreland, all the strain is accommodated in the middle part. So large displacements can be recognized by strong activity in especially the weak (putty) layers.

The strong viscous material that is located in the front of the experiment in model 5 also acts on the surrounding material. For example models

with similar or bigger bulk shortening, model 2 and 3, the deformation front is present or has passed at this distance from the backstop. Just like in model 2 and 3 strain is not expressed in structures in these domains (respectively *Fig. 44* and *Fig. 49*). In model 2 and 3 this is due to the strain transfer through the weak layer. In model 5 (*Fig. 55*) this is due to the zone of low strain around the strong viscous material and the subsequent strain localization in front of this strong viscous material.

The presence of a strong component in the system shows specific strain distribution, mainly avoiding the stronger component. In a recent study done on fold-propagation folding in relation with cover strength using discrete element modeling similar findings were presented *(Hardy and Finch, 2006)*. Making layered models with difference in strength per layer (of example strong-weak-strong) and deforming them with a simple basal thrust mechanism the deformation is being generated. In a three-layered model with, from top to bottom, strong-weak-strong rheology, deformation clearly concentrates in the middle weak layer (*Fig. 58a and b*). Fold propagation folds and other high mobility structures can describe the deformation style in this locality.

Mapping the locations where the bonds between the discrete elements were broken an image can be generated showing the high and low strain intensity domains (*Fig. 58b*). This also shows the importance of layer parallel shortening with the presence of a weak layer *(Hardy and Finch, 2006)*.

# 6. Discussion

The aim of this research is to enhance the understanding of the detailed structural development in the northeast Tyrifjorden area in light of existing regional tectonic models (*e.g. Bruton et al., 2010*). It will be tested whether the Oslo area is an area with typical foreland basin thrust system characteristics, like piggybacks, popups and possible distinct thrust levels. Special interest lies with the dominance of back thrusts in the study area *(Hjelseth, 2010; Kleven 2010; Bruton et al., 2010)* and its mechanism and sequence. Also emphasis will be put on the strong heterogeneity of structural styles and strong homogeneity of deformation in the area.

## 6.1. Structural evolution

Contractional deformation in the Oslo region



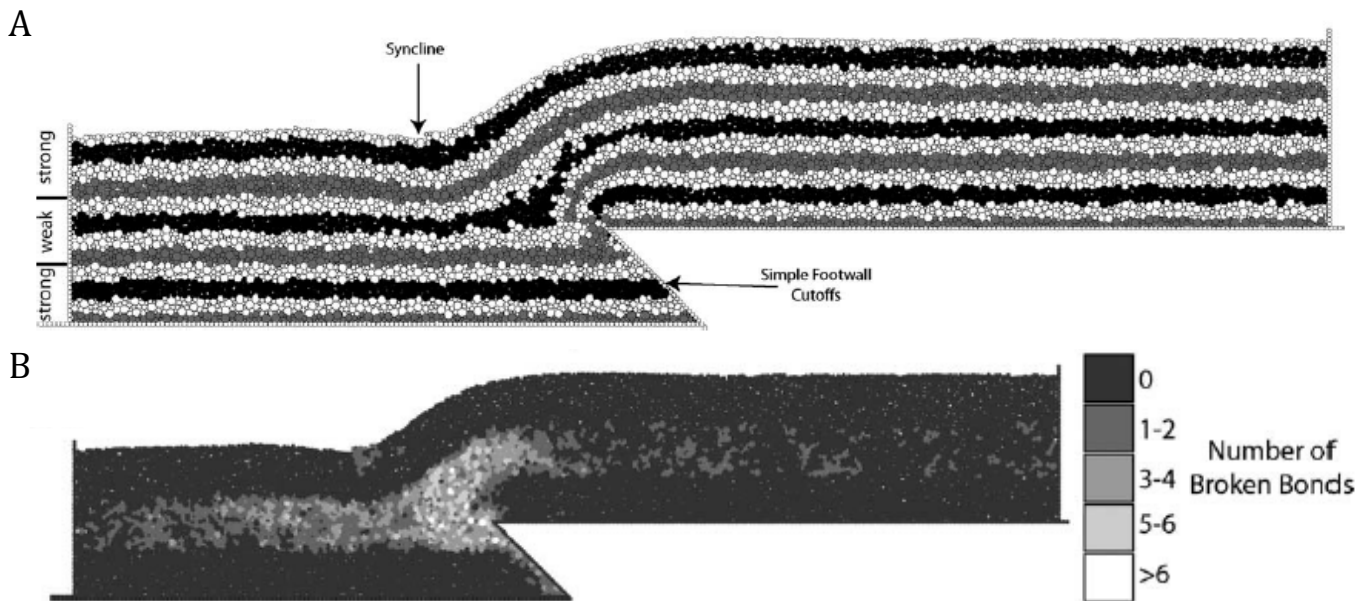Fig. 58. Some results from numerical models performed by Hardy and Finch, 2006. (A) Cross section of a strong-weak-strong experiment showing a very mobile weak layer and a minorly folded upper strong layer (strain intensity variations). (B) Diagram showing the number of broken bonds between the particles in the model from figure 57a, showing layer parallel deformation and high mobility in the weak layer.

(Osen-Røa Nappe complex) is accommodated in folding and faulting as is recognized before by numerous authors (*e.g. Murchison, 1847; Kjerulf, 1862, Nystuen, 1981; Morley, 1986a, b, 1987a, b, 1994*). The heterogeneity in structural style has also been documented (*e.g. Morley, 1994; Bruton et al., 2010*), though detailed measurements on the character of the deformation lack in particular in the studied area. Also the recognized dominance of back thrusts in the east Tyrifjorden area *(Bruton et al., 2010; Kleven, 2010; Hjelseth, 2010)* raises questions.

Data analysis shows two axial plane populations closely associated with different deformation mechanisms (faulting and folding), suggesting a difference in timing of deformation. A mechanism behind the differences in deformation style may be the amount of fluid in the system. Since evidence is found that the lower Palaeozoic sequence in the Oslo region (Osen Nappe) has undergone a maximum temperature and depth associated with the sub green schist facies (*e.g. Nystuen, 1981; Morley, 1994; Bruton et al., 2010*), it is not likely that the ductile character is solely caused by burial. An other explanation can be that the sediments were still very wet during early stages of deformation, causing intensive folding wet layers and less intensive folding in dryer layers (***Fig. 59***). Later dewatering



Fig. 59. Fault propagation and refolded folds on the west side of Utøya. Picture is taken in a N-S orienation, width of the image is approximately 2m. The disharmony in the folds can be related to the amount of fluid in the layers. The folded compentent layer may have been dryer than the refolded less competent layers, creating this outcrop. The folded competent layer may have been a dried up surface.

of the system results in strengthening of the sequence and major fault systems to form. In this reasoning the folds population was formed earlier than the faults population. The structures were most likely formed in one progressive event, as the stress field has not changed significantly between both populations and other deformation features (e.g. faults) do not show a significant change in stress orientation. Though the appearance of both populations does infer a slight change in tectonic transport direction at that time, though deviation from the NNW-SSE line is minimal. The fact that the axial planes are not on one small population but that they are fanned on a great circle suggests that after formation the orientation of the single structures has been distorted. This distortion seems to be caused by the same stress field as where the folds itself are formed in, as the fold axes of 235/2 and 72/20 are in the same order as for example the mean fold axis (62/9) of the folds itself. This again is proof for a progressive deformation event.

As mentioned above, observations in the field and analysis of the axial planes measured in the field show that the Caledonian deformation history of this area can be subdivided into two main components: a ductile sequence and a brittle sequence. The ductile sequence can be recognized in strongly folded rocks and fault propagation folds (closer to the brittle regime). For example in the Steinsfjorden Formation at the backside of Utøya (***Fig. 59***) a very ductile signature is observed. The brittle sequence consists of both fore and back thrusts; the back thrusts are most likely out of sequence, though roughly at the same time as the fore thrusts as they do not deviate from the thrusting population (***Fig. 35b***). Both sequences contribute to similar structures that can be observed nowadays. The major popup found in the south part of the study area, bounded in the north by the major back thrust at the Utstranda section (profile A-A' and C-C', ***Fig. 13 and Fig. 22***), is an example of this. In all parts of this popup both viscously induced structures as well as brittle induced structures are present. The sequences are part of a major progressive deformation event, and seem to have occurred after deposition of all the Palaeozoic lithologies in the study area. The structures are related

to the Scandian deformation event (*e.g. Nystuen, 1981; Morley, 1994; Roberts, 2003*), which was the major Caledonian event and started mid-Silurian (425Ma) to early Devonian (395Ma). The main direction of tectonic transport recognized in this study is NNW-SSE, which corresponds with the direction of tectonic transport of the Osen Nappe *(Nystuen, 1981; Bruton et al., 2010)*. Locally in the upper part of the stratigraphy (from Ringerike Group down to at least the Vik formation) in the studied area the transport direction is NNW due to dominance in back thrusting, such a geometry can be described as a popup with a relatively small fore thrust. The net transport direction in the area will most likely be SSE, as lower in stratigraphy back thrusts are less abundant (Modum, profile E-E') and a sole thrust is present causing major deformation in the foreland *(Nystuen, 1981; Morley, 1994; van den Broek, 2015; Weekenstroo, 2015)*. Detailed structural evolution with different phases of back thrusts and multiple deformation phases (D's) as documented by for example Hjelseth (2010) and Kleven (2010) are not recognized in this study, though both study areas did not have a complete overlap with the current study area. An agreement is found in the sequence that is presented above; with early folding, followed by major fore thrusts and later back thrusts, all in one progressive event, the Scandian phase.

The study of Hjelseth (2010), of which the study area is due north from the Rytteråker peninsula, four sequences of events are distinguished; two folding and two faulting (fore and back thrusting).

In the field multiple folds are recognized, though analysis shows they most likely are formed by the same mechanism and at the same time. This also applies for the thrusting and the transport directions (NNW-SSE) and structural styles (dominant back thrusting) are recognized *(Hjelseth, 2010)*.

The study done just south if this paper's study area, by Kleven (2010) has similar findings as this study. Four stages of deformation are presented, though no distinction between folding and faulting is being made. The high abundance of back thrust is being stated, which is in full agreement with this study. Also thrust orientations and fold axis are consistent throughout the area from the area of Hjelseth (2010), through this study's area, to the area of Kleven (2010).

## 6.2. Large-scale structures

The present data shows heterogeneity in deformation style, but homogeneity in principle stress orientation, this is in coherence with observations from previous studies, for example the distinction between domains with folds and faults *(Nystuen, 1981; Morley, 1994)* and homogeneous transport directions and corresponding fold axis (*e.g. Sippel et al., 2010; Bruton et al., 2010; Kleven, 2010; Hjelseth, 2010; Weekenstroo, 2015; Verdonk, 2015; Van den Broek, 2015*).

To the north of this study area (east of Hønefoss and Klekken), a major fault (Klekken fault) and footwall syncline is recognized and just north from there, in de Viul area the basal layer is
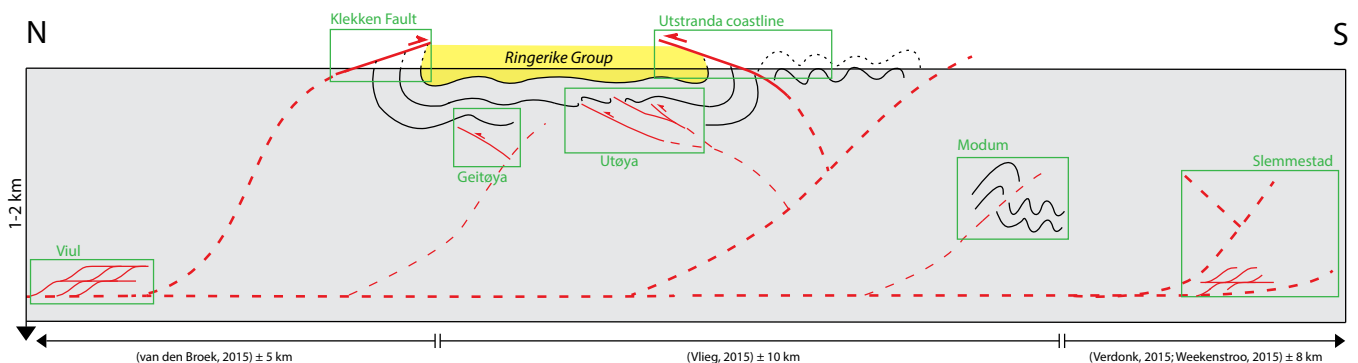


Fig. 60. Large scale profile using data from (from north to south) van den Broek, 2015; Vlieg, 2015; Verdonk 2015 and Weekenstroo, 2015. Key structures from key localities have been illustrated and correlated to create an overview schematic model of the Oslo area. From this study the major popup, strong back thrusting and competence differences are visible (see text for details).

49

recognized *(Nystuen, 1981; Morley, 1994; Bruton et al., 2010; van den Broek, 2015)*. The major footwall syncline is at the same level both stratigraphically and tectonically as this paper's study area, and deformation in between the Klekken fault and the major back thrust recognized on profiles A-A' and C-C' is limited. In between these two major structures a region of low deformation is present, with structural style that can be described by the sections through the islands (north part of A-A' and B-B'). Thus large scale open folding with lower amplitude is the structural style, which can also be recognized at the gas station of Vik, which lies along the road from this study's area and the Viul and Klekken area. At Viul, where the main lithology is a pre Cambrian bitumous shale (Alum shale), there the structuring is dominated by duplexes and shear zones. It is expected that the basal decollement is situated in this lithology and at this locality *(Nystuen, 1981; Morley, 1994; Bruton et al., 2010; van den Broek et al., 2015)*. This basal decollement can be followed towards the south until the area of Slemmestad *(Morley, 1994)*, where the last thrusts are outcropped and the basal layer dies out most likely in a blind thrust *(Nystuen, 1981; Morley, 1994; Weekenstroo et al., 2015)*. At the southernmost outcrop observed in this study (profile E-E') a structural style is recognized that is unique for this level in the stratigraphy and is also found near Oslo on Fornebu and Bygdøy beaches. This style is characterized by major fore thrusts with associated drag folding and relatively small-scale fold trains (several folds of different geometry and size in a row) in the footwalls and is present mainly in lithologies that are lower in stratigraphy than the Vik Formation.

The summarizing profile of these studies (*Fig. 60*) shows this correlation between the northern part with the basal decollement layer and the Klekken fault upsection *(Bruton et al., 2010; van den Broek, 2015)*, the southern part with the fold trains and fore thrusts in middle part of the stratigraphy *(Morley, 1994; Verdonk, 2015)* and the frontal (blind) thrust and deformation associated with the lower part of the stratigraphy *(Morley, 1994; Weekenstroo, 2015)* and area of this study, which lies in between. The overview picture (*Fig.*

*60*) shows a typical foreland thrust belt setting, as shown already by Nystuen in 1981. He proposed that the Osen nappe and the Røa nappe are one tectonic domain bounded by a basal decollement in the Precambrian shales. The Oslo region in this view lies in the Osen part of the Osen-Røa nappe and consists of the very tip of this nappe, near or just south of Slemmestad *(Nystuen, 1981; Morley, 1994; Bruton, 2010; Weekenstroo, 2015)*.

Competence contrast in the stratigraphy seems to play a major role in the distribution of strain, causing heterogeneous distribution of structural styles. Especially the presence of the strong Ringerike Group seems to have great influence on the structural style. The lack of strong deformation structures in the area between the Klekken fault and the Tyrifjorden area shows the Ringerike Group is subduing the deformation by its strong cohesive character at that level. As can be recognized at lower stratigraphic localities, for example at Modum (profile E-E', *Fig. 31*), there may be higher strain intensity levels, though they do not push through to the surface (through the Ringerike Group). The structural style typical for the level just below the Ringerike Group is very open low amplitude folding. The fact that at the Utstranda coastline this major popup is situated may imply that there was a weak zone in the Ringerike Group, causing strain to localize. This occurs both laterally (inside the popup and outside the popup a major variation in deformation intensity is present) and vertically (going down in level/stratigraphy increases strain). The presence of the popup with high internal strain also influences the strata that lies close to or under this popup, for example the footwall deformation in the Ringerike sandstone in profile C-C' and back thrusting at Geitøya en Utøya (that are located outside the popup). When going lower in stratigraphy thrusting and higher strain intensity features become more abundant *(Bruton et al., 2010)*, like for example back thrusting in the Sælabonn bay *(Hjelseth, 2010)* and the fold train and major fore thrust at Modum (profile E-E'). On a smaller scale this lithological strength difference also occurs, with less, though still visible, impact on the structural style. An example can be found in section C-C'

50

(*Fig. 22*), at the Lihøgdaveien ramp outcrop (*Fig. 23 and Fig. 24*), where the deformation style is characterized by a very brittle tight to isoclinal folding for around 50m, followed by a style with more open folds and some minor faulting just south of the ramp outcrop. The key to this style difference is again the competence, or strength difference of the lithologies, as the ramp outcrop compiles Braksøy Formation, and just south of there lays the Bruflat Formation. Due to the higher shale content in the Braksøy Formation the deformation style in this lithology is much more brittle and intensified. The Braksøy Formation may also be a layer that is significant deformed by layer parallel shortening. Since strain subduing is occurring just below the Ringerike Group, due to its strong nature, the strain that transfers from below should be directed laterally in stead of vertically, thus in layer parallel slip. A weaker shale layer like the Braksøy Formation may act as such a layer.

In order to understand how the structures we find in the field have evolved into what they are today, and what mechanisms have caused the distinctive styles to form analogue models are performed. In these models the focus for this research is on the high abundance of back thrusts and the impact of rheology (strength differences) on structural style.

## 6.3.    Mechanisms of back thrusting

In previous studies several theories are proposed as a mechanism for high abundance of hinterland-directed thrusts in foreland basins
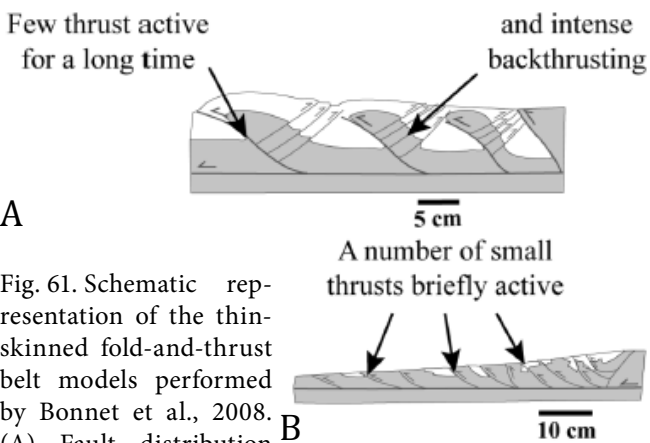


Fig. 61. Schematic representation of the thin-skinned fold-and-thrust belt models performed by Bonnet et al., 2008. (A) Fault distribution with high sedimentation rates. (B) Fault disribution with low sedimentation rates.
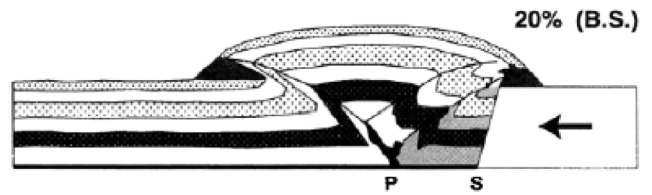


Fig. 62. Experiment with a high angle slope indenter performed by Bonini et al., 1999. Hinterland-directed (right in this image) are abundant, see text for more details.

(e.g. Bonnet et al., 2008; Bonini et al., 1999; 2000; Smit, 2003). High sedimentation intensity may induce back thrusting dominance in a thin-skinned thrust belt (*Fig. 61*) *(Bonnet et al., 2008)*. In a series of analogue experiments varying sedimentation and erosion in an inclined model set-up with silica powder and glass beads at the base the theory is demonstrated. With low amount of sedimentation more foreland-directed thrusts are formed, but the thrusts are small and are not active for a long amount of time. With high amount of sedimentation the thrusts become bigger and displace more material. Also high amount of hinterland-directed thrusts are recorded (*Fig. 61a*). It is generally know that sedimentation (and erosion) can influence thrusting and thrust direction, so it should be taken into account with the analysis of the present study's models, as no surface material transport was incorporated. It also applies to the study area, to for example the Ringerike group, which shows some significant sedimentation (*Fig. 8*) at the time of propagation of deformation. The major back thrusts in the Oslo foreland basin are also situated in the upper part of the sequence (Ringerike Group-Sælabonn) similar to the results from Bonnet et al., 2008. In the more frontal part of the foreland basin the sedimentation accumulation is lower and also less back thrusts are present *(Nystuen, 1981; Morley, 1994; Bruton et al., 2010)*.

A second theory for initiating high amount of back thrusts in a thin-skinned fold-and-thrust belt may be the presence of an obstacle in the foreland *(Bonini et al., 1999)*. Linked to the Swiss Alps models were constructed with a rigid indenter (representing the Adriatic plate) with variable front angle. These experiments cover a larger scale, though a mechanism comparison can be made
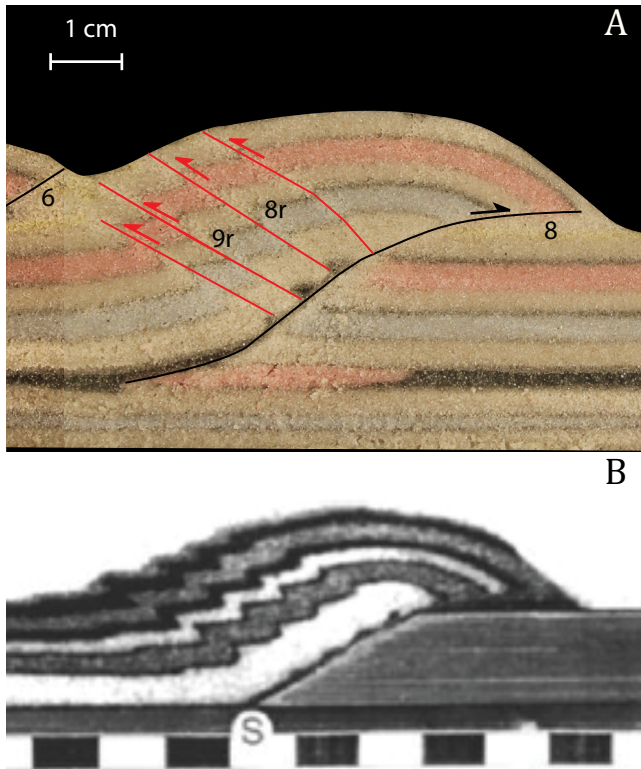
Fig. 63. Combination figure to illustrate similarities between a popup in model 2 (A) and a popup in a model from Bonini et al., 1999, with a lower angle indenter (B). In this case the left of the image is the hinterland, see text for more details

with the smaller scale models of this study. With low frontal angles a series of fore kinks form, initiated at the toe of the indenter, moving up over the footwall. With higher angles a popup is formed, with only one foreland-directed thrust and a few hinterland-directed thrusts (*Fig. 62*). Two correlations can be made between this study and Bonini et al. (1999): (1) an obstacle with high frontal angle causes back thrusting, this can be described as vertical escape between two (relatively) rigid bodies. Major displacement on large-scale hinterland-directed thrusts is key in this process; (2) an obstacle with low frontal angle causes a high amount of trusting to occur away from the indenter. In case the obstacle lies in the foreland, like in this study (opposite from Bonini et al, 1999) this would mean a high amount of hinterland directed thrusts (*Fig. 63b*), which can also be recognized in the results from model 2 (*Fig. 63a*). With higher indenter frontal angle the back thrusting would occur, only again with higher displacement and lower numbers.

As mentioned above the brittle-ductile decoupling influences the abundance of back thrusts: strongly decoupled parts of the experiments back thrusts develop *(Smit, 2003)*. Looking from a different perspective, Davis and Engelder (1987) suggested that back thrusting could be induced by non-frontward sequence thrusting, thus starting with thrusting in the foreland and developing further deformation features between the frontal thrust and the orogen. However in analogue experiments of Smit (2003) and this study, back thrusts occur in both frontward and backward sequences. This then implies that strain rate or sequence is no determinant for thrust-vergence *(Smit, 2003)*. The final argument for high dominance of back thrusts may be the above-mentioned weak BD-coupling *(Smit, 2003)* occurring possibly in the Utstranda subsurface. The cause of this weak BD-coupling may be extrusion or concentration of ductile material in the lower part of the stratigraphy, as is seen in model 1 and 2 (*Fig. 41 and Fig. 44*).

## 6.4. Impact of weak zones

A different aspect that is recognized in the analogue models is the high mobility of the weak layers. This is also documented in the indenter study of Bonini et al. (1999), where a weak basal layer is intruded into the overlying strata (vertical escape) following the faults (*Fig. 62*). From point p in the figure the fore and back thrusts propagate, suggesting a correlation of the brittle-ductile coupling and thrusting, as mentioned before. Also a proposition is made regarding the rigid indenter and the effective indenter. As can be seen in the figure, the strata close to the steep rigid indenter is not deformed, making it part of the effective indenter (*Fig. 62*). This is similar to the low strain zone that is observed in the final experiment (*Fig. 55*); the size of the effective indenter here is very significant compared to the rigid indenter. When the weak layer is at the base in an indenter study *(Bonini, 2000)* it also forms an effective indenter, or ramp. In this case deformation in the hanging wall is minimized and the brittle crust will be transported over the effective ramp. This can be recognized in one particular model from this study, the earlier mentioned nice

flat-ramp-flat structure in the middle of model 2 (*Fig. 44*) shows in its lower part this effective ramp geometry. Though probably due to the minor thickness of the weak layer and the interaction of the upper brittle part with the lower brittle ramp back thrusts have developed in the hanging wall.

Similar as in the experiments: in nature weak layers tend to localize the strain and become mobile. An analogue experiment example of the Aljibe thrust imbricate from the Gibraltar Arc *(Luján et al., 2003)* shows a strong link between rheological properties of the weak layer (in this study at the base) and the structures in the overlying thrust wedge. The models performed were constructed with different basal domains (ductile/brittle) and different geometries of the ductile domain. It is proposed that the presence of the viscous material in the model enhances the development back thrusting and the outward migration of the deformation front *(Luján et al., 2003)*. Whether there is a link between the presence of weak material and higher amount of hinterland-directed thrusts is an interesting question to ask. It may be that in a less stable system (with the presence of a weak layer) more back thrusting would occur than in a homogeneous, stable system. It is shown that the magnitude of coupling between brittle and ductile material influences thrust orientation *(Smit, 2003)*, but linking it to presence or the lack of a weak component remains a question. In nature though this may be unrealistic, as in almost every system a (relatively) weak component is present. Linking this theory directly to the Oslo foreland basin also poses problems; the basal layer is weak enough to transfer strain towards the foreland, though no structures are- or evidence is found that the weak layer has undergone viscous behavior. Rocks in the Utstranda popup do show a ductile character, which seems a combination of strong strain localization *(Bruton et al., 2010)* (as it is one of the few places where strain can be transferred up section) and presence of a lot of fluid in the system during deformation (as discussed above).

## 6.5. Natural examples

The experimental results are applied to natural foreland basins like the Ebro basin and the Zagros fold and thrust belt. The experiments are initially constructed using constraints from the Caledonide foreland basin, which has proven to be very valuable. All natural examples are typical foreland basins with characteristic lithologies and similar dimensions; therefore it is interesting to see what correlations can be made with the analogue experiments. Key in this comparison are the typical foreland basin parameters *(Chapple, 1978)* that are the basis for this modeling study.

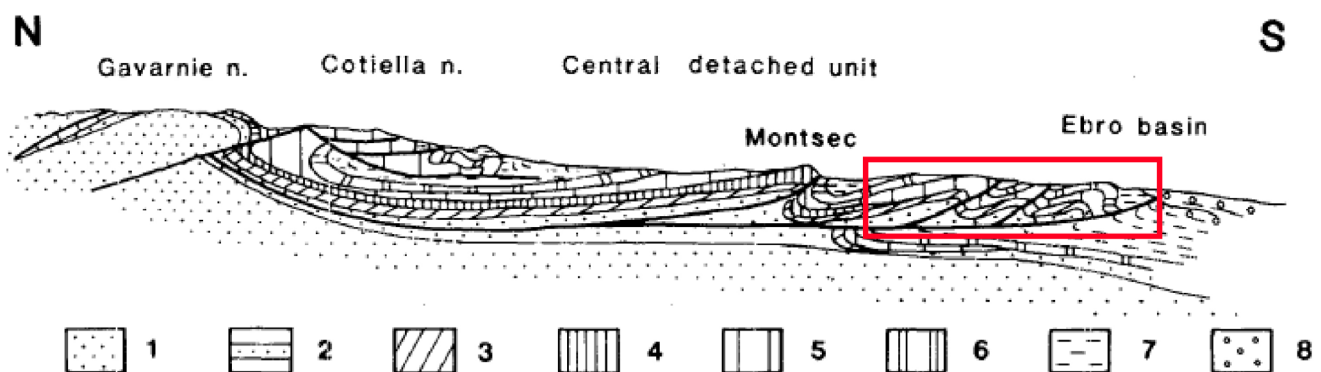A well-studied foreland basin like the Southern Pyrenees provides excellent material to



Fig. 64. Section through the Southern Pyrenees with (1) Paleazoic basement rocks; (2) Permotriassic molasse, volcanic rocks and upper Triassic evaporites; (3) Jurassic; (4) Lower Cretaceous; (5) Upper Cretaceous; (6) Eocene Alveoline bearing limestone; (7) Middle Eocene marls and flysch; (8) Upper Eocene and Oligocene molasse. Red box shows the thin-skinned frontal part of the foreland basin that has a simlar geometry as the Oslo foreland basin (Osen part of the Osen-Røa nappe complex). Figure from Sugrañes, 1983.

compare this study's results with. In the southern domain of the basin, the thin-skinned part, typical structures like ramp-flat-ramp and a basal weak layer are present *(Sugrañes, 1983; Puigdefàbregas et al., 1992; Vergés, 1995)*. Characteristic for the Southern Pyrenees are the large piggyback basins (e.g. Tremp basin), bounded by a major basal salt decollement, comparable to the Osen-Røa decollement *(Nystuen, 1981)*. The scale and character of the basal decollement differs from the Osen-Røa basal fault. As the basal friction of salt is lower than that of shale the foreland in the Pyrenees extends further out. The southernmost part of the foreland basin, which runs into the Ebro basin *(Sugrañes, 1983)*, can be correlated to the Osen-Røa nappe in the Oslo area (***Fig. 64***). The dominance in back thrusting is less apparent in the Southern Pyrenees *(Choukroune et al., 1990; Puigdefàbregas et al., 1992; Vergés, 1995; Teixell, 1996)*, this may be due to differences in rheological characteristics of the foreland basin.

Similar to the Southern Pyrenees, foreland basins south of the Zagros belt also provide good correlation material and are well studied in field (e.g. Sherkati and Letouzey, 2004; McQuarrie, 2004) and analogue studies *(Bahroudi and Koyi, 2003)*. What seems key to the evolution of the southern Zagros belt is the sedimentary infill of the foreland basins, thus strength properties of the column. Just like in the Oslo region, the southern Zagros belt seems to have a very strong cap rock (e.g. Ringerike Group), giving some interesting expressions in the distribution of strain and deformation styles in the sequence below *(Sepher et al., 2006; Sherkati and Letouzey, 2004)*. In the Zagros belt succession at some locations a strong and thick cover rock is present, where at other locations a thin and weak one is present. The alternation of structural style closely coincides with this cover rock alternation, creating large-scale box folds. Also at smaller scale, within this major box folds, the deformation is controlled by the strength of the individual layers. Apart from the dominant influence of the cover rock, there is also an important role of the basal weak layer, which in the Zagros belt the Hormuz salt will be *(Sepher et al., 2006)*. The spatial difference in structural style seen in the Zagros is due to uneven spatial distribution of the basal layer, causing for example an irregular deformation front, as is shown in analogue experiments by Bahroudi and Koyi, 2003.

# 7.  Synthesis

By varying mechanical and rheological parameters in the analogue models different end-scenarios are constructed that all project the effects caused by these variations. In the following part these end-scenarios are compared to the field observations from the Oslo foreland basin with special focus on heterogeneities in structural style and the dominance in back thrusting.

In the field four tectonic sub areas are defined, each with its own distinctive structural style; a domain with large scale, low amplitude folding (sub area 1), a fault dominated domain (sub area 2), a domain with minimal deformation (sub area 3) and a domain with small scale fold trains an less faults (sub area 4). In terms of deformation history these areas do not differ, they all have undergone the same principle stress field, visible in a region wide fold axis of 62/9 and similar fault orientations. Density plots of all the planes measured in the study area suggests an asymmetrical fold system with hinges tipping towards the NNW, which corresponds with a high amount of back thrusts, thus a local tectonic transport direction towards the NNW along the regional NNW-SSE tectonic transport line *(Nystuen, 1984; Morley, 1994; Bruton et al., 2010)*. The axial planes plot in two populations, one associated with drag folds close to major (back) thrusts and the other associated with purely folding. Both axial plane populations are folded by the same fold axis, suggesting a progressive deformation event. Combining data from the field summarized in a schematic overview, with the analogue model results clarifies the origin of the structures (***Fig. 65***).

The presence of the weak interlayer (putty 1) in the models resulted in strong evidence for layer parallel shortening (***Fig. 65b***) and high mobility of the weak layers (***Fig. 65 a, b and c***), causing strong deformation within- and around the weak
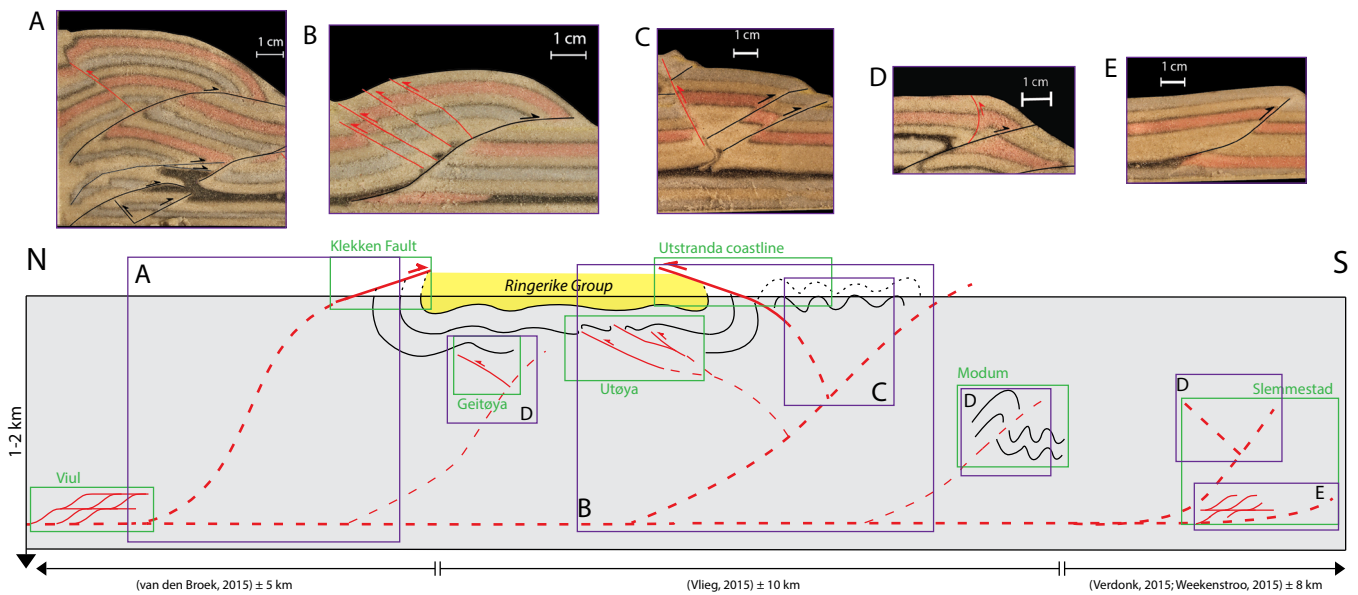
Fig. 65. Combination figure of the schematic overview image (figure 60) and several key structures from the model cross sections. (A) Back part of model 2, section B-B' (figure 45); (B) Middle part of model 2, section B-B' (figure 45); (C) Middle part of model 3, setion C-C' (figure 49); (D) Frontal part of model 5, section E-E' (figure 55) and (E) Frontal part of model 3, section C-C' (figure 49). All images from the models are mirrored to match the direction of movement of the Oslo foreland schematic section (movement direction towards the right, or S (SSE)). Examples of the structures (A-E) are the clearest illustrations, in the model sections multiple examples that fit structures in the schematic section are present. See text for more details.

layer. These are features that are also recognized in the field; the strong difference in structural style between for example the relatively undeformed Ringerike Group and the strongly faulted and folded mid- to lower Silurian sequence below illustrates this. The difference in deformation intensity, and the localization of deformation in for example the major back thrust at the Utstranda road section require layer parallel shortening in weaker layers to accommodate strain.

Also the open large-scale folding structural style in the north part of study area (and all the way to the northern Ringerike area; (*e.g. Nystuen, 1984; Bruton et al., 2010; Van den Broek (2015)*) requires layer parallel shortening along weaker layers. These weaker interlayers are relatively abundant in the sequence from the basal layer, the Alum shale *(Nystuen, 1984; Bruton et al., 2010; Van den Broek, 2015)*, up to the Steinsfjorden formation. The Ringerike Group on top of this sequence is relatively massive and strong. In the field also specific strength (and competence) contrasts have been observed. For example at the Lihøgdaveien ramp outcrop, where the Braksøy Formation is

deformed intensely between the relatively weakly deformed Steinsfjorden and Bruflat Formations (*Fig. 23 and Fig. 24*). The deformation at this locality has a very brittle signature, in contrast to for example an outcrop in profile D-D' at the cross road between the E16 and Utstranda with a very ductile character in the nodular limestones of the Steinsfjorden Formation. The latter may be the effect of high mobility of weak material in the root of the back thrust/pop up, as is also observed in the analogue models (*e.g. Fig. 41, Fig. 44, Fig. 49, Fig. 52 and Fig. 55*), or just the effect of deformation of very wet sediments as discussed above (*Fig. 59*).

The Viul area with its basal layer shows the origin of a major thrust up section (with possible levels in between *(Bruton et al., 2010)*, equivalent to the Klekken fault. In the model some major thrusts are recognized, though the example that is taken from model 2 (*Fig. 65a*) shows the occurrence of major drag folds along major fore thrusts (*Fig. 65d*). These large-scale drag folds can also be recognized in the field; just northeast of Klekken a section from the Venstøp Formation to the Steinsfjorden Formation, which is half of the

55

Palaeozoic stratigraphy in this area, is completely bended into a drag fold *(Van den Broek, 2015)*. At a smaller scale (***Fig. 65d***) these drag faults are also recognized in the Modum section, as well as in the Bygdøy and Slemmestad area *(Morley, 1994; Verdonk, 2015; Weekenstroo, 2015)*. High amount of back thrusts, as recognized in the Utstranda area (from Geitøya and Utøya to the south part of the Utstranda road section) are also observed in the experiments (***Fig. 65b***). The high mobility of the putty in the experiments caused it to move along the fore thrust, being at the root of the small pop-ups. Weak brittle-ductile coupling *(Smit, 2003)* of the viscous material in this root and the presence of a strong ramp most likely caused the dominance in back thrusting in this case. These are both theories can also be applied to the Oslo foreland basin. Apart from the back thrusts, also layer parallel shortening is observed in the images of the models (***Fig. 65b***). This occurs in the weaker viscous material, and is also recognized in weaker layers in the field (e.g. Alum shale), as discussed above. In the front of the models sometimes a frontal fore thrust occurs (***Fig. 65e***), preceded by a domain of lower deformation intensity (e.g. large scale, low amplitude folds). This can be linked to several locations in the Oslo foreland basin, though in the Slemmestad area the thrusts are in the southern most tip of the system *(Morley, 1994; Weekenstroo, 2015)*. Low deformation intensity domains are recognized all over the area; in the Slemmestad domain *(Weekenstroo, 2015)*, but also in the north of the present study area and in between the present study area and the study area of van den Broek, 2015.

As for the basal inclination that is incorporated in the models the field data correlates good. Combining the data from Verdonk (2015) and Weekenstroo (2015) with the data from Van den Broek (2015) and the present study a foreland basin system with an oblique basal layer is recognized. Also from previous studies that have analyzed the geometry of the foreland basin (*e.g. Murchison, 1847; Kjerulf, 1862; Nystuen, 1984; Morley, 1994; Bruton et al., 2010*) an increase in accommodation space is observed in the Ringerike area, compared to the Slemmestad area. Also worth to mention is the higher amount of Alum Shale outcrops in

the south (near Slemmestad and more south towards Holmestrand and Skien). The effect of this basal inclination in the models is a large area of low deformation in between the frontal thrust and structures closer to the orogen (***Fig. 65e***). In the field this is also observed in for example the area between the Klekken fault *(Van den Broek, 2015)* and the back thrust at the Utstranda road section.

The introduction of a strong viscous material in the models caused strain localization in other parts of the models (mostly in back of the models; e.g. model 5, ***Fig. 55***). In the field this is also recognized, as there are domains where almost no strain is expressed (though maybe transferred layer parallel and in large-scale folding as mentioned above) and domains with high strain (e.g. Klekken fault and the Utstranda pop-up). As the strong component in the field, the Ringerike Group, is dominantly present in almost the whole area as top sequence the effect of it on deformation is different than in the experiments, as in the experiment the strong component was only present in a small part of the model. In the field it seem like strain has localized at weak zones in the Ringerike Group. As mentioned above, the relatively strong Ringerike Group also influences its surroundings, reducing strain in layers in the direct vicinity of it, just like is observed in the experiments. It is also interesting to see the Ringerike Group more as an obstacle (for example an obstacle south of the Utstranda popup) causing strain localization in front of this obstacle as is observed in the experiments. The dominance in hinterland directed trusts could be related to this, as is discussed above *(Bonini et al., 1999; Smit, 2003)*.

Finally the tectonic level model by Bruton et al., 2010 is revised in the present study area (***Fig. 66***). The view that was presented in their paper was in the right direction, though the dominance of back thrusting (***Fig. 66***) and homogeneity in principal strain axes have been underestimated. The heterogeneity in structural style that is recognized throughout the Oslo foreland basin (*e.g. Morley, 1994; Bruton et al., 2010*) is also recognized in the present study area. Especially the large-scale folds in the north part and the thrusting in the south part are strongly contrasting.
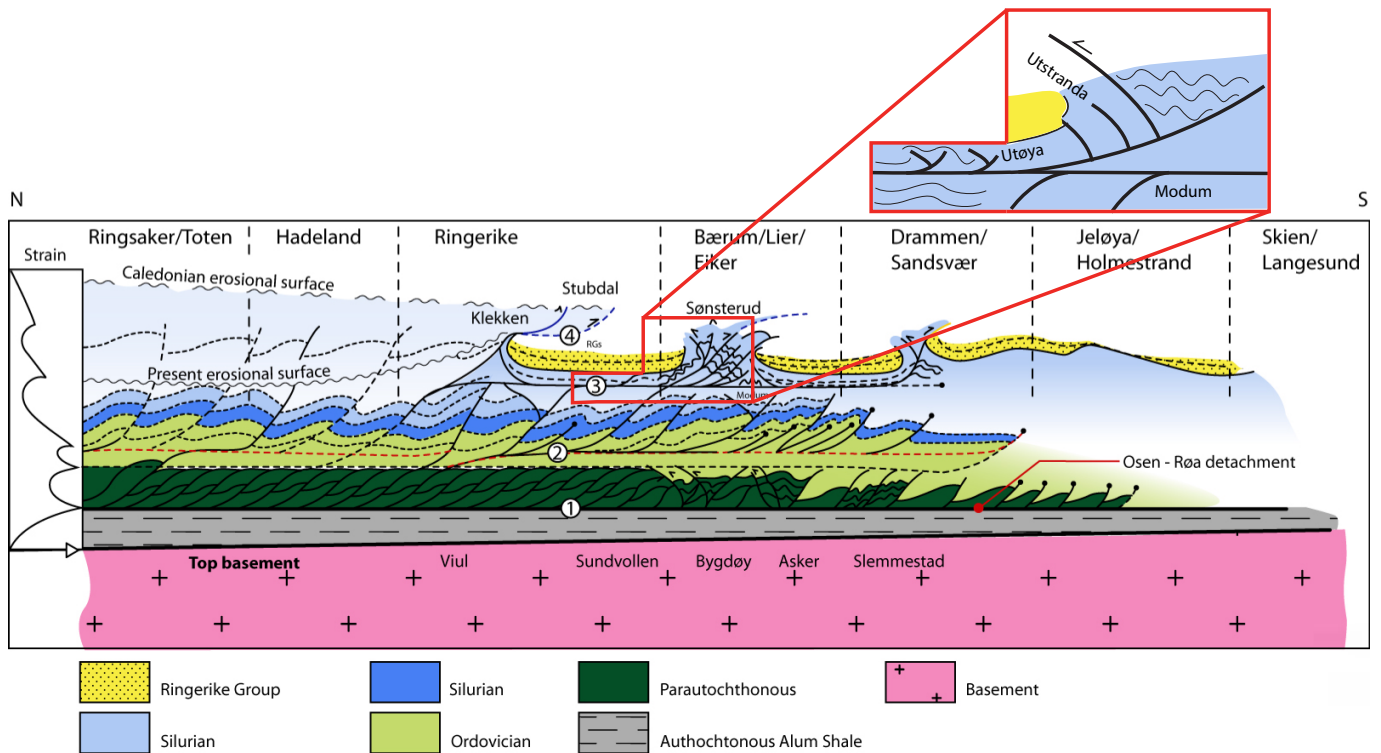
Fig. 66. Revision figure of the structural level model proposed by Bruton et al., 2010. The present study shows important details in the indicated Sønsterud to Sundvollen area. The difference in structural style, indicated by sub areas in this study, dominance in back thrusting , homogeneous deformation indicators and the analogue modeling research, are an addition to the study by Bruton et al., 2010.

The Oslo foreland basin can be linked in general to various foreland basins in the world, like for example the Southern Pyrenees and the Zagros belt. At greater detail though variations may occur but as recorded in for example the Zagros belt but also this study, variation always closely coincide with variations in rheology of the sedimentary sequence.

# 8.    Conclusions

In the Oslo region an area wide consistent fold axis is observed of 62/9 and a density plot of all the planes measured shows an asymmetrical system with shallow south dipping planes and steep north dipping planes, suggesting a (local) NW transport direction. This coincides with the dominance of back thrusts in the area. Two structure-forming events are recognized in the field from axial plane plots; an early viscous event creating refolded- and fault propagation folds, and a later brittle event creating major fore- and, in this area, mainly back- thrusts. The lithologies have

undergone a sub green schist metamorphic facies, thus the brittle/ductile contrast is related to fluid content of the strata. The apparent homogeneous stress measurements show that one progressive deformation event occurred which was the major structure forming event of the Caledonian Orogeny; the Scandian deformation event.

Fundamental questions on dominant structures and influence of rock rheology in the Oslo region are answered using analogue modeling. Besides strong dependence on a weak basal layer also the effect of a strong cover rock or obstacle is recognized, creating distinct structural styles and a possible explanation for dominance in back thrusting and the heterogeneous distribution of structural styles in the study area.

Zooming out to basin scale (from Viul to Slemmestad) and combining data from Van den Broek, 2015; Verdonk, 2015 and Weekenstroo, 2015 a structural model can be constructed that shows close resemblance with the model

from Bruton et al., 2010. The details from the present study, like for example the structural sub areas, dominance in back thrusting, homogeneous deformation indicators and analogue modeling study, can be seen as an addition to it.

# 9.   Acknowledgments

# 10.   References

Allmendinger, R. W., Cardozo, N. and Fisher, D. M. (*2011*). Structural Geology Algorithms: Vectors and Tensors. Cambridge University Press.

Bahroudi, A. and Koyi, H. (*2003*). Effect of spatial distribution of Hormuz salt on deformation style in the Zagros fold and thrust belt: an analogue modelling approach. Journal of the Geological Society **160**, *719-733*.

Bergström, J. and Gee, D. G. (*1985*). The Cambrian in Scandinavia. In: D. G. Gee & B. A. Sturt (eds.) The Caledonide Orogen–Scandinavia and Related Areas, pp *247-271*. John Wiley & Sons.

Bjørlykke, K. O. (*1901*). Overskyvninger i den norske fjeldkjæde. Naturen. Kristiania.

Bockelie, J. F. (*1978*). The Oslo region during the early Palaeozoic. In: Tectonics and geophysics of continental rifts, pp *195-202*. Springer.

Bonini, M., Sokoutis, D., Mulugeta, G. and Katrivanos, E. (*2000*). Modelling hanging wall accommodation above rigid thrust ramps. Journal of Structural Geology **22**, *1165-1179*.

Bonini, M., Sokoutis, D., Talbot, C. J., Boccaletti, M. and Milnes, A. G. (*1999*). Indenter growth in analogue models of Alpine-type deformation. Tectonics **18**, *119-128*.

Bonnet, C., Malavieille, J. and Mosar, J. (*2008*). Surface processes versus kinematics of thrust belts: impact on rates of erosion, sedimentation, and exhumation– Insights from analogue models. Bulletin de la Societe Geologique de France **179**, *297-314*.

Brenchley, P. J. and Newall, G. (*1977*). The significance of contorted bedding in upper Ordovician sediments of the Oslo region, Norway. Journal of Sedimentary Research **47**, *819-833*.

Brøgger, W. C. (*1882*). Paradoxiden Ölandicus-nicäet ved Ringsaker i Norge. GFF **6**, *143-148*.

Brueckner, H. K. and van Roermund, H. L. M. (*2004*). Dunk tectonics: a multiple subduction/eduction model for the evolution of the Scandinavian Caledonides. Tectonics **23**, *1-20*.

Bruton, D. L., Gabrielsen, R. H. and Larsen, B. T. (*2010*). The Caledonides of the Oslo Region, Norway– stratigraphy and structural elements. Norwegian Journal of Geology/Norsk Geologisk Forening **90**, *93-121*.

Byerlee, J. (*1978*). Friction of rocks. Pure and applied geophysics **116**, *615-626*.

Chapple, W. M. (*1978*). Mechanics of thin-skinned fold-and-thrust belts. Geological Society of America Bulletin **89**, *1189-1198*.

Choukroune, P., Roure, F., Pinet, B. and Team, E. P. (*1990*). Main results of the ECORS Pyrenees profile. Tectonophysics **173**, *411-423*.

Cocks, L. R. M. and Torsvik, T. H. (*2002*). Earth geography from *500* to *400* million years ago: a faunal and palaeomagnetic review. Journal of the Geological Society **159**, *631-644*.

Dallmeyer, R. D., Andréasson, P. G. and Svenningsen, O. (*1991*). Initial tectonothermal evolution within the Scandinavian Caledonide accretionary prism: constraints from *40*Ar/*39*Ar mineral ages within the Seve Nappe Complex, Sarek Mountains, Sweden. Journal of Metamorphic Geology **9**, *203-218*.

Davies, N. S., Turner, P. and Sansom, I. J. (*2005*). Caledonide influences on the Old Red Sandstone fluvial

systems of the Oslo Region, Norway. Geological Journal **40**, *83-101*.

Davis, D., Suppe, J. and Dahlen, F. A. (*1983*). Mechanics of fold-and-thrust belts and accretionary wedges. Journal of Geophysical Research: Solid Earth (*1978–2012*) **88**, *1153-1172*.

Davis, D. M. and Engelder, T. (*1985*). The role of salt in fold-and-thrust belts. Tectonophysics **119**, *67-88*.

Del Ventisette, C., Montanari, D., Sani, F., Bonini, M. and Corti, G. (*2007*). Reply to comment by J. Wickham on "Basin inversion and fault reactivation in laboratory experiments". Journal of Structural Geology **29**, *1417-1418*.

Essex, R. M., Gromet, L. P., Andréasson, P. G. and Albrecht, L. (*1997*). Early Ordovician U-Pb metamorphic ages of the eclogite-bearing Seve nappes, Northern Scandinavian Caledonides. Journal of Metamorphic Geology **15**, *665-676*.

Finch, E., Hardy, S. and Gawthorpe, R. (*2003*). Discrete element modelling of contractional fault-propagation folding above rigid basement fault blocks. Journal of Structural Geology **25**, *515-528*.

Gaál, G. and Gorbatschev, R. (*1987*). An outline of the Precambrian evolution of the Baltic Shield. Precambrian Research **35**, *15-52*.

Gale, G. H. and Roberts, D. (*1974*). Trace element geochemistry of Norwegian Lower Palaeozoic basic volcanics and its tectonic implications. Earth and Planetary Science Letters **22**, *380-390*.

Gayer, R. A., Rice, A. H. N., Roberts, D., Townsend, C. and Welbon, A. (*1987*). Restoration of the Caledonian Baltoscandian margin from balanced cross-sections: the problem of excess continental crust. Transactions of the Royal Society of Edinburgh: Earth Sciences **78**, *197-217*.

Gee, D. G. (*1975*). A tectonic model for the central part of the Scandinavian Caledonides. American Journal of Science **275**, *468-515*.

Gee, D. G. (*1986*). Middle and upper crustal structure in the central Scandinavian Caledonides. Geologiska Föreningen i Stockholm Förhandlingar **108**, *280-283*.

Gee, D. G. and Sturt, B. A. (*1985*). The Caledonide orogen: Scandinavia and related areas. *1266* pp. Wiley.

Gunby, I. J., Siedlecka, A., Tveten, E. and Larsen, B. T. (*2003*) Berggrunnskart *1814* IV Lier *1:50000*. Norges Geologiske Underskolse.

Halvorsen, T. (*2003*). Sediment infill dynamics of a foreland basin: the Silurian Ringerike Group, Oslo Region, Norway., University of Oslo. *166* pp.

Hartz, E. H. and Torsvik, T. H. (*2002*). Baltica upside down: a new plate tectonic model for Rodinia and the Iapetus Ocean. Geology **30**, *255-258*.

Henningsmoen, G. (*1978*). Sedimentary rocks associated with the Oslo Region lavas. In: J. A. Dons & B. T. Larsen (eds.) The Oslo Paleorift. A Review and Guide to Excursions, pp *17-24*. Norges Geologiske Undersøkelse.

Hjelseth, E. (*2010*). Caledonian structuring of the Silurian succession at Sundvollen, Ringerike, southern Norway, University of Oslo, Oslo. *156* pp.

Holtedahl, O. (*1920*). The Scandinavian 'Mountain Problem'. Quarterly Journal of the Geological Society **76**, *387-403*.

Hossack, J. R. and Cooper, M. A. (*1986*). Collision tectonics in the Scandinavian Caledonides. Geological Society, London, Special Publications **19**, *285-304*.

Hubbert, M. K. (*1937*). Theory of scale models as applied to the study of geologic structures. Geological Society of America Bulletin **48**, *1459-1520*.

Kirkland, C. L., Daly, J. S., Chew, D. M. and Page, L. M. (*2008*). The Finnmarkian Orogeny revisited: an isotopic investigation in eastern Finnmark, Arctic Norway. Tectonophysics **460**, *158-177*.

Kleven, M. K. H. (*2010*). Caledonian (Silurian) out-of-sequence thrusting at Sønsterud, Holsfjorden, Ringerike, University of Oslo, Oslo. *130* pp.

Larsen, B. T., Olaussen, S., Sundvoll, B. and Heeremans, M. (*2008*). The Permo-Carboniferous Oslo Rift through six stages and *65* million years. Episodes **31**, *52*.

Luján, M., Storti, F., Balanyá, J.-C., Crespo-Blanc, A. and Rossetti, F. (*2003*). Role of décollement material with different rheological properties in the structure of the Aljibe thrust imbricate (Flysch Trough, Gibraltar Arc): an analogue modelling approach. Journal of Structural Geology **25**, *867-881*.

McQuarrie, N. (*2004*). Crustal scale geometry of the Zagros fold–thrust belt, Iran. Journal of Structural Geology **26**, *519-535*.
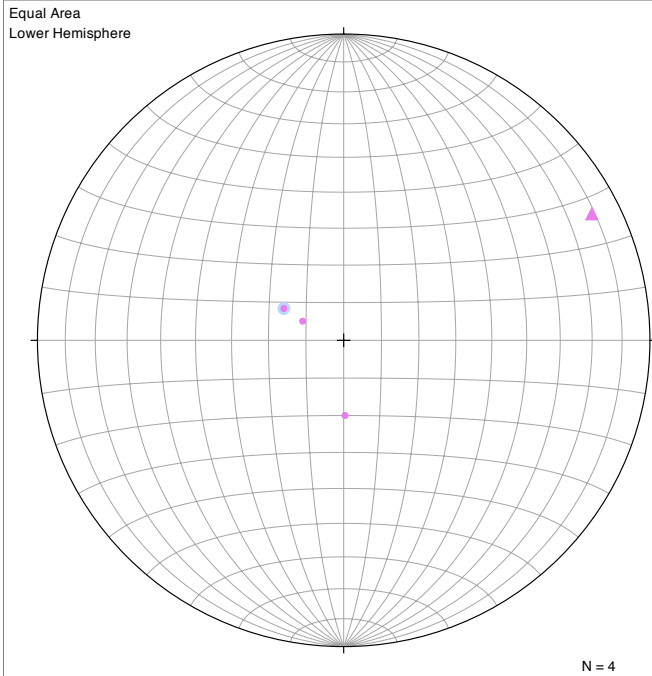
Mørk, M. B. E., Kullerud, K. and Stabel, A. (*1988*). Sm-Nd dating of Seve eclogites, Norrbotten, Sweden—evidence for early Caledonian (*505* Ma) subduction. Contributions to Mineralogy and Petrology **99**, *344-351*.

Morley, C. K. (*1986*). The Caledonian thrust front and palinspastic restorations in the southern Norwegian Caledonides. Journal of Structural Geology **8**, *753-765*.

Morley, C. K. (*1986*). Vertical strain variations in the Osen-Røa thrust sheet, North-western Oslo Fjord, Norway. Journal of structural geology **8**, *621-632*.

Morley, C. K. (*1987*). Lateral and vertical changes of deformation style in the Osen-Røa thrust sheet, Oslo Region. Journal of structural geology **9**, *331-343*.

Morley, C. K. (*1987*). The structural geology of north Hadeland. Norsk geologisk tidsskrift **67**, *39-49*.

Morley, C. K. (*1994*). Fold-generated imbricates: examples from the Caledonides of Southern Norway. Journal of Structural Geology **16**, *619-631*.

Nielsen, A. T. and Schovsbo, N. H. (*2006*). Cambrian to basal Ordovician lithostratigraphy in southern Scandinavia. Bulletin of the Geological Society of Denmark **53**, *47-92*.

Nystuen, J. P. (*1981*). The late Precambrian" sparagmites" of southern Norway; a major Caledonian allochthon; the Osen-Roa nappe complex. American Journal of Science **281**, *69-94*.

Nystuen, J. P. (*1983*). Nappe and thrust structures in the Sparagmite Region, southern-Norway. Norges Geologiske Underskolse Bulletin **70**, *67-83*.

Oftedahl, C. (*1943*). Om sparagmiten og dens skyvning innen kartbladet Øvre Rendal. Aschehoug & Company.

Olaussen, S. (*1981*). Marine incursion in Upper Palaeozoic sedimentary rocks of the Oslo region, southern Norway. Geological Magazine **118**, *281-288*.

Owen, A. W. (*1990*). The Ordovician successions of the Oslo region, Norway. Norges geologiske undersøkel.

Puigdefàbregas, C., Muñoz, J. A. and Vergés, J. (*1992*). Thrusting and foreland basin evolution in the southern Pyrenees. In: Thrust tectonics, pp *247-254*. Springer.

Ramberg, H. (*1981*). The role of gravity in orogenic belts. Geological Society, London, Special Publications **9**, *125-140*.

Ramsay, J. G. and Huber, M. I. (*1987*). The techniques of modern structural geology. *391* pp. Academic press.

Roberts, D. (*1980*). Mélange in Trondheim Nappe, central Norwegian Caledonides. Nature **285**, *593*.

Roberts, D. (*2003*). The Scandinavian Caledonides: event chronology, palaeogeographic settings and likely modern analogues. Tectonophysics **365**, *283-299*.

Roberts, D. and Gee, D. G. (*1985*). An introduction to the structure of the Scandinavian Caledonides. The Caledonide orogen–Scandinavia and related areas **1**, *55-68*.

Roberts, D., Heldal, T. and Melezhik, V. (*2001*). Tectonic structural features of the Fauske conglomerates in the Lovgavlen Quarry, Nordland, Norwegian Caledonides, and regional implications. Norsk Geologisk Tidsskrift **81**, *245-256*.

Sepehr, M., Cosgrove, J. and Moieni, M. (*2006*). The impact of cover rock rheology on the style of folding in the Zagros fold-thrust belt. Tectonophysics **427**, *265-281*.

Sherkati, S. and Letouzey, J. (*2004*). Variation of structural style and basin evolution in the central Zagros (Izeh zone and Dezful Embayment), Iran. Marine and petroleum geology **21**, *535-554*.

Sippel, J., Saintot, A., Heeremans, M. and Scheck-Wenderoth, M. (*2010*). Paleostress field reconstruction in the Oslo region. Marine and Petroleum Geology **27**, *682-708*.

Smit, J. H. W., Brun, J. P. and Sokoutis, D. (*2003*). Deformation of brittle-ductile thrust wedges in experiments and nature. Journal of Geophysical Research: Solid Earth (*1978–2012*) *108*.

Sokoutis, D., Burg, J.-P., Bonini, M., Corti, G. and Cloetingh, S. (*2005*). Lithospheric-scale structures from the perspective of analogue continental collision. Tectonophysics **406**, *1-15*.

Stephens, M. B. and Gee, D. G. (*1985*). A tectonic model for the evolution of the eugeoclinal terranes in the central Scandinavian Caledonides. In: D. G. Gee & B. A. Sturt (eds.) The Caledonide orogen–Scandinavia and related areas, pp *953-978*. John Wiley and Sons.
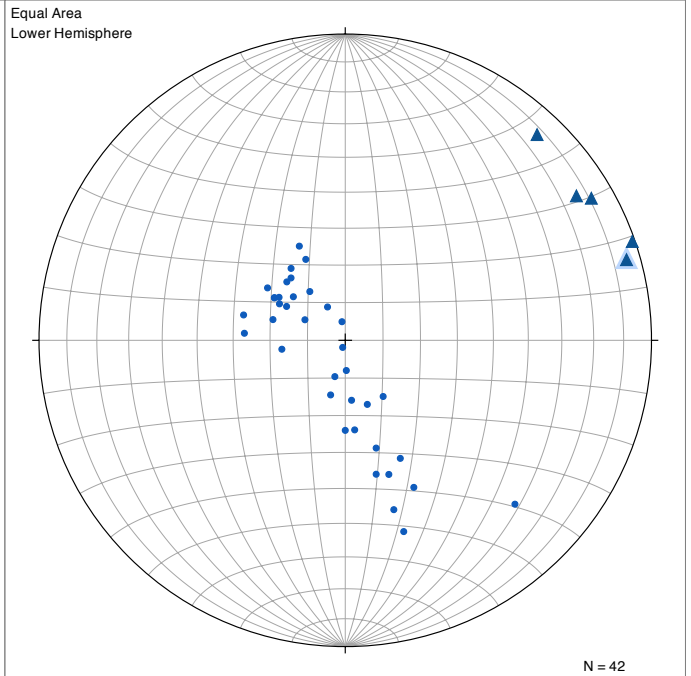
Sturt, B. A., Pringle, I. R. and Ramsay, D. M. (*1978*). The Finnmarkian phase of the Caledonian orogeny. Journal of the Geological Society **135**, *597-610*.

Sundvoll, B. and Larsen, B. T. (*1994*). Architecture and early evolution of the Oslo Rift. Tectonophysics **240**, *173-189*.

Sundvoll, B., Larsen, B. T. and Wandaas, B. (*1992*). Early magmatic phase in the Oslo Rift and its related stress regime. Tectonophysics **208**, *37-54*.

Sugrañes, L. S. (*1983*). Discussion about the emplacement of some of the Southern Pyrenees nappes (Spain). Acta geológica hispánica **18**, *47-53*.

Teixell, A. (*1996*). The Ansó transect of the southern Pyrenees: basement and cover thrust geometries. Journal of the Geological Society **153**, *301-310*.

Thon, A. (*1985*). The Gullfjellet ophiolite complex and the structural evolution of the major Bergen arc, west Norwegian Caledonides. In: D. G. Gee & B. A. Sturt (eds.) The Caledonide Orogen: Scandinavia and related areas, pp *671-677*. New York: Wiley and Sons.

Törnebohm, A. E. (*1888*). Om fjällproblemet. Geologiska Föreningen i Stockholm Förhandlingar **10**, *328-336*.

Törnebohm, A. E. (*1896*). Om användandet af termerna arkeisk och algonkisk på skandinaviska förhållanden. Geologiska Föreningen i Stockholm Förhandlingar **18**, *285-299*.

Torsvik, T. H., Eide, E. A., Meert, J. G., Smethurst, M. A. and Walderhaug, H. J. (*1998*). The Oslo Rift: new palaeomagnetic and *40*Ar/*39*Ar age constraints. Geophysical Journal International **135**, *1045-1059*.

Torsvik, T. H. and Rehnström, E. F. (*2001*). Cambrian palaeomagnetic data from Baltica: implications for true polar wander and Cambrian palaeogeography. Journal of the Geological Society **158**, *321-329*.

Torsvik, T. H., Smethurst, M. A., Meert, J. G., Van der Voo, R., McKerrow, W. S., Brasier, M. D., Sturt, B. A. and Walderhaug, H. J. (*1996*). Continental break-up and collision in the Neoproterozoic and Palaeozoic—a tale of Baltica and Laurentia. Earth-Science Reviews **40**, *229-258*.

Van den Broek, J. (*2015*). Unknown, University of Utrecht, Utrecht. *70* pp.

Verdonk, A. (*2015*). Unknown, University of Utrecht, Utrecht. *70* pp.

Vergés, J., Millán, H., Roca, E., Muñoz, J. A., Marzo, M., Cirés, J., Den Bezemer, T., Zoetemeijer, R. and Cloetingh, S. (*1995*). Eastern Pyrenees and related foreland basins: pre-, syn-and post-collisional crustal-scale cross-sections. Marine and Petroleum geology **12**, *903-915*.

Weekenstroo, M. (*2015*). Unknown, University of Utrecht, Utrecht. *70* pp.

Weijermars, R. and Schmeling, H. (*1986*). Scaling of Newtonian and non-Newtonian fluid dynamics without inertia for quantitative modelling of rock flow due to gravity (including the concept of rheological similarity). Physics of the Earth and Planetary Interiors **43**, *316-330*.

Wickham, J. (*2007*). Comment on "Basin inversion and fault reactivation in laboratory experiments". Journal of Structural Geology **29**, *1414-1416*.

Worsley, D., Aarhus, N. and Bassett, M. G. (*1983*). The Silurian succession of the Oslo region. Trondheim: Universitetsforlage.

Zwaan, K. B. and Larsen, B. T. (*2003*) Berggrunnskart *1814* III Hønefoss *1:50000*. Norges Geologiske Undersokelse.

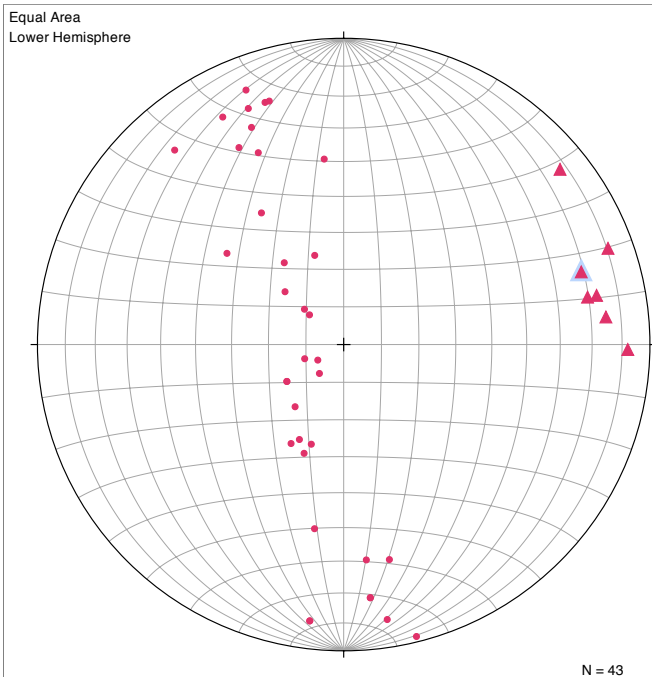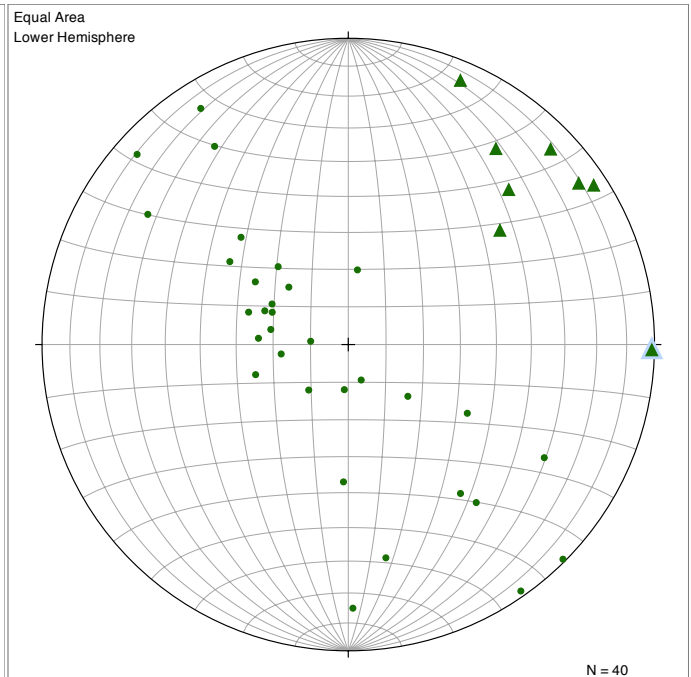## Appendix A: Stereodata per location.
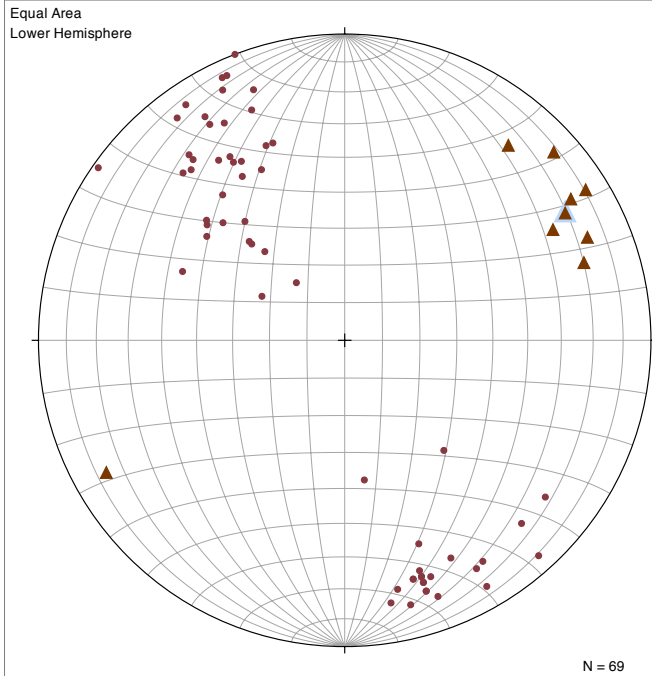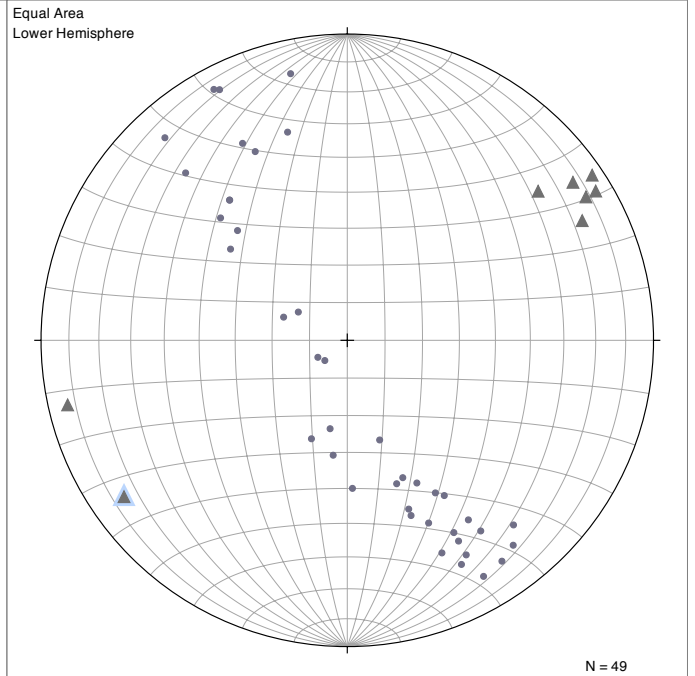
Rytteråker

Storøya

Geitøya

Utøya

## Crossroad Utstranda-E16

Equal Area
Lower Hemisphere

N = 69

## Utstranda coastline

Equal Area
Lower Hemisphere

N = 49

## Sonsterud coast

Equal Area
Lower Hemisphere

N = 7

## Utstranda road

Equal Area
Lower Hemisphere

N = 128
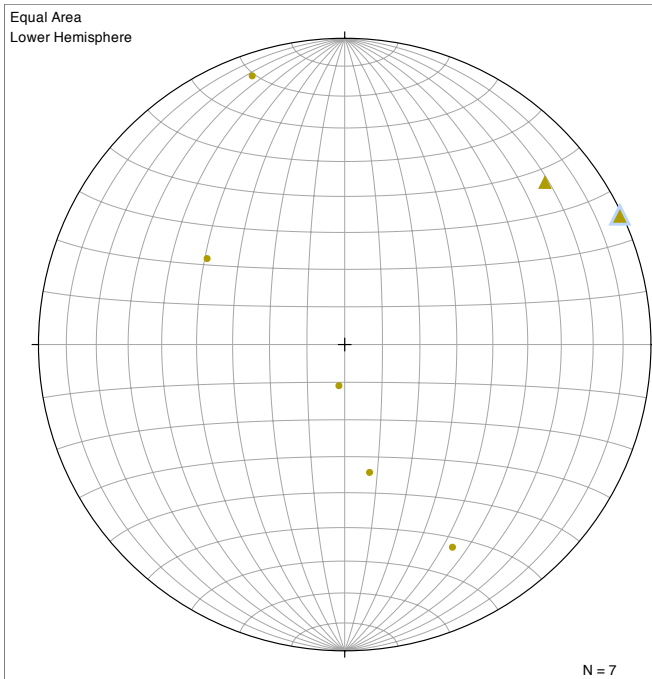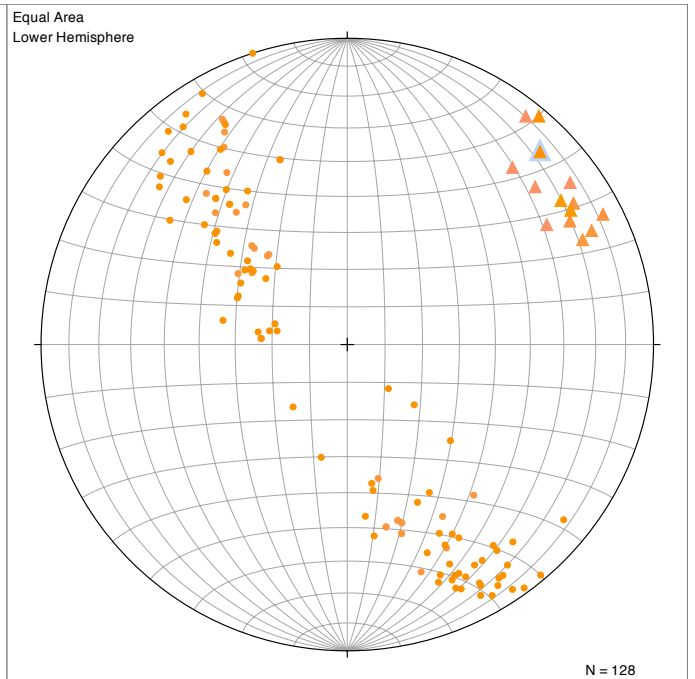
## Appendix B: Strength profiles

| Model # | Model setup* | Mechanical setup |
|---|---|---|
| 1 | *Backstop* — 2, 60, 20, Putty 1, 0,5, 1 | Basal (strong) quartz layer with a thin centered (weak) putty layer on top, followed by a thick section of quartz sand. *BS (bulk shortening): 13%, v (velocity of convergence): 5 cm/h.* |
| 2 | 2, 30, 5, 30, 15, 0,5, 1 | Basal (strong) quartz layer with a discontinuous (weak) putty layer on top (which lays closer to the backstop), followed by a thick section of quartz sand. *BS: 20%, v: 5 cm/h.* |
| 3 | 2, 60, 15, 0,5, 2, 1,5° | Basal (strong) quartz layer with a thin, centered (weak) continuous putty layer on top, followed by a thick section of quartz sand. Basal inclination of 1,5°. *BS: 15,5%, v: 5 cm/h.* |
| 4 | 2, 20, 5, 20, 15, Putty 2, 0,5, 2, 1,5° | Additional discontinuity in the putty layer, putty 2 is very strong compared to putty 1. Basal inclination of 1,5°. *BS: 10%, v: 5 cm/h.* |
| 5 | 0,2, 1, 2, 7, 0,8, 0,5, 20, 3, 20, 15, 2, 1,5° | Additions: Shorter sand part inbetween two putties and the introduction of a second stage of weak layer in the upper part. Basal inclination of 1,5°. *BS: 13%, v: 5 cm/h.* |

*Thicknesess and lengths are given in cm.*